9950-338

DOE/JPL-954929-80/7

DRD Line Item No. SE-7

INVESTIGATION OF RELIABILITY ATTRIBUTES AND ACCELERATED STRESS FACTORS ON TERRESTRIAL SOLAR CELLS

SECOND ANNUAL REPORT

J.W. Lathrop and J.L. Prince

Department of Electrical and Computer Engineering

Clemson University

Clemson, SC, 29631

APRIL 1980

PREPARED FOR
JET PROPULSION LABORATORY

PREPARED BY
CLEMSON UNIVERSITY, CLEMSON, SOUTH CAROLINA 29631

DRD Line Item No. SE-7 DOE/JPL - 954929-80/7

ENGINEERING AREA

INVESTIGATION OF RELIABILITY ATTRIBUTES AND ACCELERATED STRESS FACTORS OF TERRESTRIAL SOLAR CELLS

SECOND ANNUAL REPORT

J. W. Lathrop and J. L. Prince

Department of Electrical and Computer Engineering

Clemson University

Clemson, SC 29631

April 1980

The JPL Low-Cost Silicon Solar Array Project is sponsored by the U.S. Department of Energy and forms part of the Solar Photovoltaic Conversion Program to initiate a major effort toward the development of low-cost solar arrays. This work was performed for the Jet Propulsion Laboratory California, Institute of Technology by agreement between NASA and DOE.

ACKNOWLEDGEMENTS

The authors acknowledge the contributions of the following Clemson University Electrical Engineering students in the conduct of this program: Graduate Students: F. Christ, R. Hartman, K. Labib, and C. Saylor; Undergraduate Students: D. Hawkins and W. Stacy. Special Acknowledgement is made of the contribution of Dr. F. W. Morgan, Department of Mathematical Sciences.

Mr. E. L. Royal was the Jet Propulsion Laboratory Technical Manager for this work.

ABSTRACT

The work covered in this report represents the second year's effort of a continuing program to determine the reliability attributes of terrestrial solar cells. Three main tasks were undertaken during the reporting period: 1) a study of the electrical behavior of cells in the second (reverse) quadrant, 2) the accelerated stress testing of three new state of the art cells and 3) the continued bias-temperature testing of four Block II type silicon cells at 78°C and 135°C. Electrical characteristics measured in the second quadrant were determined to be a function of the cell's thermal behavior with breakdown depending on the initiation of localized heating. This implied that high breakdown cells may be more fault tolerant when forced to operate in the second quadrant--a result contrary to conventional thinking. The accelerated stress tests used in the first (power) quadrant were bias-temperature, bias-termperature-humidity, temperature-humidity, thermal shock, and thermal cycle. The new type cells measured included an EFG cell, a polycrystalline cell, and a Czochralski cell. Electrical parameters measured included I_{SC}, V_{OC}, P_M, V_M, and I_M. Incorporated in the report are the distributions of prestress electrical data for all cell types. Significant differences in the response to the various stress tests were observed between cell types. A microprocessed controlled, short interval solar cell tester was designed and construction initiated on a prototype for use in the program.

SUMMARY

The second year of the accelerated reliability testing program extended the first year's effort and included the stress testing of three additional cell types. In a separate effort the second quadrant behavior of cells was investigated. Stress test results again showed a wide variability among cell types in their ability to withstand the effect of various stresses. For example:

1) Bias-temperature stress testing showed significant degredation, consistent in time, for one cell type and only moderate degredation for another cell type. The final cell type showed no significant degredation at all.
2) Bias-temperature-humidity stress testing showed significant degredation, consistent in time, for one cell type and only moderate degredation for the other cell types. Furthermore, these two cell types actually showed less degredation towards the end of the test.
3) Sensitivity to thermal cycle and thermal shock stress varied both in severity and in characteristic failure mode from cell type to cell type.
4) One cell type gave an indication of infant mortality failure--the first that has been observed in two years of testing.
5) The cell types tested appeared to be less prone to the increased series resistance failure mode, which was predominant in the first year's effort. Instead, much of the degredation could be related to I_{sc} reduction.

6) It appeared that EFG material, at least in the configuration tested, was more sensitive to thermal cycle/thermal shock than either Czochralski or polycrystalline material.

The second quadrant studies confirmed that breakdown is a thermal phenonmenon and to a first approximation the temperature of a cell at the breakdown knee is a constant, independent of where the knee occurs. Techniques are described for observing the occurrence of a non-uniform temperature distribution across the cell.

New test jigs were constructed to hold cells during bias-temperature testing. A microprocessor controlled, short interval tester was designed to eliminate the problems of temperature variations during measurement. A prototype system is presently under contruction.

TABLE OF CONTENTS

TABLE OF CONTENTS (continued)

LIST OF FIGURES

LIST OF FIGURES (continued)

LIST OF FIGURES (continued)

LIST OF FIGURES (continued)

LIST OF FIGURES (continued)

LIST OF TABLES

1.0 INTRODUCTION

1.0 INTRODUCTION

The reliability characteristics of solar cells intended for low-cost terrestrial applications, either central power generation or distributed residential usage, will be a key factor in the determination of the economic feasibility of such systems. DOE cost goals for terrestrial photovoltaic systems, for example, are based on the assumption of a 20-year module life. Interpretation of such specific module life figures, however, is only meaningful when done in terms of system life cycle costs. Minimization of a system's life cycle costs will involve developing strategies for repair and replacement of modules as well as the design acceptance of some performance degredation. The concept of module life is analagous in many respects to the concept of lifetime of any consumer product. The term, 5-year life, when applied to an automobile, for example, does not mean that it will perform as new during those 5 years, but rather that repairs will be minimal and that performance remains satisfactory. It is in this same context that the 20-year photovoltaic module goal should be viewed.

The fact that system reliability goals must, of necessity, be somewhat nebulous, however, does not mean that reliability studies are unnecessary. It is important to establish the methodology and to acquire the data for assessing the reliability attributes of state of the art technology. Clemson University has been engaged in a program to investigate the reliability attributes of terrestrial solar cells and to define applicable accelerated test procedures which can be used for such monitoring. This report describes the program's second year activities.

The reliability test program, being performed by Clemson University as part of DOE's Low Cost Solar Array (LSA) Project under contract to the

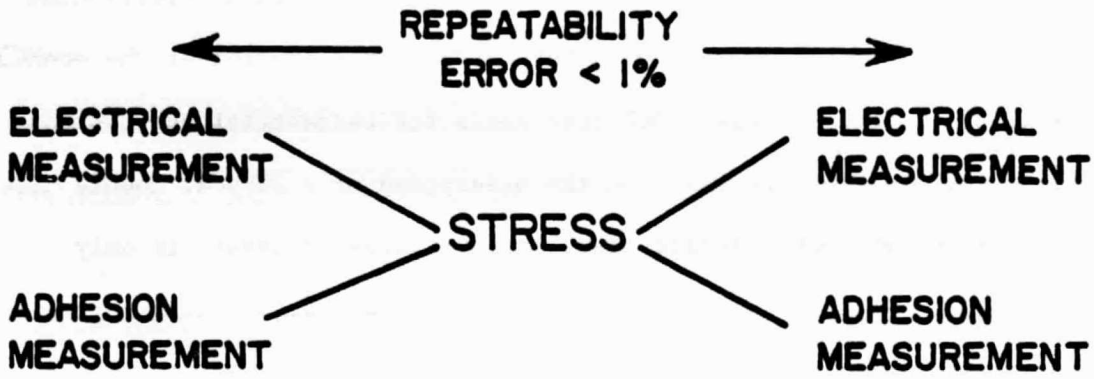

ELECTRICAL PARAMETERS

V_{oc} I_{sc} R_s V_m I_m P_m

INSPECTION

LOW POWER MAGNIFICATION

PHOTOGRAPHY

Figure 1.1. Reliability Methodology Second Year Program.

Jet Propulsion Laboratory, was started in Decmeber 1977 and represented the first known systematic attempt by independent investigators to define the basic reliability attributes of terrestrial solar cells. Results of the first year's program were reported in the First Annual Report, DOE/JPL-954929-79/4, May 1979. The program developed test metholodology and accumulated baseline accelerated stress reliability data on four different cell types identified as A, B, C and E. The cells, which were representative of commercial, state-of-the-art cells used in JPL/LSA Block II and III solar cell module procurements, were unencapsulated so that the reliability attributes encountered were a function only of the basic cell structure and not of the encapsulation. Results of the first year's program included a preliminary reliability qualification test schedule, development of reproducible electrical measurement techniques, and implementation of a computerized system for reliability data managemnt and analysis. Quantities of A, B, C and E cells were continued under bias-temperature stress at two different temperatures throughout the second year program and the results reported.

The second year program has refined and extended many of the techniques developed under the first year's program. Accelerated environmental stress testing were performed on three new cell types, indentified as F, G and H, representing quite different technologies from the original four cell types. Table 1.1 lists the physical characteristics of all cell types tested to date. The program utilized the conventional reliability methodology illustrated in Figure 1.1.1. The cells were initially electrically measured and visually inspected. Quantities of cells were then subjected to various stresses for various lengths of times and remeasured. This sequence of

TYPE	SIZE (in)	THICKNESS (mils)	AR COATING	TECHNOLOGY	METAL
A	4,DIA	24	NO	P/N	SOLDER
B	3,DIA	19	YES	N/P	THIN FILM Ti/Pd/Ag
C	2,DIA	20	YES	N/P	SOLDER
E	3,DIA	15	NO	N/P	THICK FILM Ag
F	3.9 x 0.8 EFG SILICON	13	YES	N/P	SOLDER
G	3,DIA	12	YES	N/P	SOLDER
H	2 x 2 POLY-SILICON	12	YES	N/P (IMPLANTED)	THIN FILM Ti/Pd/Ag

Table 1.1. Physical Characteristics of Cells Tested in Clemson Program.

measure-stress-measure was repeated many times for each stress test. The measurement repeatability insured that electrical degredation due to stress as small as $\pm$ 2% could be detected.

In addition to environmental stress involving factors such as temperature and humidity, it has become evident that operational factors can play a significant role in cell reliability. Specifically, module field failure can result from the shifting of a cell's operating point from normal operation in the first or power quadrant of the VI characteristic to the second or reverse quadrant. Because large amounts of power can be dissipated in the cell in the second quadrant the cell overheats in this mode leading to possible early failure. A separate task of the second year's program involved a preliminary investigation of the behavior of cells in the second quadrant with the objective of developing techniques for more detailed quantitative second quadrant characterization and correlation with reliability factors.

The technical portion of this report is organized to present the second quadrant studies first, followed by a description of the accelerated stress testing program and its results. The report focuses primarily on the events which occurred during the second year's effort. Small amounts of descriptive material presented in the First Annual Report are repeated for clarification where necessary, but in general the Second Annual Report should be viewed as the second volume in a series, rather than as a stand alone document.

2.0 SECOND QUADRANT STUDY

Page intentionally left blank

2.0 SECOND QUADRANT STUDY

2.1 Introduction

The deeper one becomes involved with terrestrial solar cell reliability the more evident it becomes that the problem of cell reliability is not just confined to normal operation in the first quadrant. Through the effects of VI characteristic mismatch within a module, variable rates of aging, shadowing, cell fractures, etc., cells are often forced to operate in the second (power consuming) quadrant. Therefor, as a separate effort during the second year of work, the characteristics of different cell types were studied in the second quadrant and initial results presented in this report.

The second quadrant characterization work at Clemson was concerned mainly with correlating cell thermal stresses with their electrical characteristics and was done under controlled laboratory conditions. In the field, where second quadrant operations in modules can occur, the interaction between cells presents complicating factors which were not investigated in this work.

2.2 Pulsed Second Quadrant VI Characteristics

A Tektronix Model 176 pulsed high current fixture was acquired for use with a 576 curve tracer in order to measure second quadrant characterisitics with heating. This plug-in fixture permits solar cell characteristics to be taken under pulsed conditions to 200 amperes peak current. The pulse width is 300 sec at a 60 Hz repetition rate resulting in a duty cycle of less than 2%. the second quadrant VI characteristics thus can be traced out with only minor heating effects which, for the most part, may be neglected. Figure 2.1 shows typical traces obtained for type A and Type G cells. Breakdown occurs at approximately 78 volts. Two curves are shown for each cell: the lower

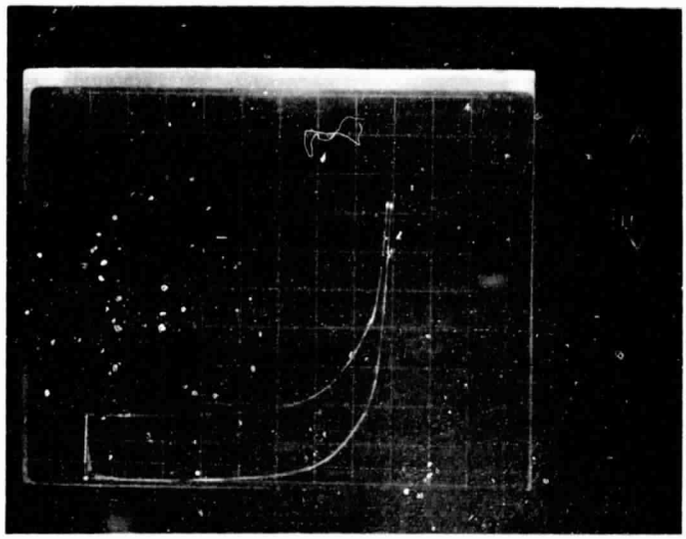

a) A Cell

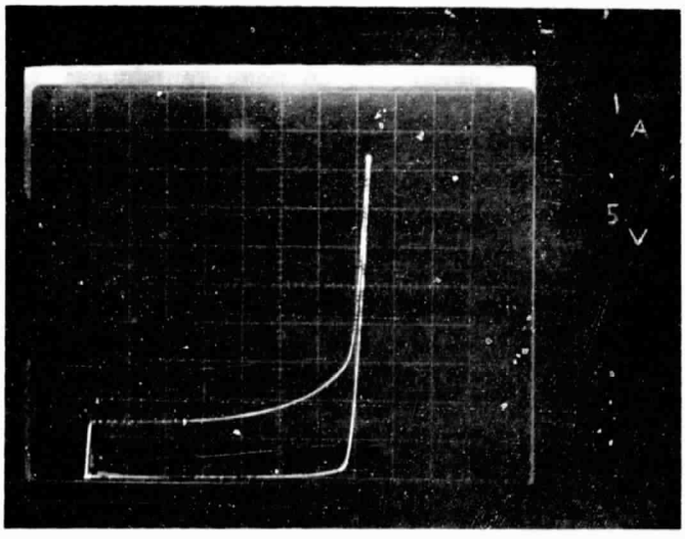

b) G Cell

Figure 2.1. Typical Second Quadrant Characteristics Made with Model 176 Cruve Tracer Attachment.

trace was taken in the dark while the upper trace was under 100 mW/cm^2 illumination. To a first approximation the illuminated characteristic is the same as the dark characteristic shifted by I_{sc}. Since the characteristics measured in this fashion are independent of localized thermal effects they may be denoted as "intrinsic", meaning they are a function of the cell construction only and not of the particular heat sinking used.

A number of measurements were made of intrinsic second quadrant characteristic on different cell types. While there was appreciable variation from cell to cell within a given cell type population a typical second quadrant "signature" could be observed which was characteristic of each type. Figure 2.2 is a comparison of typical intrinsic second quadrant characteristics for the different types measured. Cell type A consistently had the highest breakdown voltage while cell types E and G consistently had the lowest. Note also the low shunt resistance asssociated with type E cells.

In order to obtain statistical information, cell voltage was read at 2 times I_{sc} , (V_{02}), and at 3 times I_{sc} , (V_{03}). The closer these two values are together, the sharper the knee of the second quadrant. The voltage values and their standard deviations are shown in Table 2.1 together with the ratio $\frac{V_{03} - V_{02}}{V_{02}}$, which is a crude measure of breakdown sharpness. The "soft" characteristic caused by low shunt resistance is clearly evident for type E cells.

The breakdown mechanism associated with pulsed measurement is avalanch multiplication, i.e. the voltage across the p-n junction increases to the point where the leakage current flowing across the space change creates additional carriers by impact ionization. This type of breakdown has a

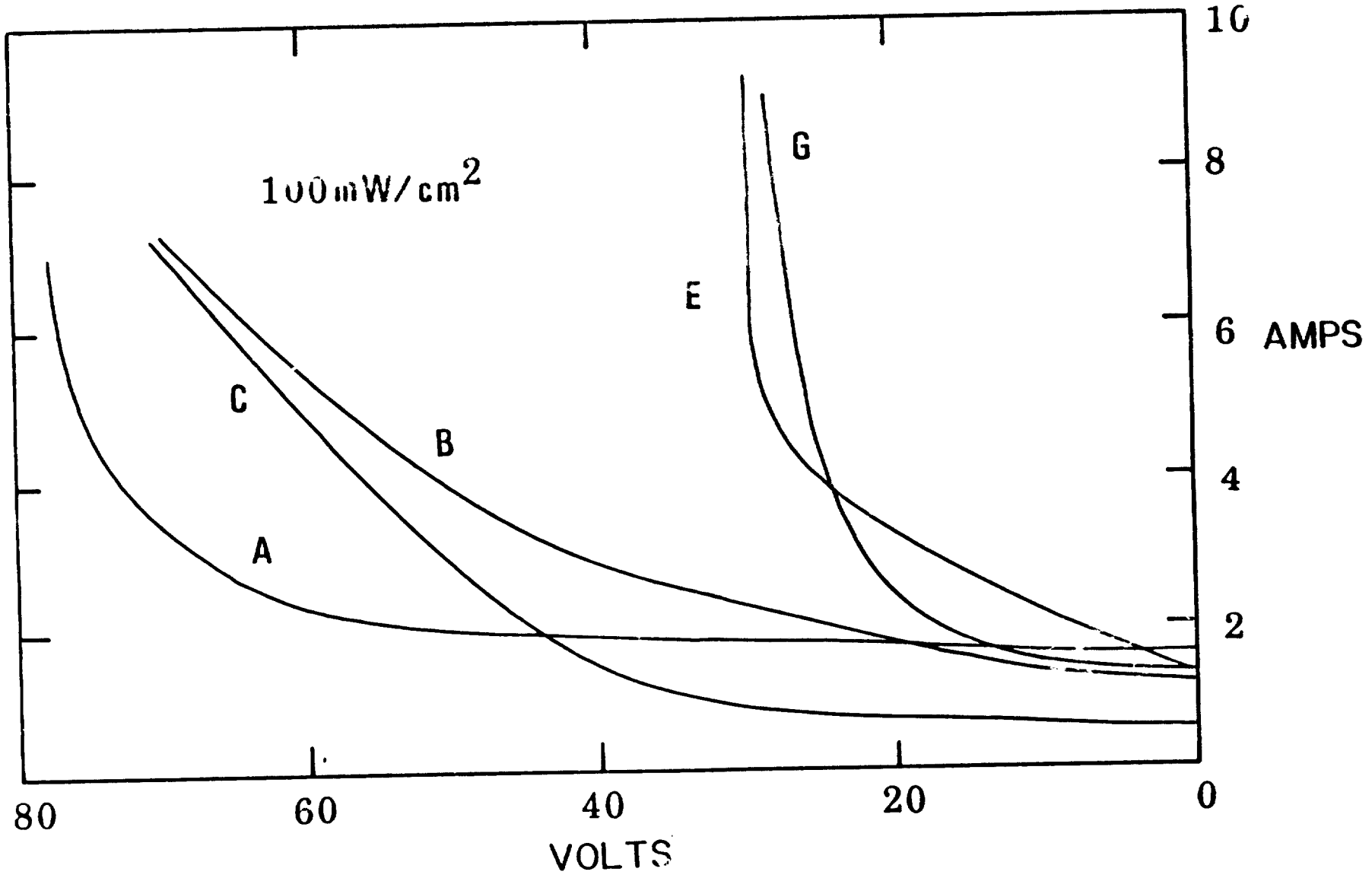

Figure 2.2. Typical Intrinsic Second Quadrant Characteristics.

Cell Type	V @ $2I_{sc}$ V_{02} (Volts)	V @ $3I_{sc}$ V_{03} (Volts)	$\frac{V_{03} - V_{02}}{V_{02}}$ %
A	62 ± 28	69 ± 32	11
B	37 ± 21	46 ± 19	24
C	39 ± 14	50 ± 15	28
E	12 ± 2	21 ± 3	75
G	25 ± 6	29 ± 5	16

Table 2.1 Second Quadrant Votages Measured at Two and Three Times I_{sc} Under Pulsed Conditions.

positive temperature coefficient; i.e. the breakdown voltage increases as the temperature increases, and is the type of breakdown normally found in semiconductor diodes. However, pulsed and steady state breakdown in a semiconductor diode tend to be the same whereas this is not the case for a solar cell. The fact which causes the difference is the tremendous amount of power being dissipated in the second quadrant by virtue of the cell being illuminated. This will be discussed in detail in the next section.

2.3 Steady State Second Quadrant VI Characteristic

At the opposite extreme to low duty cycle pulsed measurement is steady state measurement. In this technique the voltage across a cell is raised very slowly so that the cell remains in quasi thermal equilibrium. The power being dissipated in the illuminated cell is roughly the short circuit current, I_{sc}, times the voltage across the cell. Figure 2.3 represents the x-y recorder trace of an A cell measured in this fashion while suspended in free air with no heat sinking. Superimposed on the VI characteristic are a family of constant power hyperbolas. Notice that although the maximum power the cell can deliver is only 0.8 Watt, 10 to 50 Watts can be dissipated in the reverse direction by virtue of the photon generated current. Notice from Figure 2.3 that the steady state breakdown is much less than the pulsed breakdown shown in Figure 2.2. Since the cell is obviously much hotter in steady state than when pulsed, the mechanism must be different in the two cases, otherwise the steady state breakdown voltage would be greater than the pulsed.

The mechanism which causes the current to increase (deviate from the straight line) as the reverse voltage of Figure 2.3 approaches 15 volts is the increase in leakage current due to the thermal generation of carriers.

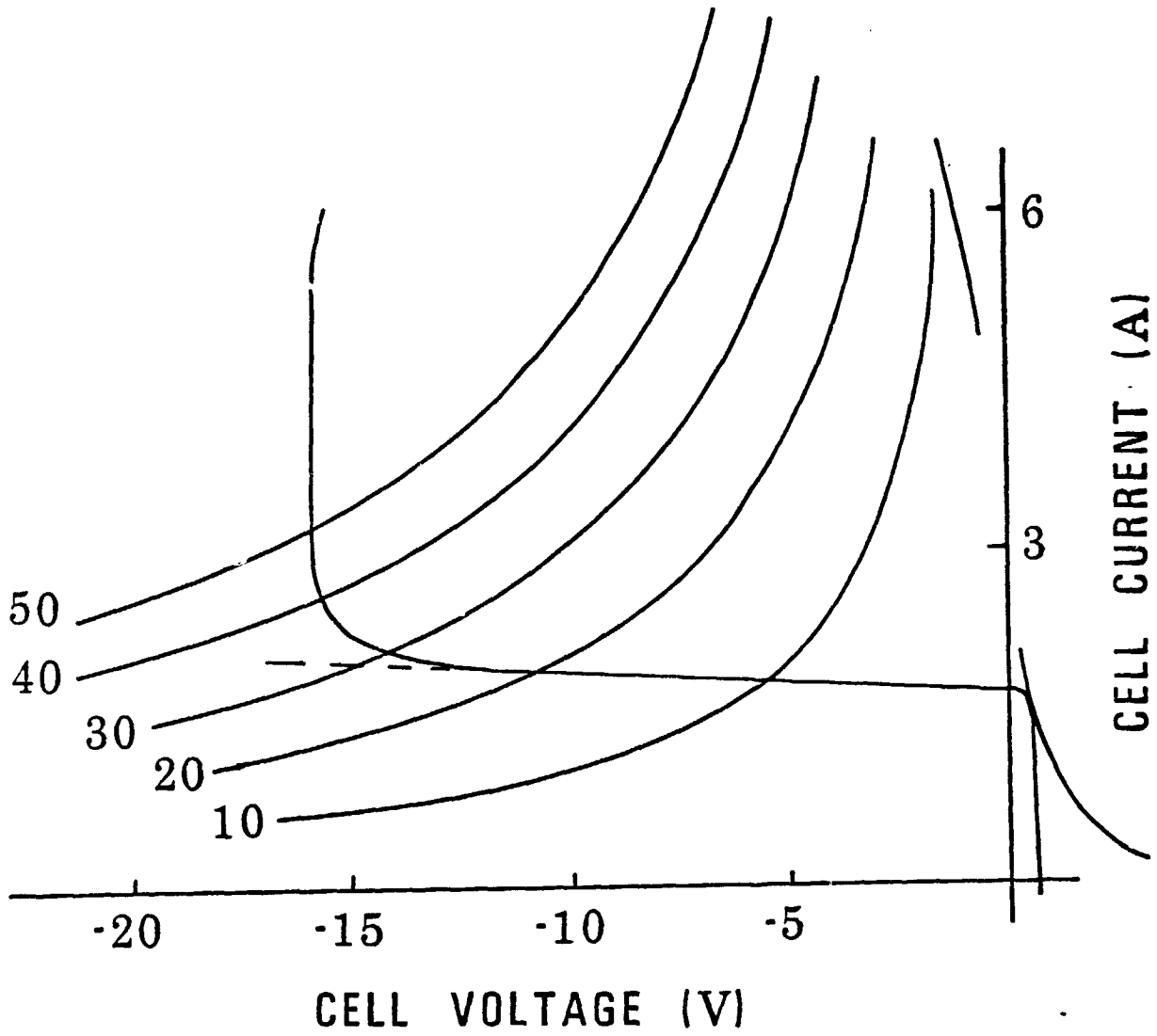

Figure 2.3. Second Quadrant A Cell Characteristics Made Under Steady State Conditions.

Thermally generated leakage current at this value of reverse voltage has become an appreciable fraction of the photon generated current. As previously discussed, the heat which thermally generates the hole-electron pairs comes from this photon current and the reverse potential. In silicon, the thermal generation of hole-electron pairs results in an intrinsic concentration of electrons and holes per cubic centimeter given by

$$n_i = 1.69 \times 10^{19} \frac{T}{300}^{3/2} e^{-0.55/KT}.$$

At 300 K the intrinsic concentration is $1.38X10^{10}$ cm^{-3}, and is negligible compared to ordinary doping levels. Consequently any thermally generated leakage at this temperature will be orders of magnitude less than the reverse diode diffusion current derived from doping levels, which, in turn, is orders of magnitude less than the photon generated current. However, N_i increases rapidly with temperature, approximatley doubling for every 11^oC rise in temperature, and at high temperatures generation will become the dominant process of hole-electron production.

Figure 2.4 is a plot of the temperature at which the concentration due to thermal effects, n_i, becomes equal to the original concentration of the base as a function of the base doping level. This temperature is termed the intrinsic temperature, θ_i. It can be seen that for normal base doping levels the intrinsic temperature is the order of 300^oC. Below θ_i, the carrier concentration in silicon is relatively temperature independent, while above θ_i it rises exponentially with temperature. At temperatures below θ_i the power dissipated in the slice due to the photon generated reverse current causes the cell to heat uniformly and operation is inherently stable.

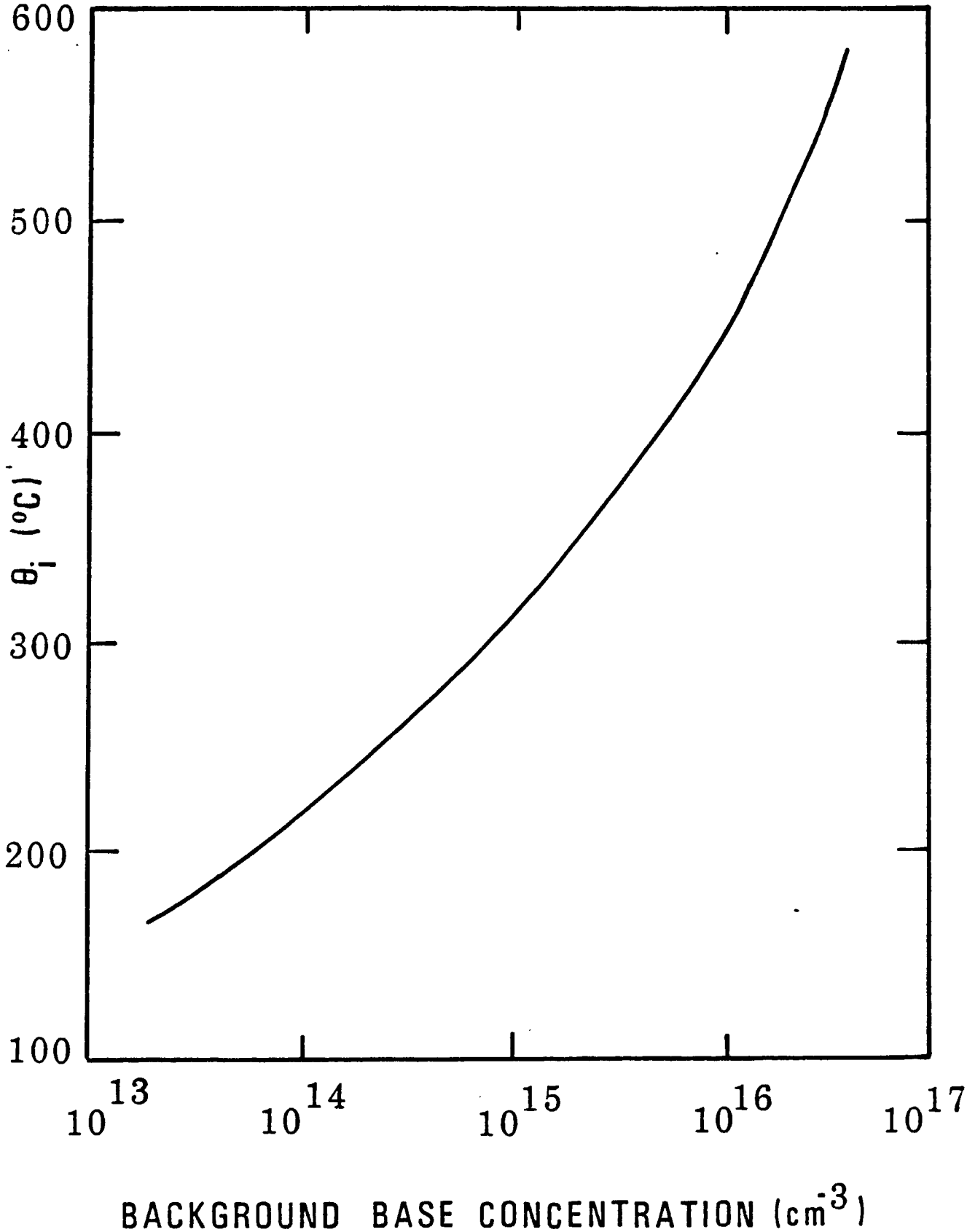

Figure 2.4. Intrinsic Temperature vs. Doping Level.

As the reverse voltage is further increased, the localized temperature at some point in the cell will exceed θ_i due to an inhomogeneity. When this occurs, current at this point becomes appreciable compared to the photon current, increasing the localized power dissiption and temperture still further resulting in a positive feedback situation capable of producing thermal runaway. It is said at this point that a localized mesoplasma has formed. Current through the device becomes limited only by the external circuit with possible catastrophic results. A highly negative resistance can appear with a discontinous drop in voltage as shown in the characteristic of Figure 2.3.

Steady state second quadrant characteristic data was taken on different devices and catagorized in the same fashion as was done for the pulsed case. This is shown in Table 2.2. Notice that although there is a 2 to 1 spread in the voltage breakdown from cell type to cell type, all types show low values--less than 15 volts, and all types display a sharp knee characteristic.

	V @ $2I_{sc}$	V @ $3I_{sc}$	$\frac{V_{03} - V_{02}}{V_{02}}$
Cell Type	V_{02} (Volts)	V_{03} (Volts)	(%)
A	14 $\pm$ 3	13 $\pm$ 3	-8
B	8 $\pm$ 1	8 $\pm$ 1	0
C	13 $\pm$ 2	13 $\pm$ 2	0
E	7 $\pm$ 2	7 $\pm$ 2	0
G	13 $\pm$ 3	13 $\pm$ 2	0

Table 2.2. Second Qaudrant Voltages Measured at Two and Three Times I_{sc} Under Steady State Conditions.

2.4 Cell Temperature Measurement

Second quadrant electrical characteristics are inherently tied to a cell's thermal characteristics. If a cell could be supplied with an infinite heat sink, then the characteristics (steady state) would appear as in Figure 2.2. With no heat sink (free air) the characteristics would appear as in Figure 2.3. For practical heat sinks the steady state characteristics will lie between these two extremes. Furthermore, the cell's thermal time constant will dictate its response to sudden changes in operating conditions. For example, if the operating point is suddenly shifted from forward to reverse it is possible for a localized mesoplasma to form, whereas if the same shift were performed gradually, none would occur because the heat generated would have had time to redistribute itself, and the temperature θ_i would never be reached. An example of a transient phenomenon of this sort is shown in Figure 2.5. In this case the operating point was suddenly shifted from short circuit, $I = I_{sc}$, to the second quadrant, $I = 2I_{sc}$, a point where the cell had previously operated in a stable fashion under steady state conditions. In the transient case, however, a mesoplasma formed in which the core temperature exceeded the melting point of silicon, 1412°C, causing a hole to be formed through the cell.

It is obvious from events of this sort that measurement of cell temperature and cell temperature distribution in the second quadrant is of great significance and two measurement approaches were investigated. The first involved the use of temperature sensitive paints which are availale under the trade name Temprobe. The texture of these paints changes markedly at a particular temperature. Each paint composition has its own characteristic transition temperature value. Since the paint must be applied to the solar

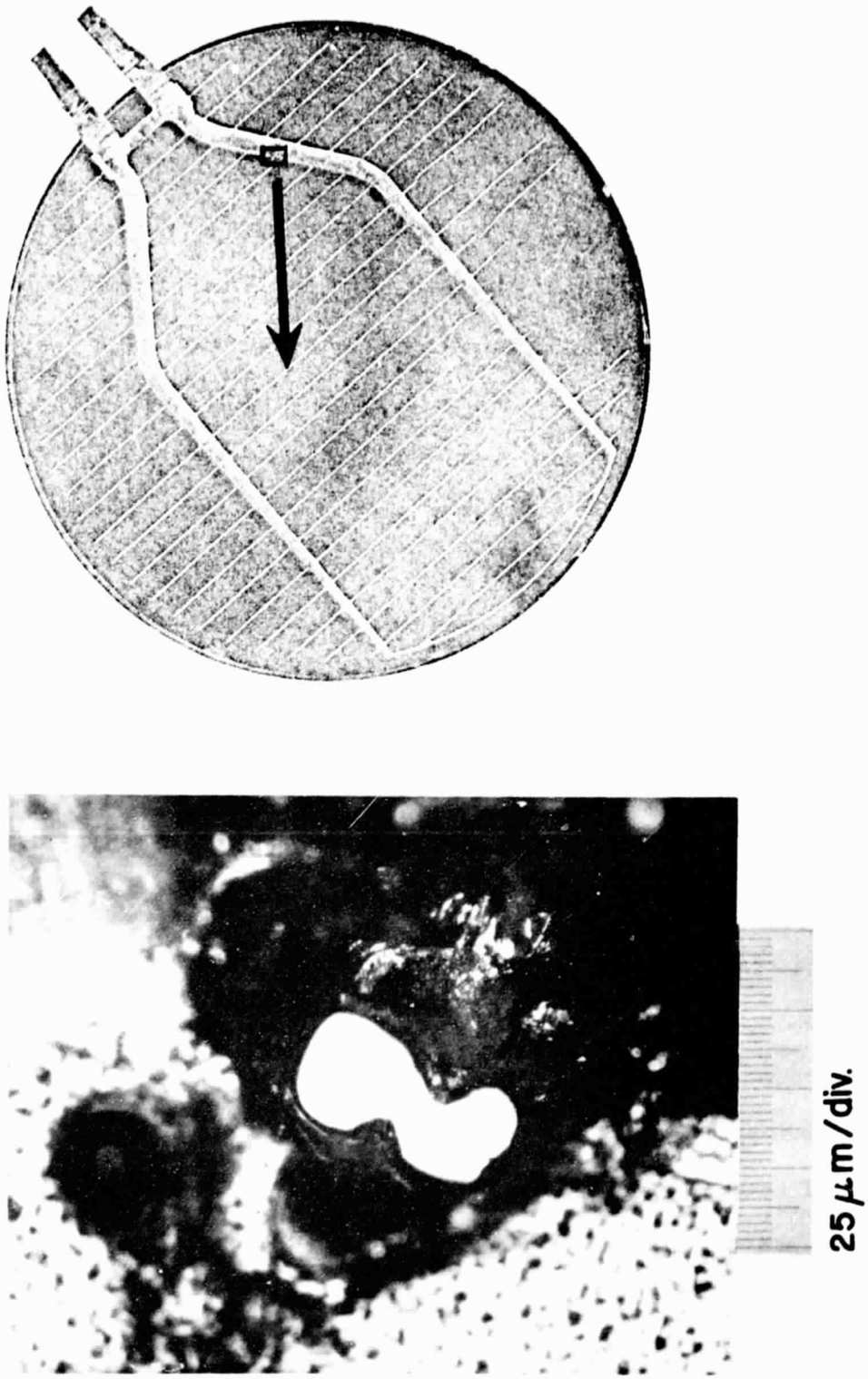

Figure 2.5. Hole Formed in Cell as a Result of Mesoplasma Formation.

cell in such a way as not to block the light, it was applied in the form of a grid to the top surface. By using 3 grids, 3 different temperatures could be detected. Figure 2.6 schematically illustrates how grids indicating 204°C, 288°C, and 427°C were applied to a cell. The grids were observed as the reverse characteristic, illustrated in Figure 2.7, was traced out. Figures 2.8, 2.9 and 2.10 are photographs of a "gridded" G cell taken at points 1, 2 and 3 respectively of Figure 2.7. Figures 2.8, taken at V = 0 (point 1), shows all three grids undisturbed. Figure 2.9 taken at V = 7 volts (point 2) shows a change in the 204°C grid between the current probes. Figure 2.10 taken at V = 9 volts (point 3) shows changes in both the 204°C and 288°C grid in this same region, but the 427°C grid is undisturbed.

Results of experiments with the temperature sensitive point seemed to confirm the operational hypothesis stated in Section 2.3 relating to mesoplasma formation at $T = \theta_i$. However, while the method is satisfactory for observing regional cell temperature variations it does not have sufficient resolution to view localized mesoplasmas. To accomplish this, experiments were run using temperature sensitive phosphors* coatings applied to the back side of cells. A schematic of the measurement method is shown in Figure 2.11 and a photograph of the actual apparatus is shown in Figure 2.12. In this technique a temperature sensitive phosphor (see Appendix C) is applied to the back of a cell. The front side of the cell is illuminated from underneath with the solar spectrum while the phosphor coated back side is illuminated from above with an ultra violet lamp. Figure 2.13 shows how the temperature distribution can be observed at different points along the characteristic of Figure 2.14. The formation of a

*This approach was first suggested to us by personnel at the National Bureau of Standards who had used similar techniques to study second breakdown in power transistors.

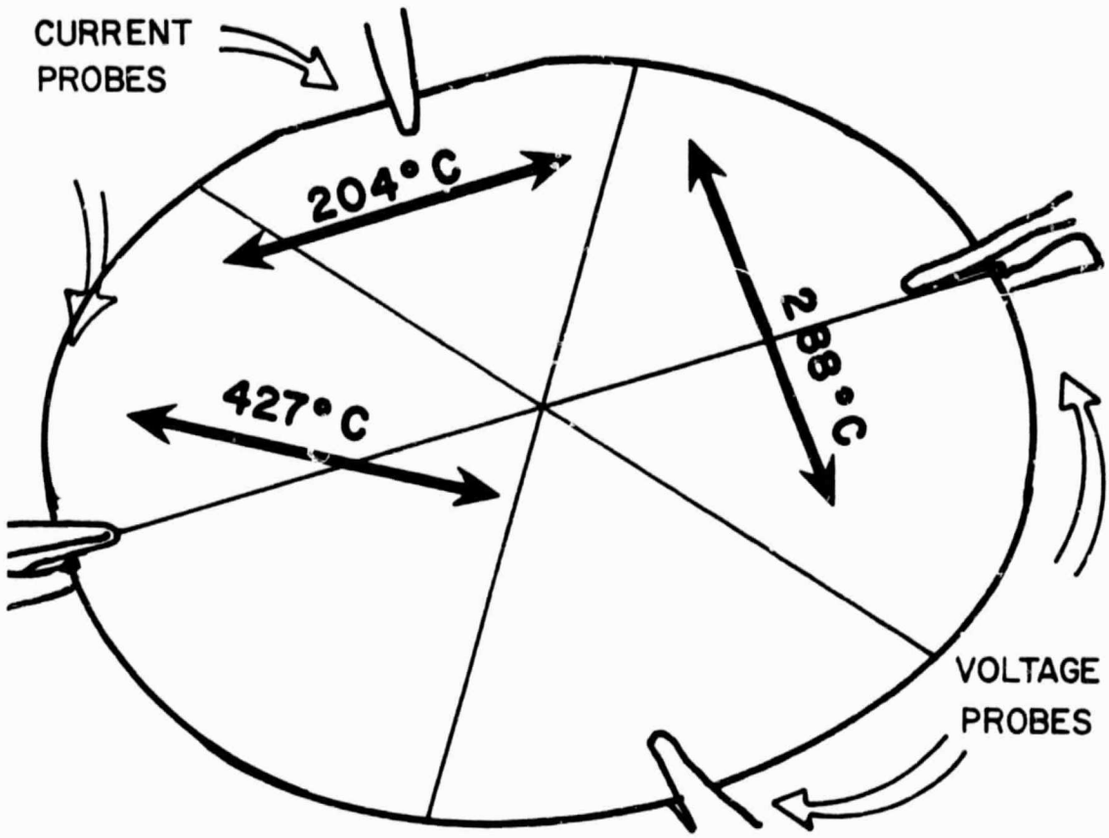

Figure 2.6. Temperature Sensing Grid Geometry.

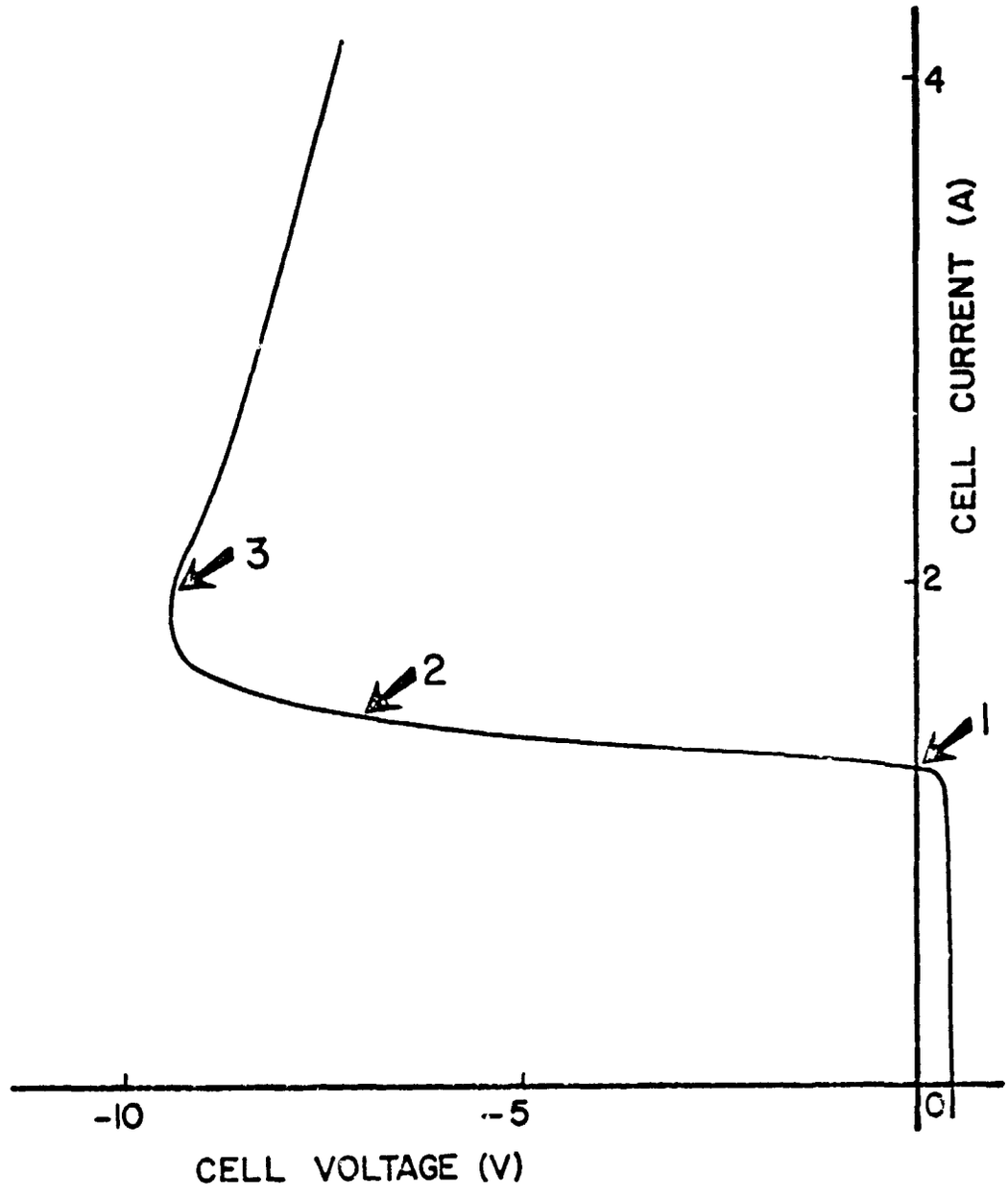

Figure 2.7. Second Quadrant Characteristics of Gridded Cell.

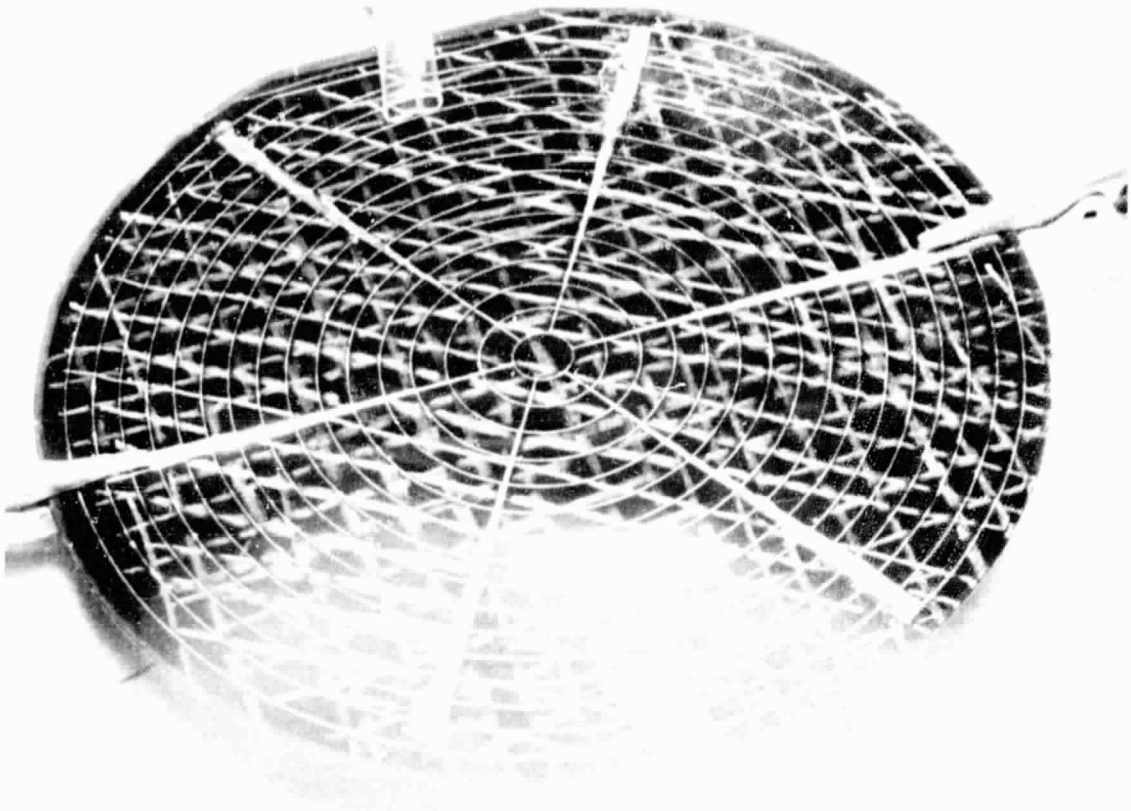

Figure 2.8. Photograph of Gridded Cell Taken at Point 1 of Figure 2.7.

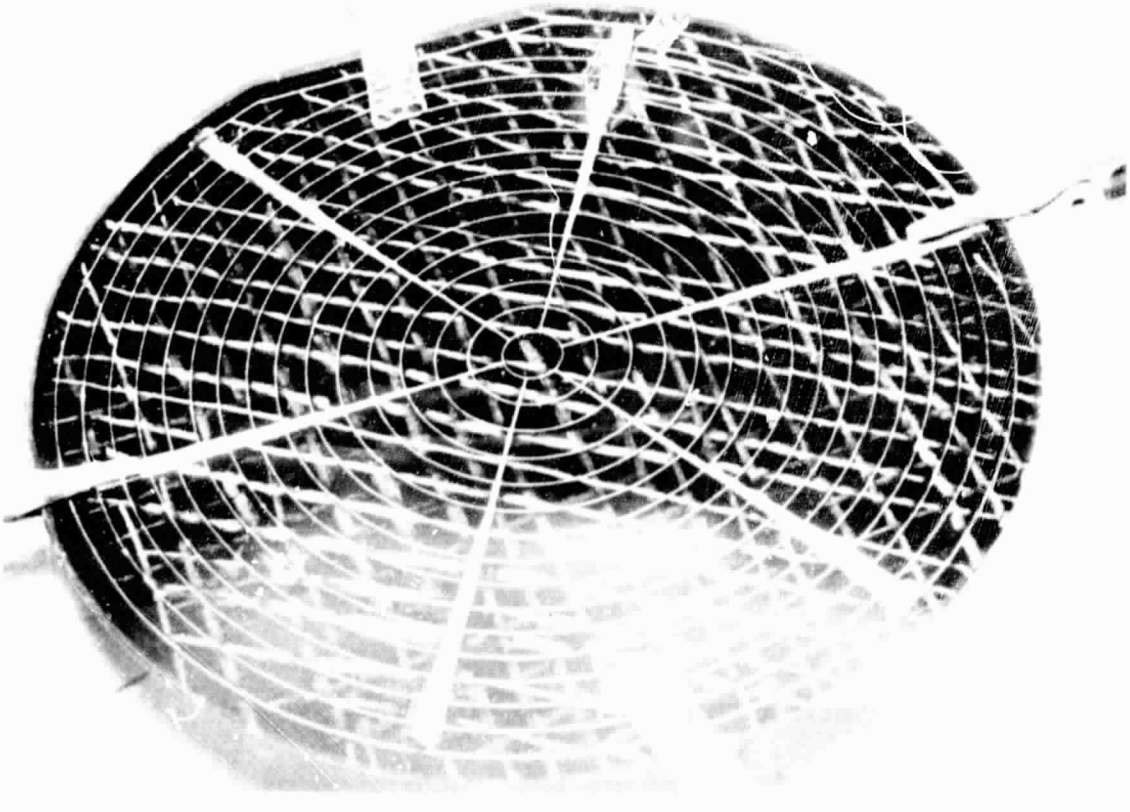

Figure 2.9. Photograph of Gridded Cell Taken at Point 2 of Figure 2.7.

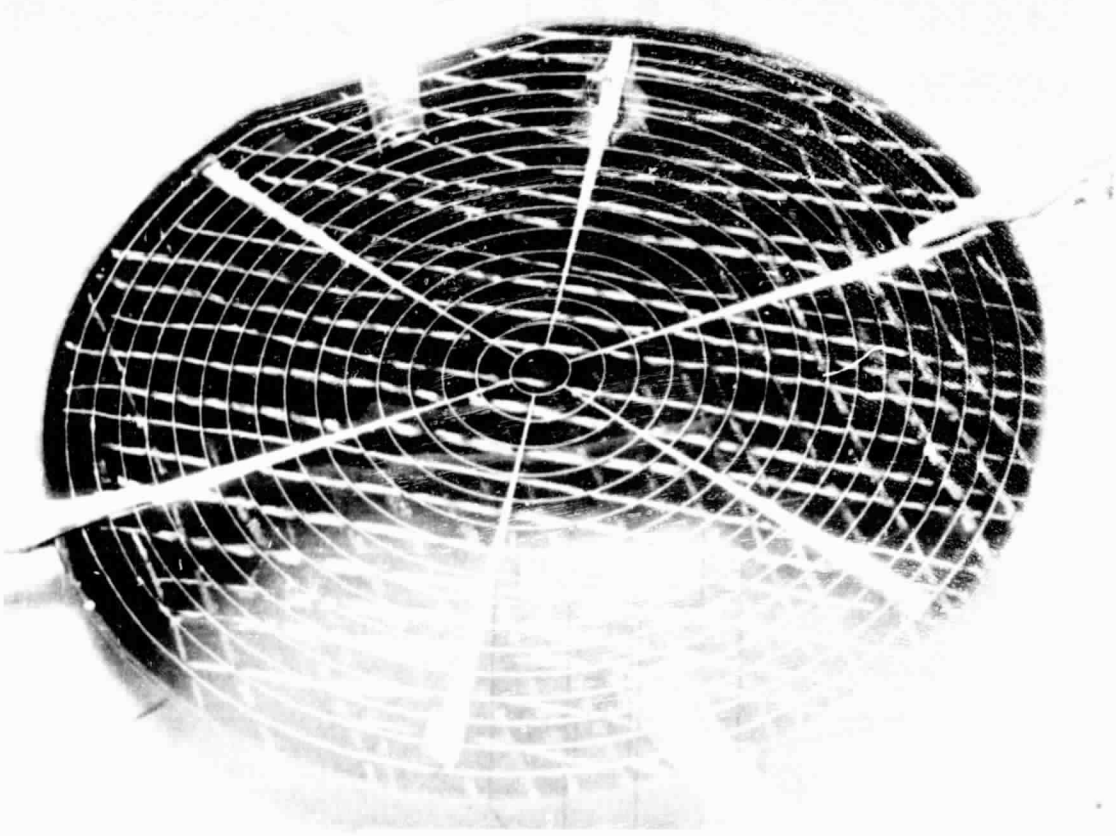

Figure 2.10. Photograph of Gridded Cell Taken at Point 3 of Figure 2.7.

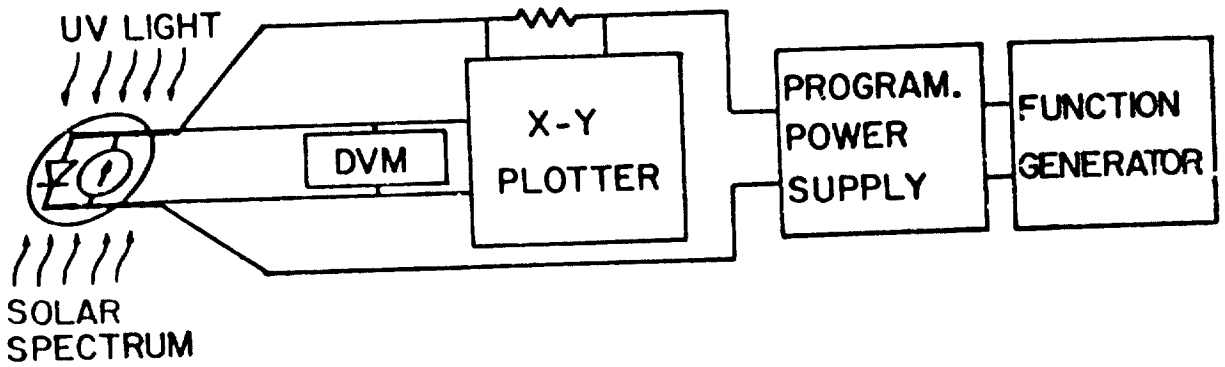

Figure 2.11. Phosphor Decoration Measurement System.

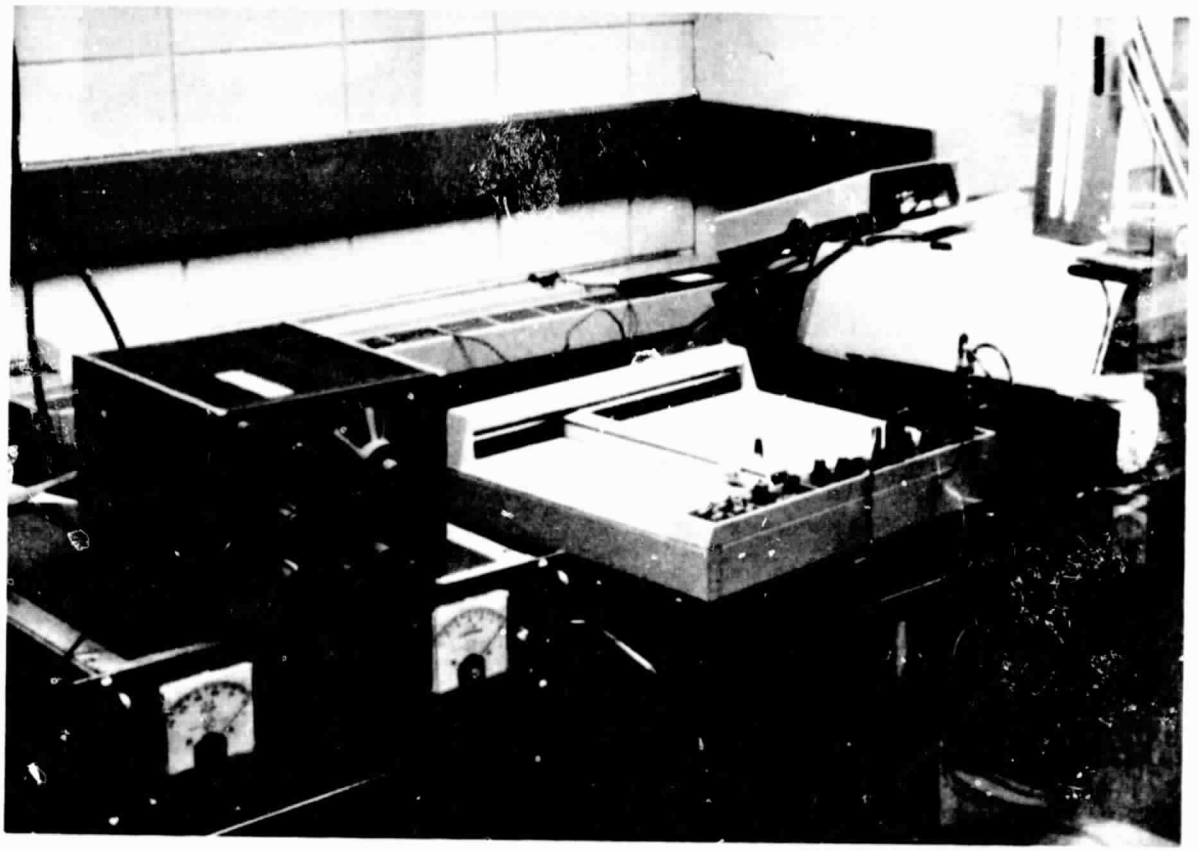

Figure 2.12. Photograph of Phosphor Decoration Temperature Measuring System.

1

2

3

4

Figure 2.13. Photographs of Phosphor Decorated Cell at Different Second Quadrant Operating Points (See Figure 2.14).

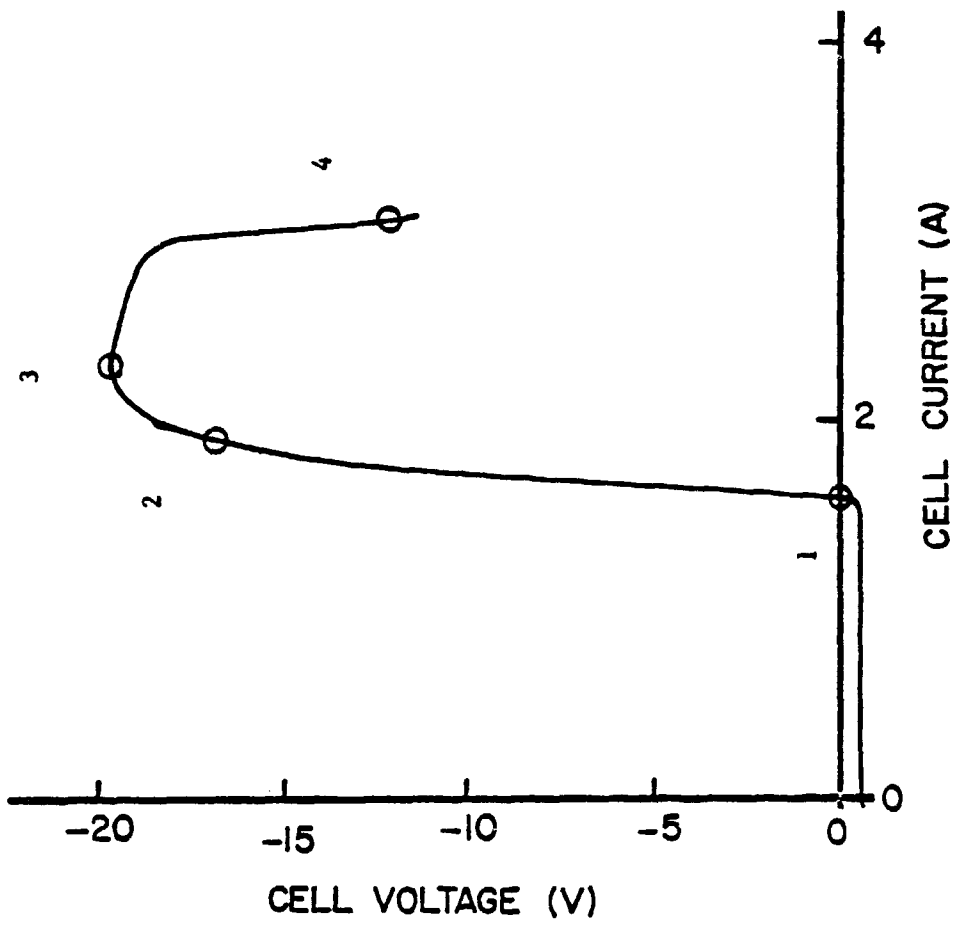

Figure 2.14. Second Quadrant Cell Characteristic Showing Points at Which Photos of Figure 2.13 were Taken.

localized mesoplasma is clearly evident from these photographs. The programmable power supply was current limited to prevent irreversible damage from occurring to the cell.

2.5 Conclusions on Second Quadrant Studies

A preliminary look at a limited number of cells has verified the thermal nature of the solar cell's second quadrant. Three operational ranges can be defined as shown by the schematic second quadrant characteristic of Figure 2.15.

Region A. In region A the temperature of the cell is less than 170°C and uniform, but much higher than when operating normally in the first quadrant. In this region the failure modes should be the same as in the first quadrant and the electrical characteristics of the cell should degrade in exactly same fashion as if the cell were on accelerated stress test in the first quadrant. Region A can be referred to as the accelerated failure mode region.

Region B. In region B the temperature is greater than 170°C (melting point of solder), but less than θ_i. In this region the temperature is also uniform (or nearly so), but the failure modes are ones not encountered in accelerated testing, such as molten solder effects, blistering and delamination of the encapsulant, and cracking of cells due to thermal mismatch. Region B can be termed the high temperatue mode region.

Region C. Finally in region C the temperature reaches θ_i in a localized region. Temperature is very non-uniform across the cell with a mesoplasma forming at a single spot. Unless externally limited in some fashion catastrophic melting will occur. Region C is termed the catastrophic mode region.

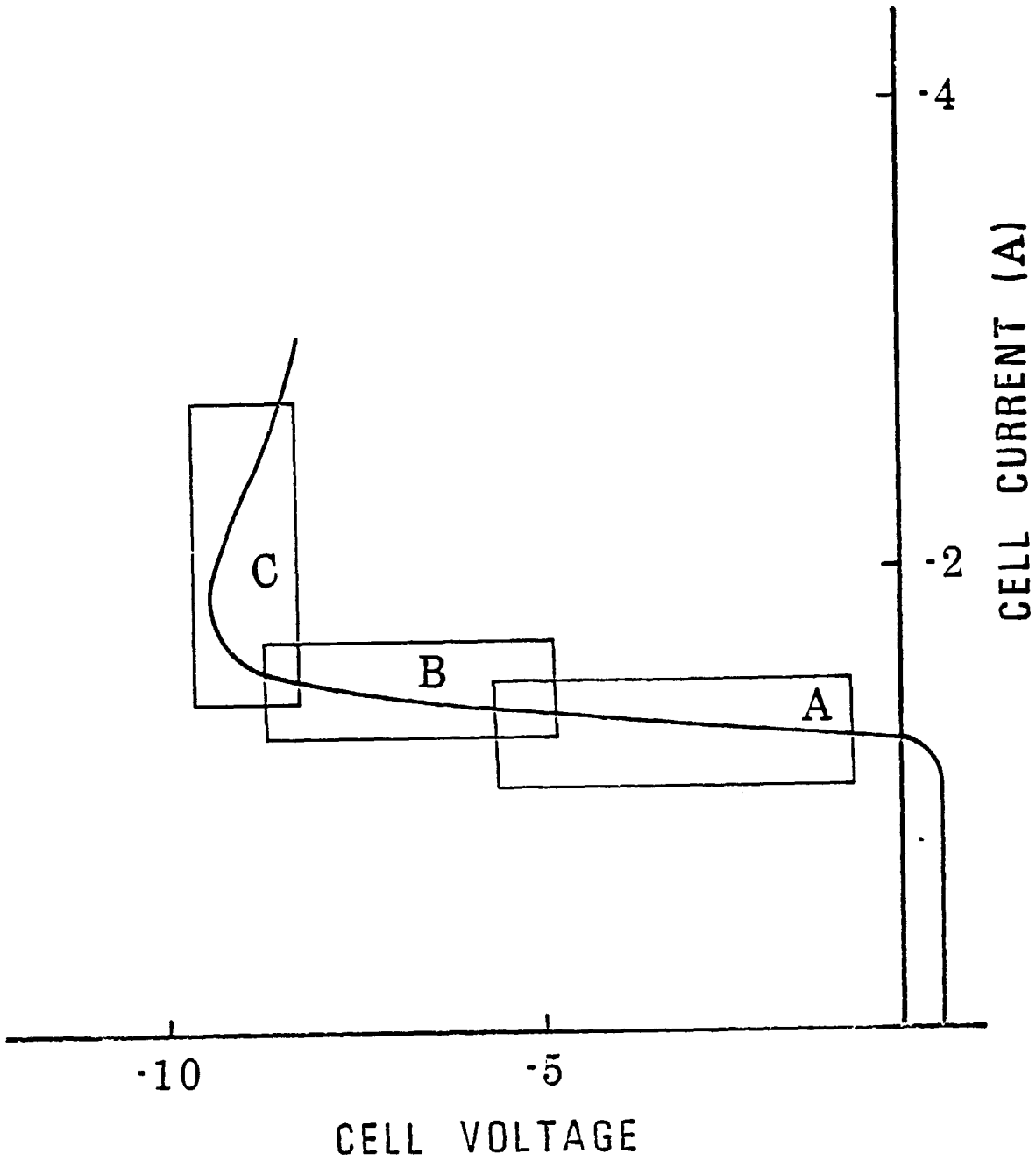

Figure 2.15. Second Quadrant Characteristics Showing Three Reliability Mode Ranges.

As defined above for steady state conditions, operation in the second quadrant is characterized by three different failure mode regions--all of which are more severe than first quadrant operation. It is obvious, however, that the lower the cell temperature, the less severe the stress. Thus cells operating in the second quadrant should be kept as far below the knee as possible. Furthermore, since the temperature at the knee is roughly θ_i, independent whether the knee occurs at low voltage or high voltage, a cell with a high breakdown should be able to survive second quadrant operation better than a cell with a low breakdown, all other characteristics being equal. This conclusion conflicts with some of the current thinking, which is based on limiting reverse power dissipation by low knee devices. The falacy is that limiting power dissipation, unless it is accomplished by a different mechanism such as a forward biased diode, does not limit temperature and it is temperature which is the reliability stress factor, not power.

3.0 ACCELERATED STRESS PROGRAM

3.0 ACCELERATED STRESS PROGRAM

3.1 Procedures

Accelerated testing was performed on three new cell types: F, G and H. The physical characteristics of these cells was shown in Table 1.1. In addition B-T testing was continued on A, B, C and E cells at 75°C and 135°C. Cells were inspected and photographed prior to testing, as described in the First Annual Report. The stress tests used in the second year's effort differed slightly from those used in the first year's program as shown in Table 3.1. The 165°C bias-temperature test was dropped becaause it was felt this temperature was too close to the melting point of solder. The power cycle test was also dropped because it had failed to show any effect when applied to the A, B, C and E cells in the first year program. Two additional tests were added: pressure cooker and 85/85 without bias, in an attempt to determine if bias was of any significance in temperature-humidity stressing. The mechanical pull strength tests performed on selected A, B, C and E type cells, have not yet been performed on the E, G and H type cells. An additional factor to be noted is that the quantity of cells available for the second year's program was less than for the first year's program. The specific numbers and a discussion of their significance will be given in Section 5.

3.2 Stress Test Fixturing

One major change in the accelerated test procedures was a change in the method of supporting and contacting cells during bias-temperature testing. The reader will recall that in the first year program miniature alligator chips were used to suspend and interconnect cells in both B-T and B-T-H chambers. This technique, while inexpensive, had many disadvantages, parti-

Lot # 1st Year (A,B,C,D)	Lot # 2nd Year (F,G,H)	Stress Test
10	10	75°C Bias - Temerature
11	11	135°C Bias - Temperature
12	12	150°C Bias - Temperature
13	--	165°C Bias - Temperature
14	14	121°C/15 Psig Steam Bias - Temp - Humidity
--	19	121°C/15 Psig Steam Temperature - Humidity
15	15	85°C/85%RH Bias - Temp - Humidity
--	20	85°C/85%RH Temperature - Humidity
16	--	Power Cycle
17	17	Thermal Cycle
18	18	Thermal Shock

Table 3.1 Stress Test and Lot Identification for First and Second Year Programs

cularly for B-T testing where the number of cells was large and oven capacity limited. In order to overcome these jigging problems a new cell test holder was developed. Specific advantages of the new design are:

1. Elimination of stress applied to cell tabs and tab attachment points.
2. Greatly reduced loading and unloading times.
3. Elimination of the need to locate shorted cells after loading.
4. Increased interconnection flexibility.
5. Increasing packing density while maintaining comparable air flow over cells.

An exploded view of the new-design cell holder is shown in Figure 3.1. Figure 3.2 shows a photograph of the test holder being loaded. The frame consists of vertical metal rods covered with insulating teflon tubing and a stablizing bottom plate. Series connection of cells is achieved through the use of convoluted beryllium-copper springs which connect the top surface lead pattern of one cell to the bottom of the overhead plate, which is in turn directly connect to the back of the next cell, and so on. As used in the B-T stress tests a completed "stack" consists of 3 parallel connected sets of cells; each set is in turn composed of 5 serially connected cells. Insulation of one set from the other is achieved through an insulating glass spacer between the top plate of one set and the bottom plate of the next. Additional insulation of cell leads is performed through the use of teflon adhesive tape. Tightening of the top nuts compresses the stack and ensures good electrical connection.

All jig materials were chosen for reliable performance at elevated temperatures. The spring metal was made of beryllium-copper which retains

its springiness, electrical conductivity and stability to temperatures of 175°C -- well above the highest test temperature of 150°C. Preliminary tests showed tarnishing of the beryllium-copper, but this does not seem to affect the alloy's performance. The plates were made of 30 mil stainless steel to ensure good electrical conductivity, stability and rigidity allowing each plate to support the column of plates and cells above it without bending, thus reducing the stress on the cells.

No difficulties have been encountered with the new jigs and the design appears ideal for B-T stress testing. It has not been usd in B-T-H testing where cell quantities are smaller and the miniature alligator clip technique has worked satisfactorily.

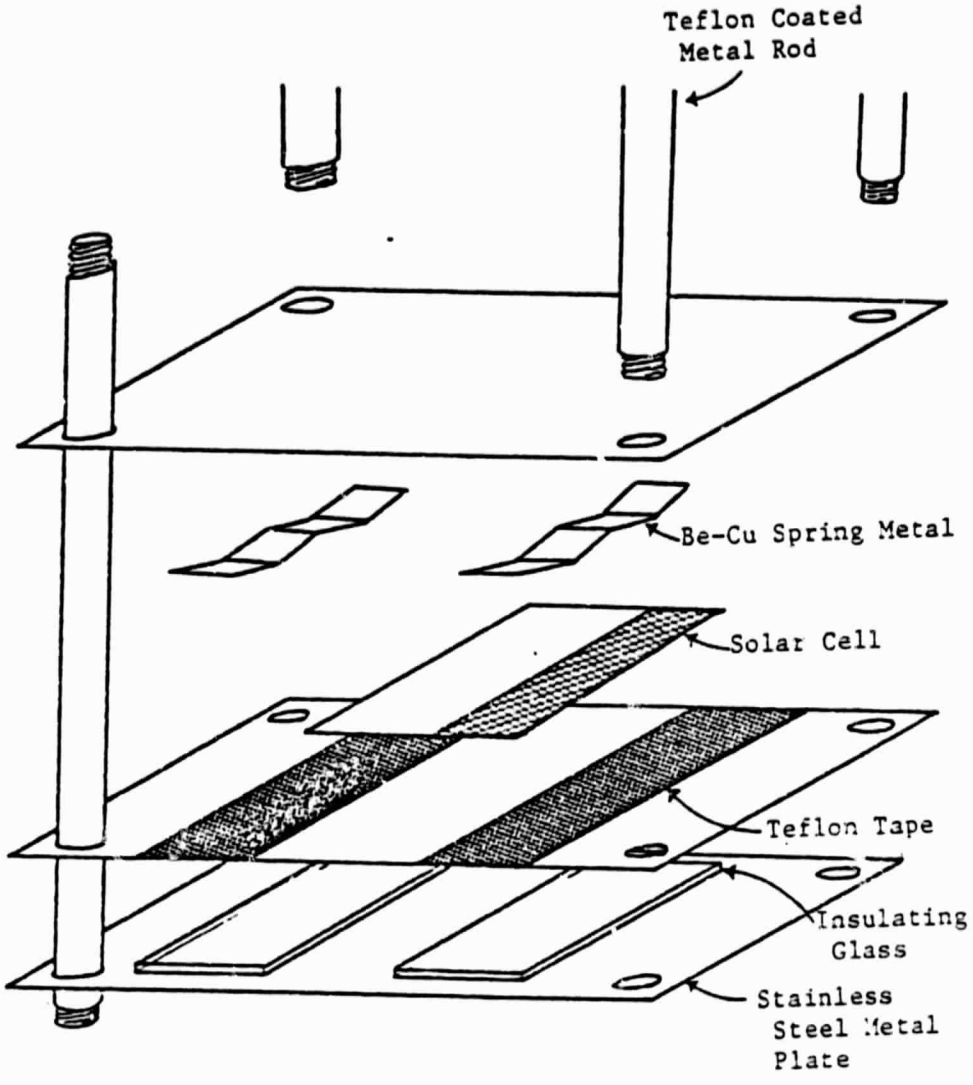

Figure 3.1. Schematic Exploded View of New-Design Stress Testing Jig.

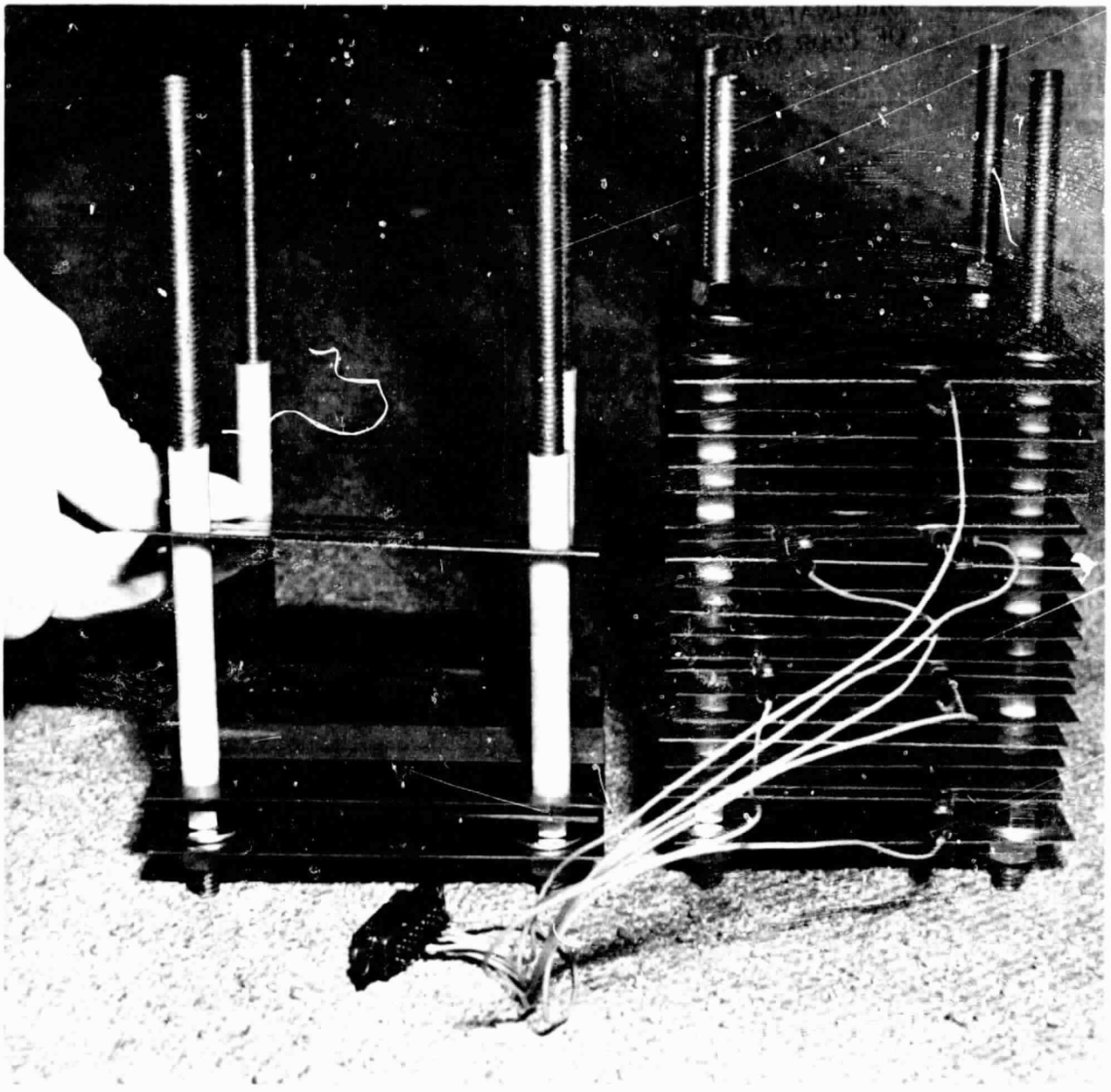

Figure 3.2. Photograph of New-Design Stress Testing Jig Being Loaded.

4.0 MEASUREMENT TECHNIQUES

4.0 MEASUREMENT TECHNIQUES

4.1 General

Reliability testing involves repeated sequences of electrical measurement, followed by stress, followed by electrical measurement. Comparison of before and after measurements are used to detect the irreversible changes brought about by stressing. Since these changes may be small, an accurate and highly reproducible measurement system is required in order to distinguish between random errors and effects brought about by stress. Since the "after" measurements may be taken weeks or even months after the "before" measurements, the repeatability requirement is particularly severe. The measurement technique used in the second year of the program was the equilibrium method, which was developed in the first year of the program and reported in detail in the First Annual Report. This method, which is capable of $\pm$ 1% repeatability, requires a fairly long measurement time during which the cell temperature must be held constant at 28 $\pm$ 0.5°C. The cells are held down to a water cooled heat sink by air pressure (vacuum holddown) and contacted on the back side by a spring loaded thermocouple. The temperature of the cooling water is adjusted until a temperature balance is achieved between the heat coming from the ELH simulator and that being removed by the heat sink, so that an equilibrium cell temperature of 28 $\pm$ 0.5°C is achieved. With flat cells, which make uniform contact with the heat sink, each cell will reach the same temperature as other cells and the temperature only needs to be adjusted once for each cell type. However, this is not the case if the cell surface is irregular as shown schematically in Figure 4.1. In this case, not only does the heat removed by the sink vary from cell to cell because of the variable contact area, but there is also an undetermined

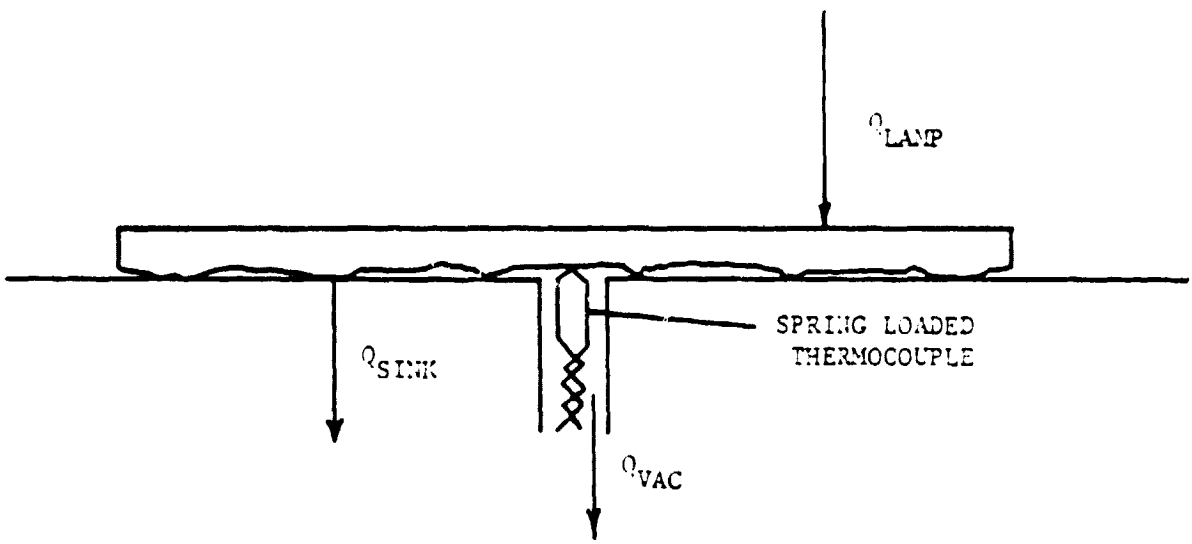

Figure 4.1. Heat Flows in Cell Measurement Jig.

amount lost by air leakage across the back into the vacuum system. The F cells constructed from EFG ribbon were particularly bad in this respect. It was obvious that it was not practical to adjust the water temperature for each cell, as this would involve an impractical amount of time. The approach followed on the F, G and H cells was to experimentally determine the variation of the measurement parameters with temperature and use this information to perform a software correction on the raw date. In addition a program was initiated to develop an instrument capable of measuring a cell in less than 1 second exposure time. Such a short time would preclude the cell heating up during measurement. Additional improvements in jig and simulator design over the first year's effort are also discussed in this section.

4.2 Simulator Design

The ELH solar simulator was redesigned as shown in Figure 4.2 to make the changing of bulbs easier and to facilitate alignment of the light pattern. An elapsed time indicator was installed in the control panel so that a running record could be kept concerning bulb life. Average bulb life has been found to be approximately 60 hours. At $15 per bulb and 4 bulbs per simulator this works out to $1/hour in bulb replacement costs. The new bulb mounts incorporated a 3-point adjustment mechanism which permitted each bulb to be independently tilted. The intent was to achieve a more constant profile over the cell area. In actuality, however, tilting the bulbs appeared to have only limited effect on the profile, probably due to the long reflective barrel. Nevertheless, a completely satisfactory profile was achieved, with a maximum variation of $\pm$ 2.5% across the cell field. Furthermore, this intensity variation was obtained without the use of a diffuser such as was used on the A, B, C and E cells.

Figure 4.2. Improved Arrangement of Bulbs in New Light Source.

4.3 Measurement Jig Design

The electrical measurement jigs were redesigned, for testing F, G and H cells, to use a common vacuum chamber with individual water cooling contacting plates for each cell type. Figure 4.3 is a photograph of the jig assembly for the rectangular F-cell, Figure 4.4 is a photograph of the jig assembly for the round G-cell, and Figure 4.5 is a photograph of the square H cell jig. As with the earlier jigs these incorporate a spring loaded thermocouple/voltage probe. Also built into each jig was a photodiode (Motorola MRD-510) which was used to continously monitor light intensity. The light intensity was originally set as discussed in earlier reports (see Second Quarterly Report, August 1, 1978, p.12) using a reference cell and a standard cell. Since reference cells were not supplied with any of the new cell types, the cell type B reference cell was arbitrarily used for all. One cell from each of the three new test populations was set aside and designated as a standard cell. It was measured prior to measuring any group of cells and the data served as a check on the system's calibration. The photodiode was monitored between measurements, and if changes were observed the standard cell was remeasured. This technique avoided any problem of lamp drift. The photodiode, being in reality a miniature solar cell is itself a function of temperature. Its output was made insensitive to temperature, however, by heat sinking to the jug (constant temperature water bath) and by proper choice of the diode load resistor value.

Type G cells presented a unique jig design problem since they were received from the manufacturer without suitable test tabs. A Kapton® coated copper sheet had been soldered to the metalized contact pattern at 6 points, around the periphery of the cell, but could not be used for electrical

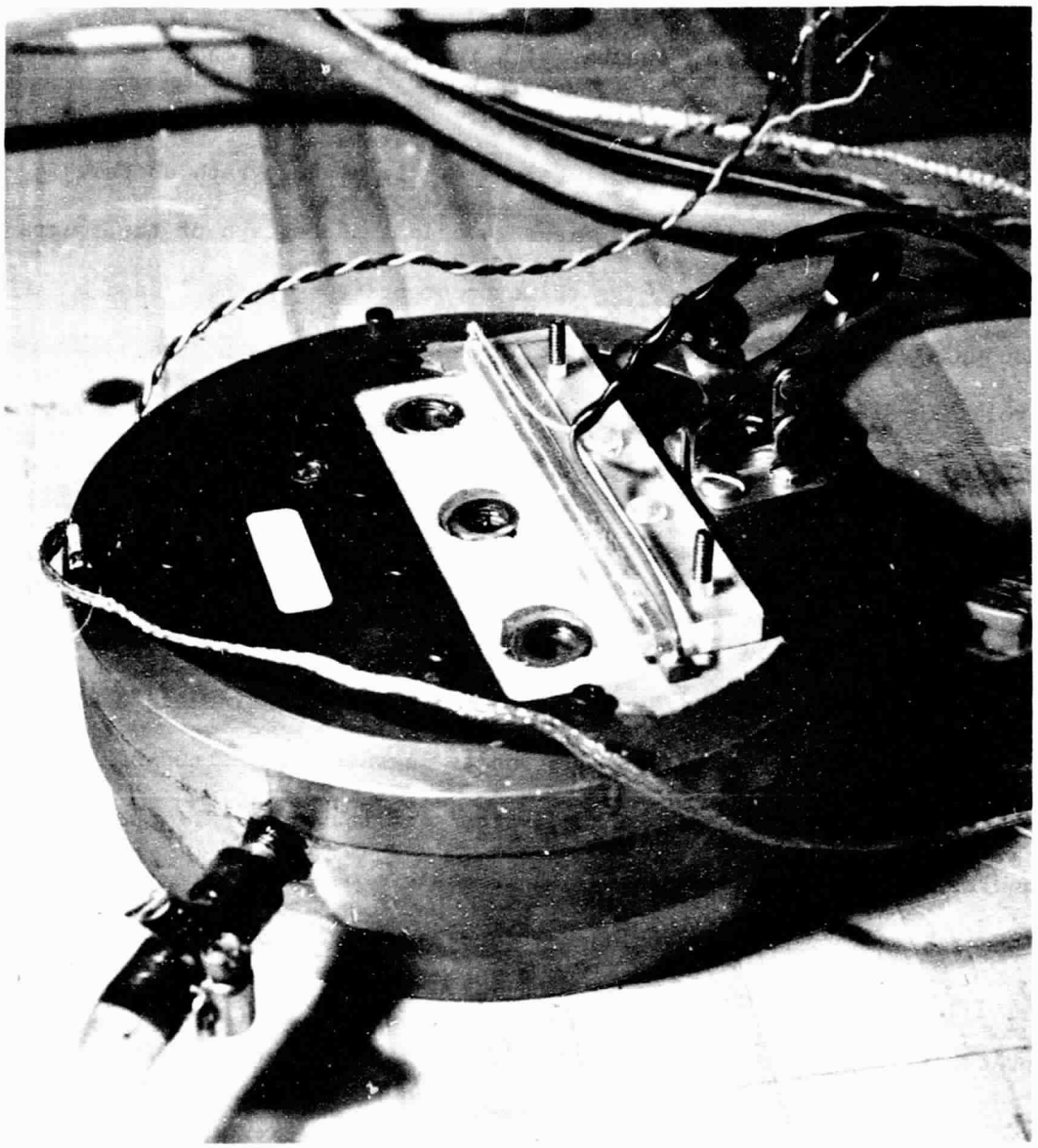

Figure 4.3. Type F Cell Electrical Measurement Jig.

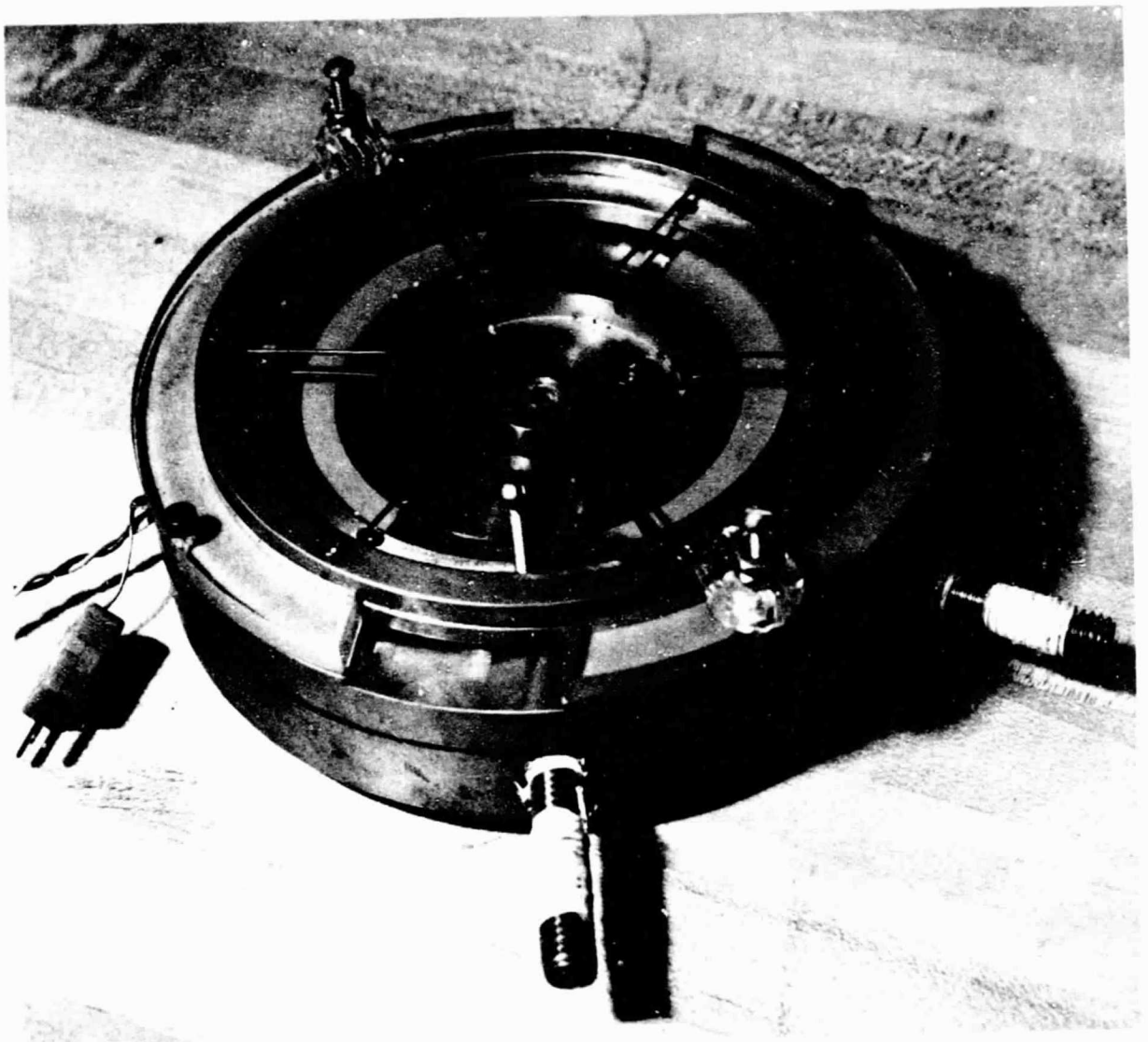

Figure 4.4. Type G Cell Electrical Measurement Jig.

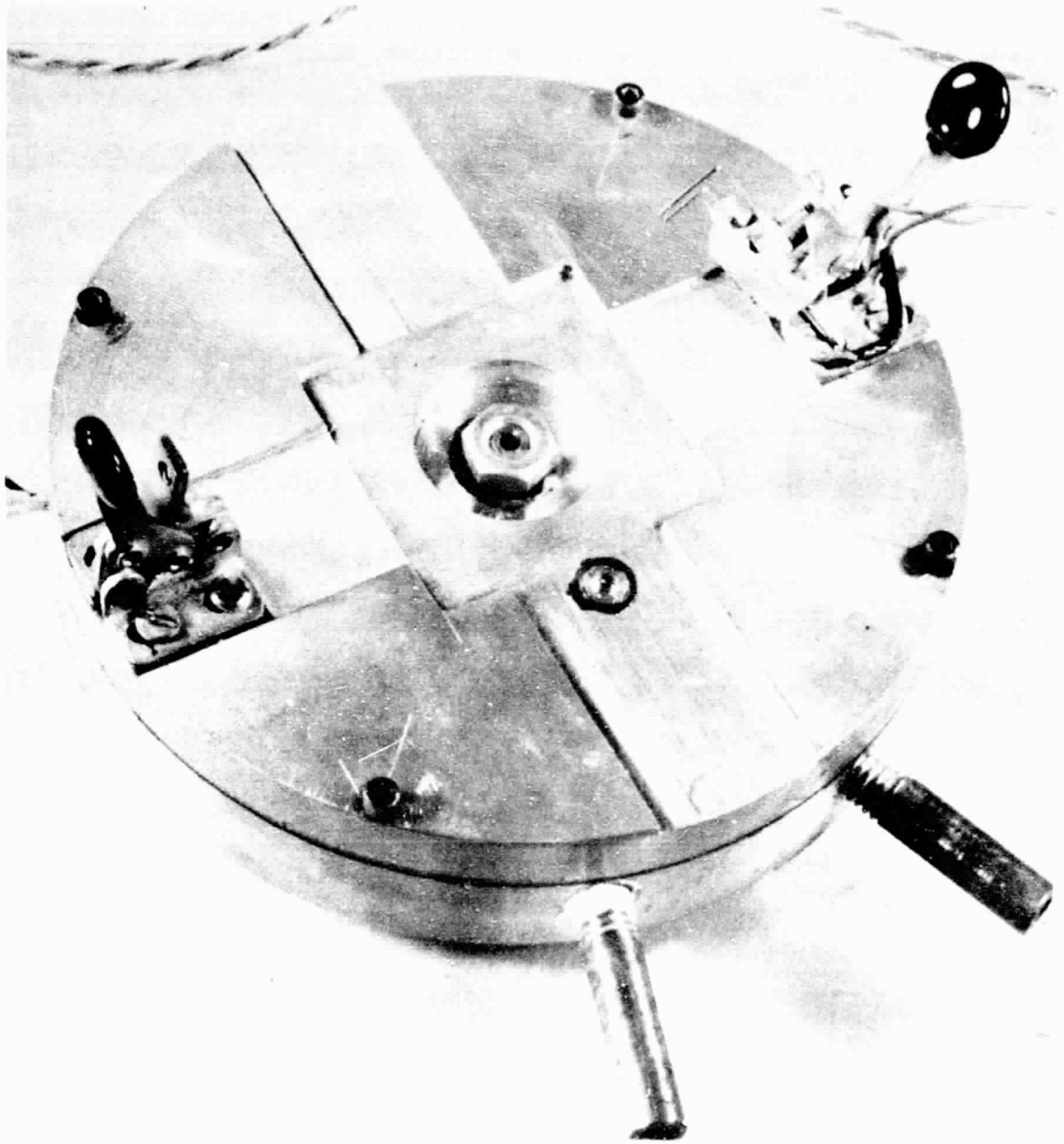

Figure 4.5. Type H Cell Measurement Jig.

connection. The copper sheet was therefore removed by cutting (no heat or force was used) and electrical test connections were made using probes rather than older connections. Since in the manufacturing process the cell had been solder dipped with subsequent reflow, the back side was generally irregular except in the center where the solder coating was relatively smooth (see Figure 4.6). Consequently, in the electrical measurement jig design the vacuum hold down was restricted to this smooth central region, but the cell periphery was allowed to rest on the jig as well for additional heat removal.

Contact to the top surface metalization of the G cells was via 6 pairs of voltage and current probes. All voltage probes were connected together as were all current probes, but the two sets were insulated from each other and separate connections brought out. The current probes were located closest to the outside of the cell. The probes could be easily and quickly aligned by eye and the cells were placed in the jig the same way each time using the flat for orientation. Reproducibility was satisfactory, but not as good as tabbed cells. Because of the G cell dimensions the photodiode incorporated in the jig was covered during cell testing, but was used to monitor lamp intensity between tests.

4.4 Variation of parameters with Temperature

As has been pointed out, lack of cell flatness made it impractical to measure each cell at the same temperature. Consequently, the temperature of each cell was allowed to stabilize at its unique value during measurement. This value was recorded and used to calculate the parametric values at 28°C. The distribution of cells shown in Figure 4.7 gives an indication of the

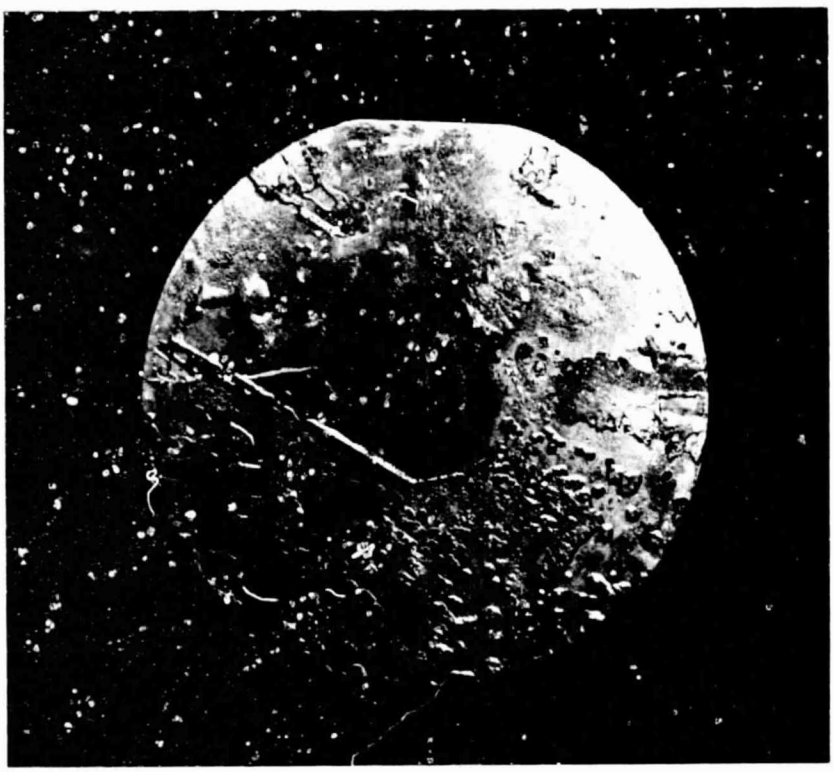

Figure 4.6. Back Side of Typical Type G Cell Showing Solder Irregularities.

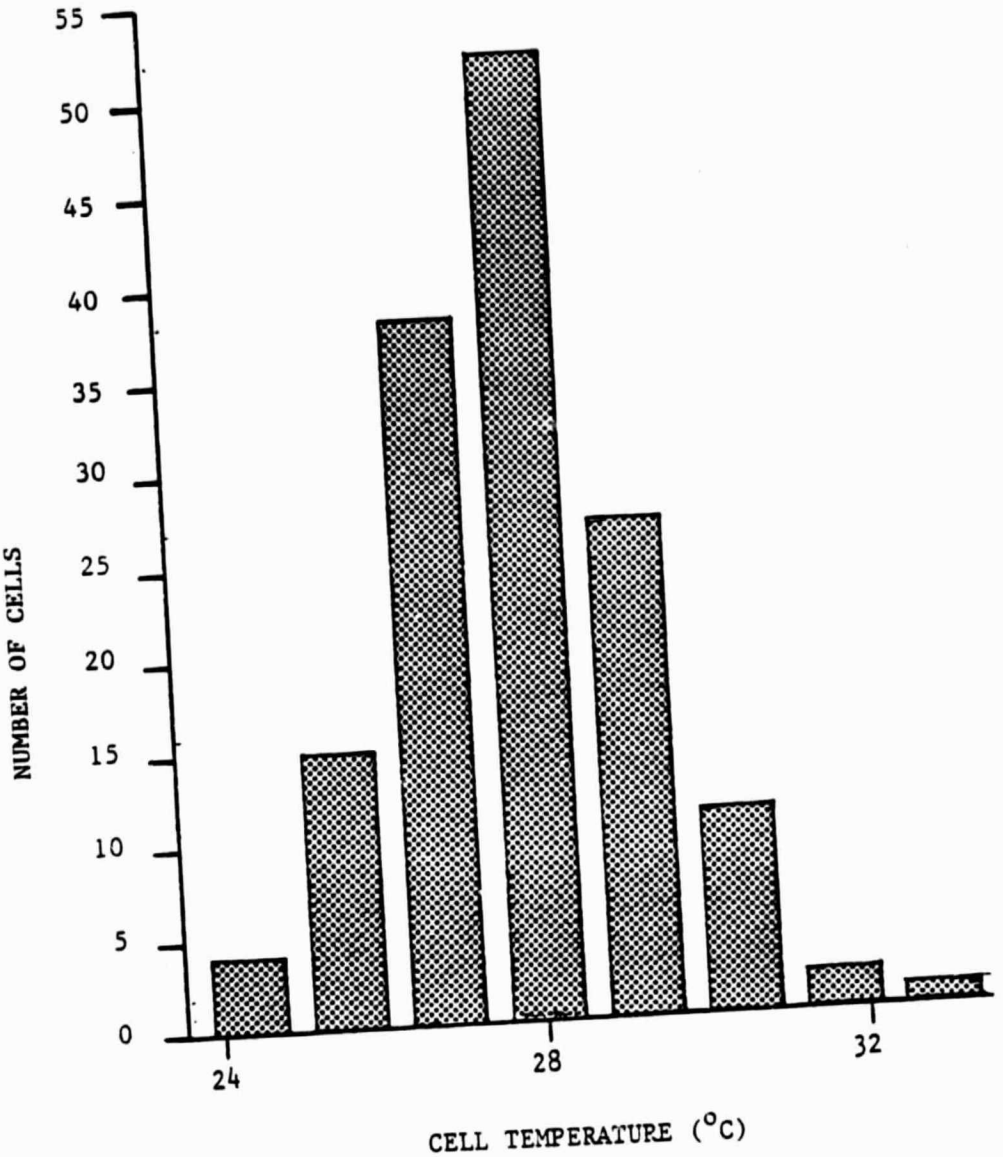

Figure 4.7. Type F Cell Temperature Distribution Under Electrical Measurement Conditions, Water Bath Temperature 26°C.

temperature vairation that was observed during measurement. In order to determine the appropriate correction factors to apply, 5 cells of each type were measured over a temperature range from 20°C to 45°C. Although absolute values of V_{OC} , I_{SC} , and P_M varied from cell to cell, each cell within a given cell type showed the same parametric variation with temperature. Typical curves for the three cell types are shown in Appendix B. A summary of the 5 cell sample, least squares fitted, averages is given in Table 4.1 for the 3 cell types studied during the second year's effort as well as for B and E cells measured during the first year's program. Note the 3 to 1 variation in I_{SC} sensitivity between cell types, and the fact that the temperature sensitivity of V_{OC} and I_{SC} apparently has little to do with the sensitivity of P_M to temperature. The values listed in Table 4.1 were used in the following formulas to determine the parametric values at 28°C:

$$V_{OC}\ (28°) = V_{OC}\ (T) - \frac{\Delta V_{OC}}{\Delta T}\ (T-28°)$$

$$I_{SC}\ (28°) = I_{SC}\ (T) - \frac{\Delta I_{SC}}{\Delta T}\ (T - 28°)$$

$$P_M\ (28°) = P_M\ (T) - \frac{\Delta P_M}{\Delta T}\ (T - 28°)$$

where T is the equilibrium temperature of the cell during measurement, expressed in °C.

4.5 Development of Microprocessor Controlled Solar Cell Tester

The temperature correction of data, as discussed in the previous section, does introduce an additional source of repeatability variation. In addition, it would be difficult to measure encapsulated cells, or cells which could not be conveniently heat sunk, using the equilibrium method. For these

Cell Type	$\frac{\Delta V_{oc}}{\Delta T}$ (mV/°C)	$\frac{\Delta I_{sc}}{\Delta T}$ (mA/°C)	$\frac{\Delta P_m}{\Delta T}$ (mW/°C)
B	-2.3	.8	-2.65
E	-2.0	1.7	-1.82
F	-2.45	.639	-0.962
G	-2.16	.537	-2.92
H	-2.28	.988	-0.737

Table 4.1 Parametric Temperature Sensitivity for Various Cell Types

reasons a short interval tester was carried through conceptual design during the second year program, with the goal of subsequent fabrication. Conceptually a short interval tester lies between an equilibrium tester and a flash tester of the type used for modules. The short interval tester keeps the simulator on continously for stability, but exposes the cells for less than a second, using a shutter, so that the temperature rise can be ignored. A block diagram of the short interval tester is shown in Figure 4.8. The power supply is an analog programmable supply which need not be reversible in current, but must be capable of both + and - voltage operation. This dual polarity is required for an accurate reading of short circuit current and to take data in the second quadrant. In general, however, because of limitations on the supply voltage the short interval tester has not been designed to appreciably reverse bias cells. As has been pointed out in Sction 2.0 on second quadrant studies, however, reverse breakdown in solar cells is a thermal phenomenon and therefore should be measured under equilibrium conditions. Thus second quadrant characteristics can not be meaningfully measured using a short interval tester, whereas the effect on the first quadrant characteristic of the cell's power dissipation can be ignored. Since the supply must be capable of supplying the short circuit current of the largest cell to be tested it must have at least a 2A rating. The power supply controller is essentially a very accurate D/A converter which interfaces between the computer and the power supply.

Internal operation of the system is as follows: The microcomputer, using a stored program, sets the power supply to a specific current value. The data acquisition board makes successive measurements of the cell voltage as a function of time. The microcomputer compares succeeding values and

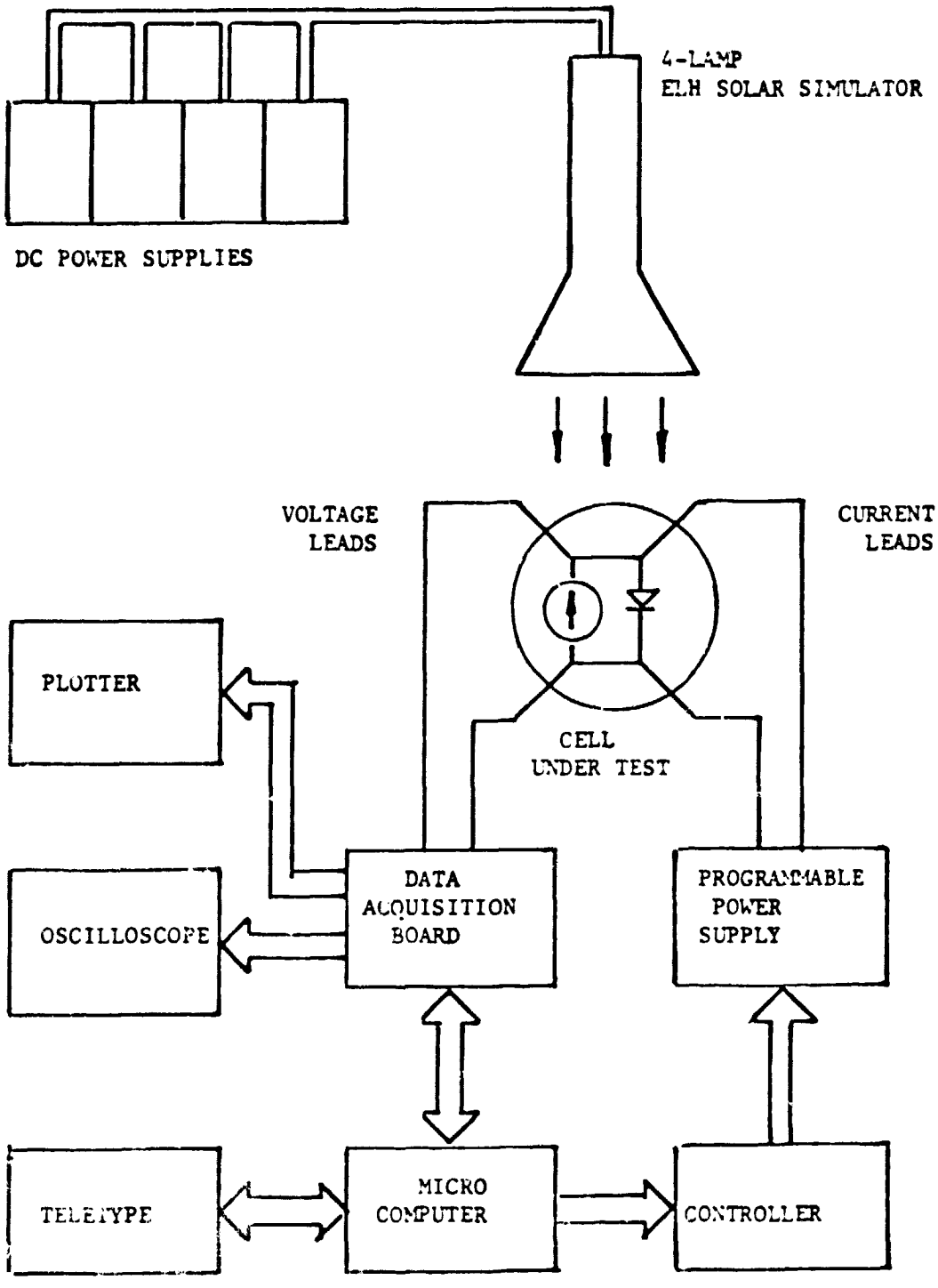

Figure 4.8. Microcomputer Controlled Short Interval Solar Cell Tester.

when no change is detected from one reading to the next it recognizes that the steady state value has been reached and then stores this reading in memory together with the current reading. Note that because of the highly accurate controller it is not necessary to measure current, only set it. Once a reading has been stored the computer advances the power supply to a new current setting and the process repeats itself until the entire V-I characteristic has been determined and stored in memory. The microcomputer then computes the maximum power point and the slopes of the characteristic curve at I_{SC} (measure of shunt resistance) and at V_{OC} (measure of series resistance).

Externally the measurement sequence is initiated by typing the cell indentification number on the teletype and pressing a selected key. This opens the shutter, exposing the cell to the ELH simulator, starting the measurement sequence just described. At the conclusion of the test the microcomputer outputs to the teletype the measured values of V_{OC} , I_{SC} , V_M , I_M , P_M , R_{SH} , and R_S as well as the ambient temperature measured independently using a thermocouple. The entire characteristic is simultaneously displayed on an oscilloscope or other monitor. If hard copy is desired, a command can be entered on the teletype and the characteristic plotted on the analog plotter. Both plotter and scope presentations make use of the D/A converters on the data acquisition board. It is intended that in addition to a printed record the teletype will produce a punched paper tape of the data which can be translated directly to punched cards suitable for IBM 370 processing without further human intervention.

Because of the short measurement time it is necessary to operate the ELH simulator lamps on DC voltage. This has been confirmed by observing the

ripple using an oscilloscope when the lamps are operated on AC. Since measurements can be taken at rates as high as 20 KHz this ripple would make accurate readings impossible. Use of DC lamp supplies does not require a separate line regulator, however.

5.0 CONTINUING STRESS TEST RESULTS - A, B, C, E TYPE CELLS

Page intentionally left blank

5.0 Continuing Stress Test Results - A, B, C, E Type Cells

5.1 Introduction

A, B, C and E type cells were subjected to various stress combinations during the first year's program and the results reported in the First Annual Report. Two tests, 75°C and 135°C B-T, were continued for 50 cells of each cell type during the second year program in order to obtain nearly 9000 cumulative test hours at these temperatures.

5.2 B-T Stress Test Results

The results obtained from the long-term BT testing of type A, B, C and E cells are shown in Figures 5.1 and 5.2. In these figures the mean percent descrease of P_m for the four cell types, calculated on a cell-by-cell basis, is shown versus stress time for the stress tests. The results confirm some results reported in the First Annual Report and help to explain some other puzzling effects noted in that work. For example, types B and C cells are seen to be unaffected by BT stress even at long times; this is in agreement with earlier results obtained using higher temperatures, in which type B cells were unaffected up to 1200 hours at 165°C and type C cells showed only very small P_m degradation up to 1200 hours at 165°C (2). Long-term results for type A cells shown in Figures 5.1 and 5.2 are consonant with results reported earlier for testing at high temperatures. These degradation results are quite significant since normal operating cell temperatures can range up to 50°C - 60°C under reasonable module field conditions. The apparent tendency toward saturation of the degradation for type A cells is actually due to a logarithmic dependence of P_m degradation on stress test time. The mechanism for the degradation shown in the figures results in series resistance increase with time, as discussed in the First Annual Report.

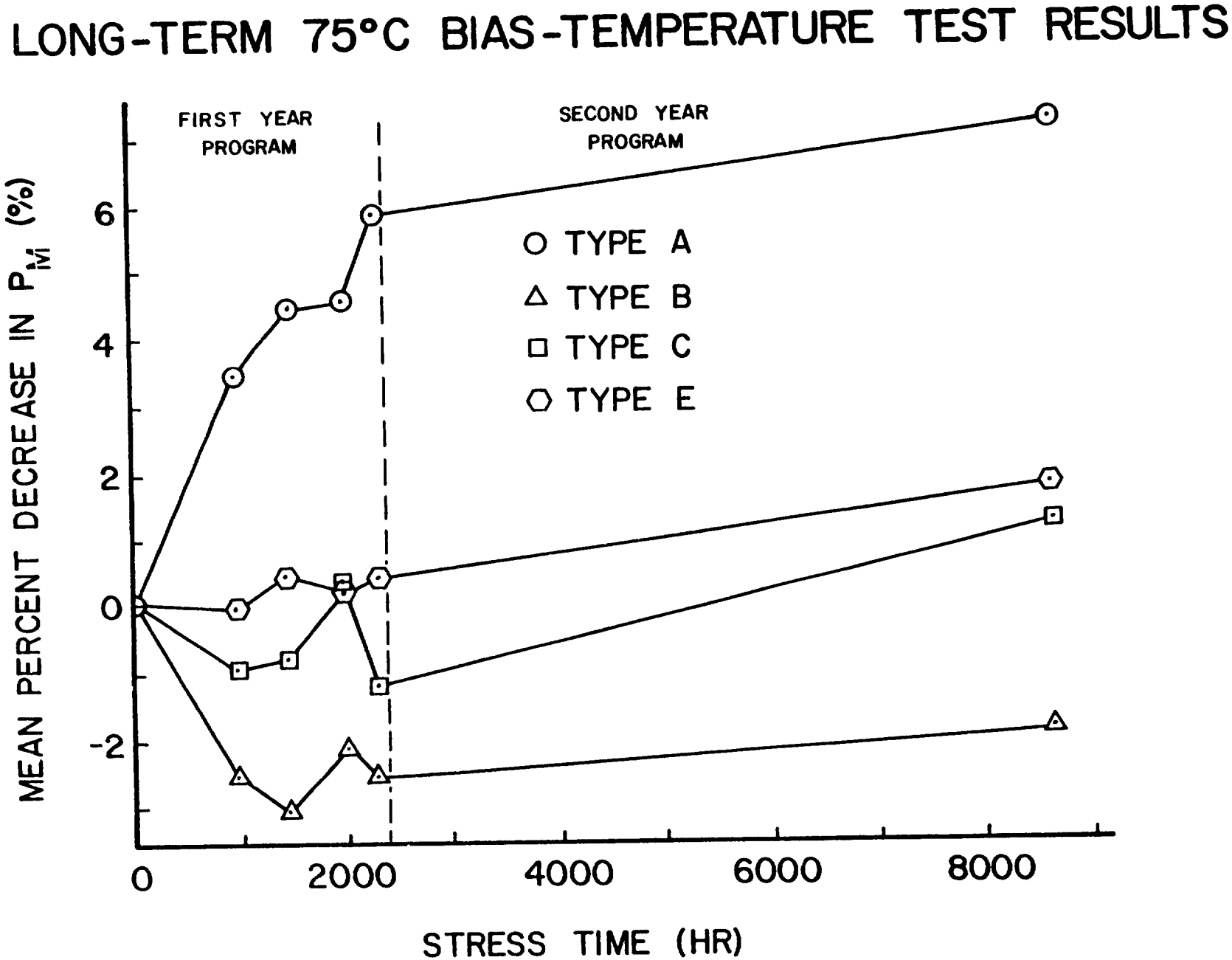

Figure 5.1. Mean Percent Decrease in P_m for 75°C B-T Stress Test, Cell Types A, B, C, and E.

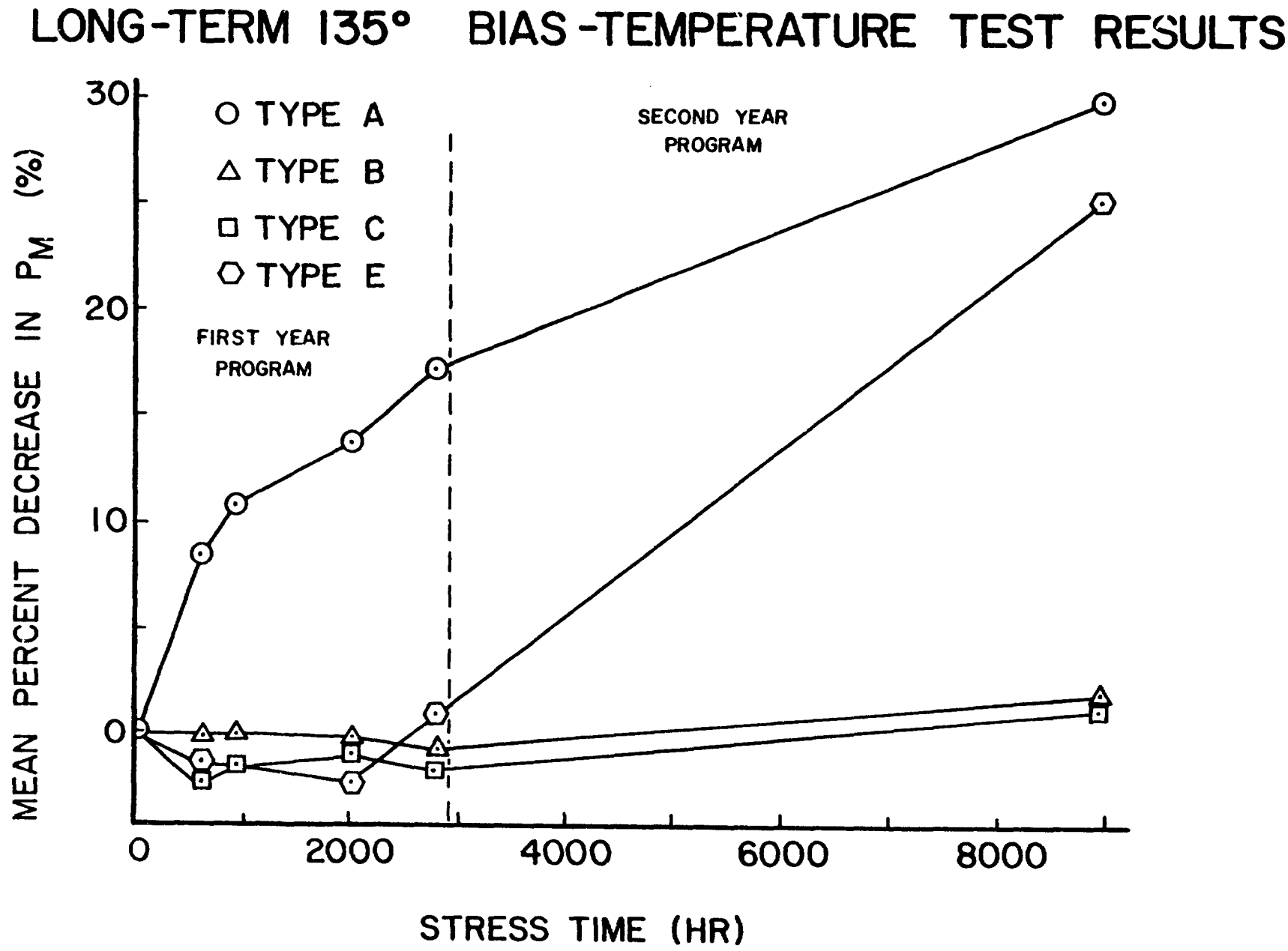

Figure 5.2. Mean Percent Decrease in P_m for 135°C B-T Stress Test, Cell Types A, B, C, and E.

The abrupt onset of degradation for type E cells shown in Figure 5.2, beginning at a time greater than 2300 hours, is of interest because the same sort of behavior was observed for this cell type under 165°C BT stress. In the higher temperature case the onset of degradation began at approximately 600 hours and amounted to 20% degradation at 1200 stress test hours. Thus, what once was observed as a puzzling phenomenon now appears to be consistent behavior for this cell type, when stressed sufficiently over time and temperature. The mechanism responsible for this behavior has not yet been identified, but some clues have been noted. The mechanism does not affect all cells equally; as seen from the P_m distributions of Figure 5.3 approximately 50% of the lot population did not degrade appreciably under stress. The other 50% of the population experienced both a decrease in mean P_m and an increase in variance. Close examination of parametric point-data and cell I-V characteristics showed that an increase in series resistance had occurred. This can be seen in the far-forward portion of the characteristic in Figure 5.4. Oxidation of the silver metalization, or metal-semiconductor contact effects, or both, are suspected as the cause(s) of this series resistance increase. Another contributor to the P_m degradation was an apparent decrease in shunt resistance R_{SH}, evident in the slope of the I-V characteristic of Figure 5.4 near V=0. Since no shunting metallic deposits were evident (none were expected) in the stress-tested cells, this effect must be due to junction degradation, or at least bulk/junction effects. Experimental results indicate that the degraded stress-tested cells showed a "photon-degradation" effect (3) much larger after stress test-induced degradation than before degradation occurred. This effect, somewhat misnamed, results in a decrease or an increase in P_m with illumination

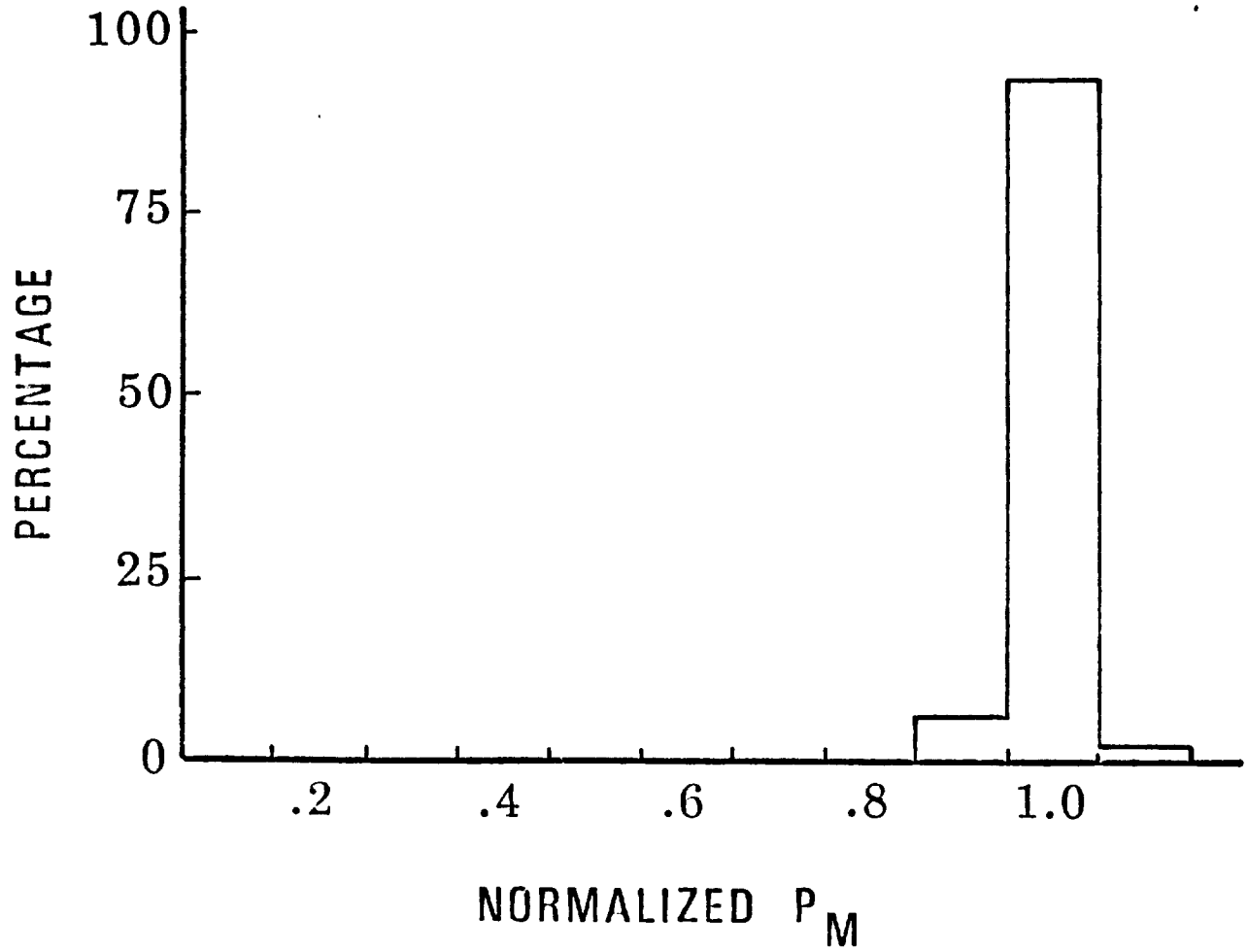

Figure 5.3. Type E Cell P_m Distributions, Prestress (a) and after 8960 Hours (b) or 135°C $^{m}_{BT}$ Stress.

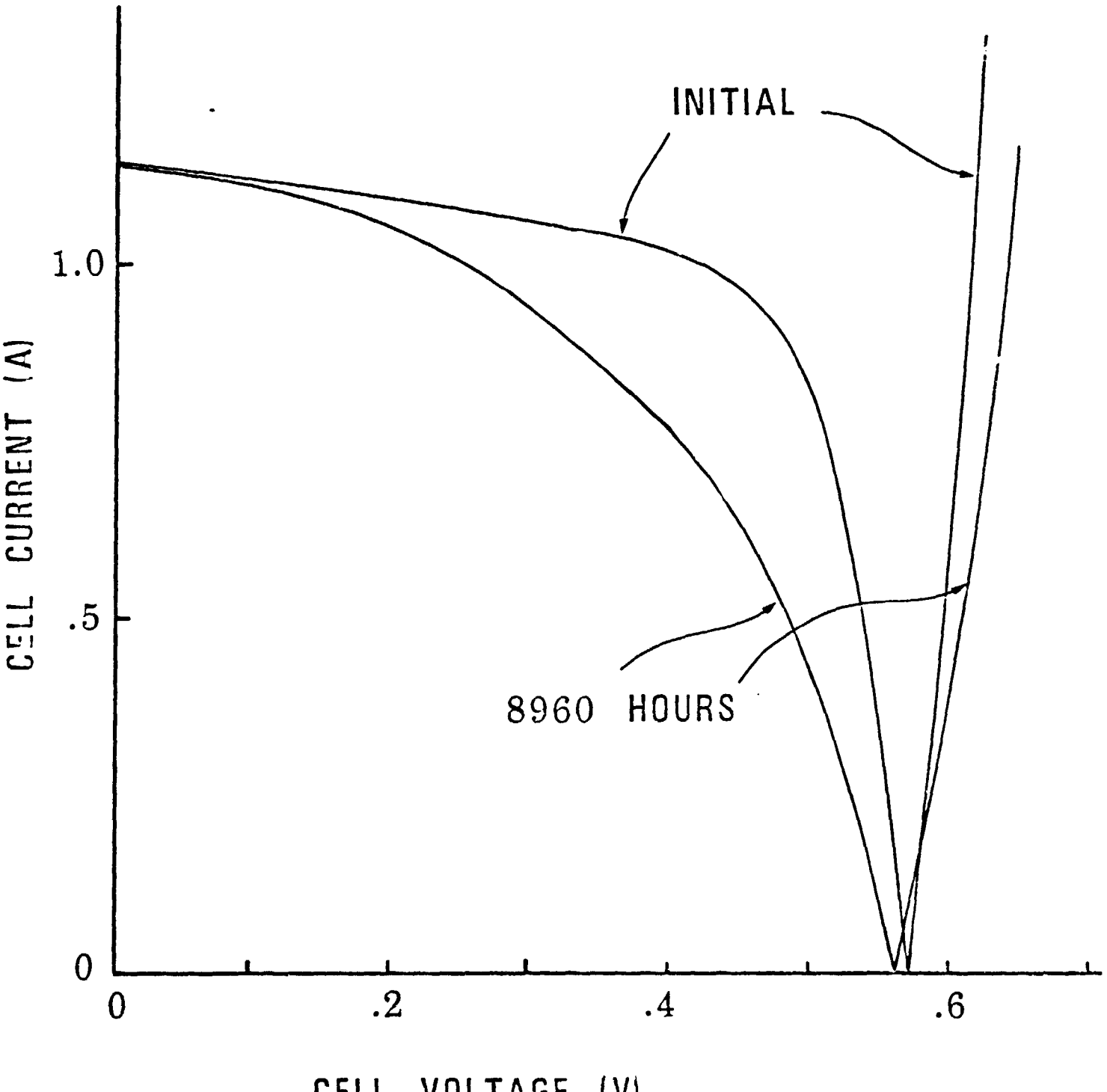

Figure 5.4. Degraded Type E Cell I-V Characteristics, Prestress and After 8960 Hours of 135°C BT Stress.

(depending on cell type) and is ill-understood even for virgin solar cells. For the case at hand, substantial but not total recovery of P_m and improvement of the apparent shunt resistance of the degraded devises was noted with increasing illumination time. It is of significance, or at least of interest, that the effect must not be surface-related since R_{SH} was decreased. Penetration of the junction region (but not junction "spiking") by heavy metal atoms and the concomitant formation of deep trapping levels is suspected as the fundmental mechanism, but the phenomenon must be investigated further.

6.0 STRESS TEST RESULTS--NEW CELL TYPES F, G AND H

Page intentionally left blank

6.0 Stress Test Results -- New Cell Types F, G and H

6.1 Introduction

A total of 437 cells of three types were subjected to accelerated stress testing in the second year's program. Table 6.1 shows the stress test schedule, and lot sizes for the various tests. Figure 6.1 shows measurement and inspection downtimes during the stress testing program.

The prestress electrical parameters of all cells intended for the stress tests were obtained and used as the basis for determining subsequent cell degradation. Tables 6.2, 6.3 and 6.4 show means and standard deviations of the prestress parameters for all cell types F, G and H, respectively. Detailed distributions of the prestress parameters are shown in Appendix A. The values shown for the parameters are those appropriate to 28°C $\pm$ 0.5°C, and 100 mW/cm^2.

Results of the accelerate stress testing will be discussed in the following section. The discussion is arranged by generic category; e.g., all B-T stress test results for all cell types are covered in a single section.

Stress Test	Type F and G Cell Quantities	Type H Cell Quantities
Forward Bias-Temperature, 75°C	30	20
Forward Bias-Temperature, 135°C	25	9
Forward Bias-Temperature, 150°C	25	9
Temperature-Humidity (Pressure Cooker)		
Forward Biased	20	10
Unbiased	15	4
Temperature-Humidity (85%°C/85%RH)		
Forward Biased	20	9
Unbiased	15	0
Thermal Cycle	15	8
Thermal Shock	15	8

Table 6.1 Stress Test Lot Sizes

Parameter	Number	Mean	Standard Deviation
V_{OC} (V)	186	0.547	0.010
I_{SC} (A)	186	0.506	0.021
V_M (V)	186	0.445	0.011
I_M (A)	186	0.444	0.025
P_M (W)	186	0.198	0.015

Table 6.2 Mean Values and Standard Deviations of Prestress Electrical Parameters, Type F Cells

Parameter	Number	Mean	Standard Deviation
V_{OC} (V)	194	0.589	0.004
I_{SC} (A)	194	1.343	0.021
V_M (V)	194	0.494	0.007
I_M (A)	194	1.223	0.033
P_M (W)	194	0.603	0.020

Table 6.3 Mean Values and Standard Deviations of Prestress Electrical Parameters, type G Cells

Parameter	Number	Mean	Standard Deviation
V_{OC} (V)	82	0.520	0.011
I_{SC} (A)	82	0.566	0.063
V_M (V)	82	0.423	0.020
I_M (A)	82	0.498	0.054
P_M (W)	82	0.211	0.028

Table 6.4 Mean Values and Standard Deviations of Prestress Electrical Parameters, Type H Cells

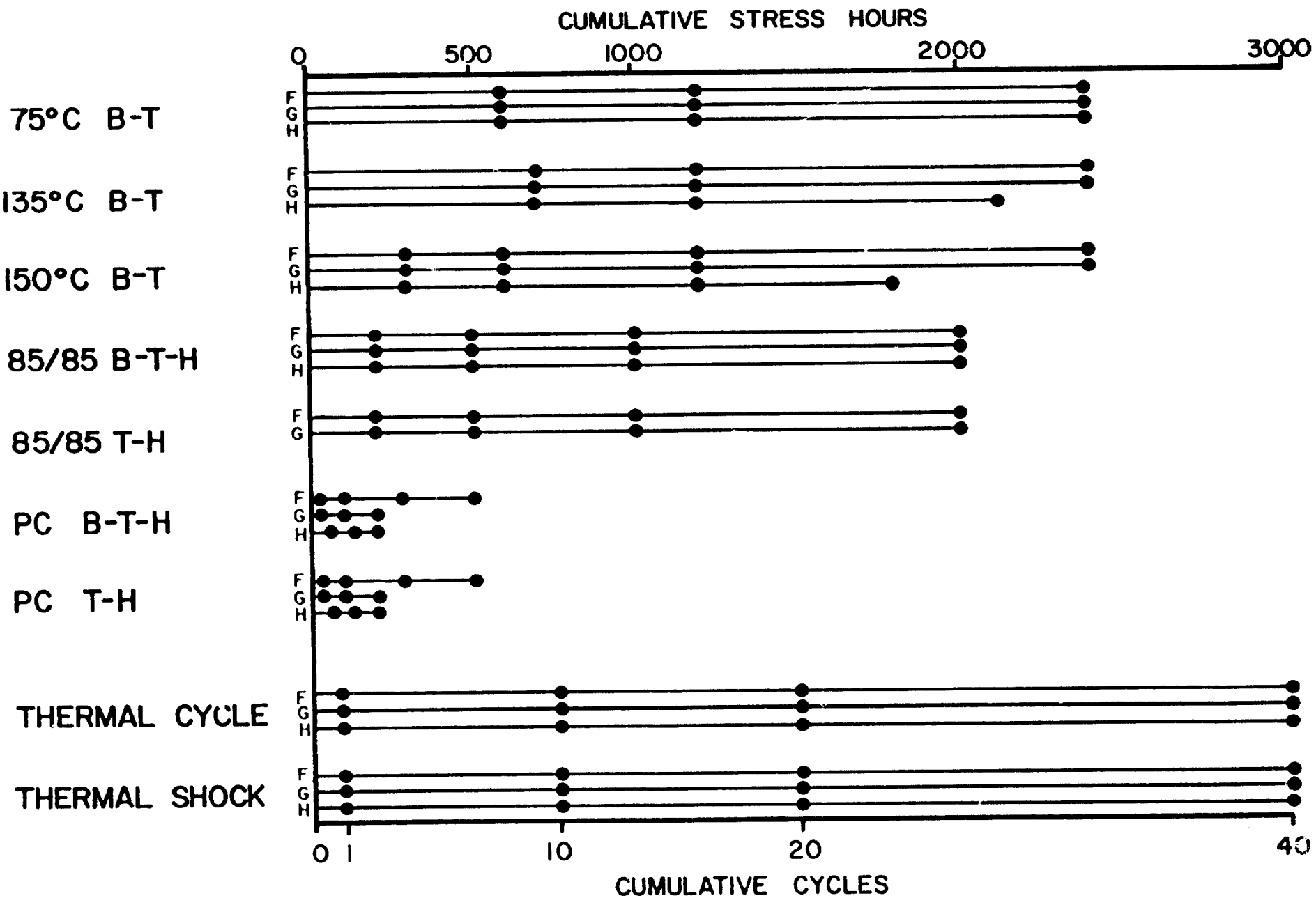

Figure 6.1. Stress Testing Schedule and Downtimes.

6.2 Bias-Temperature Stress Test Results

The behavior of the mean percent decrease in P_m with bias-temperature (B-T) stress is shown in Figure 6.2 for type F cells. Examination of detailed type F cell data shows that for the 75°C and 135°C stress tests a significant contribution to the decrease shown in Figure 6.2 came from one cell in each test. An example of the behavior of a "freak" cell can be seen in Figure 6.3 which shows the prestress and post-2400 hour P_m distribution for the cell type F, 75°C B-T test. The same sort of degradation as shown in Figure 6.3 was also observed for I_{sc} for the same "freak" cell. The mechanism involved is apparently not severe series or shunt resistance change since the decrease in I_m is approximately the same as the degradation in I_{sc}, and practically no effect on V_m was observed. For example, the freak cell in the 75°C B-T test population showed a decrease in P_m from 0.16W to 0.06W, and in I_{sc} from 0.48A to 0.21A, while V_m showed an increase from 0.441V to 0.450V during the same test. Quite different behavior was shown by the cells subjected to 150°C B-T stress. In this case, in addition to one cell which showed anomalously large decrease in P_m (and I_{sc}), there was a more general trend downward in P_m for the whole population. This effect can be clearly seen from the P_m and I_{sc} distribution of Figures 6.4 and 6.5. Again, the trend in P_m was apparently due to I_{sc} decreases, independent of series or shunt resistance changes, because I_m was affected and little or no change in V_m was evident. The freak cell in this population was an exception to the general trend in that it showed substantial decrease in both V_m and I_m, as well as in P_m and I_{sc}.

Visual inspection of B-T stress-tested cells showed that small, hollow bubbles were formed in the back solder metalization under stress. The

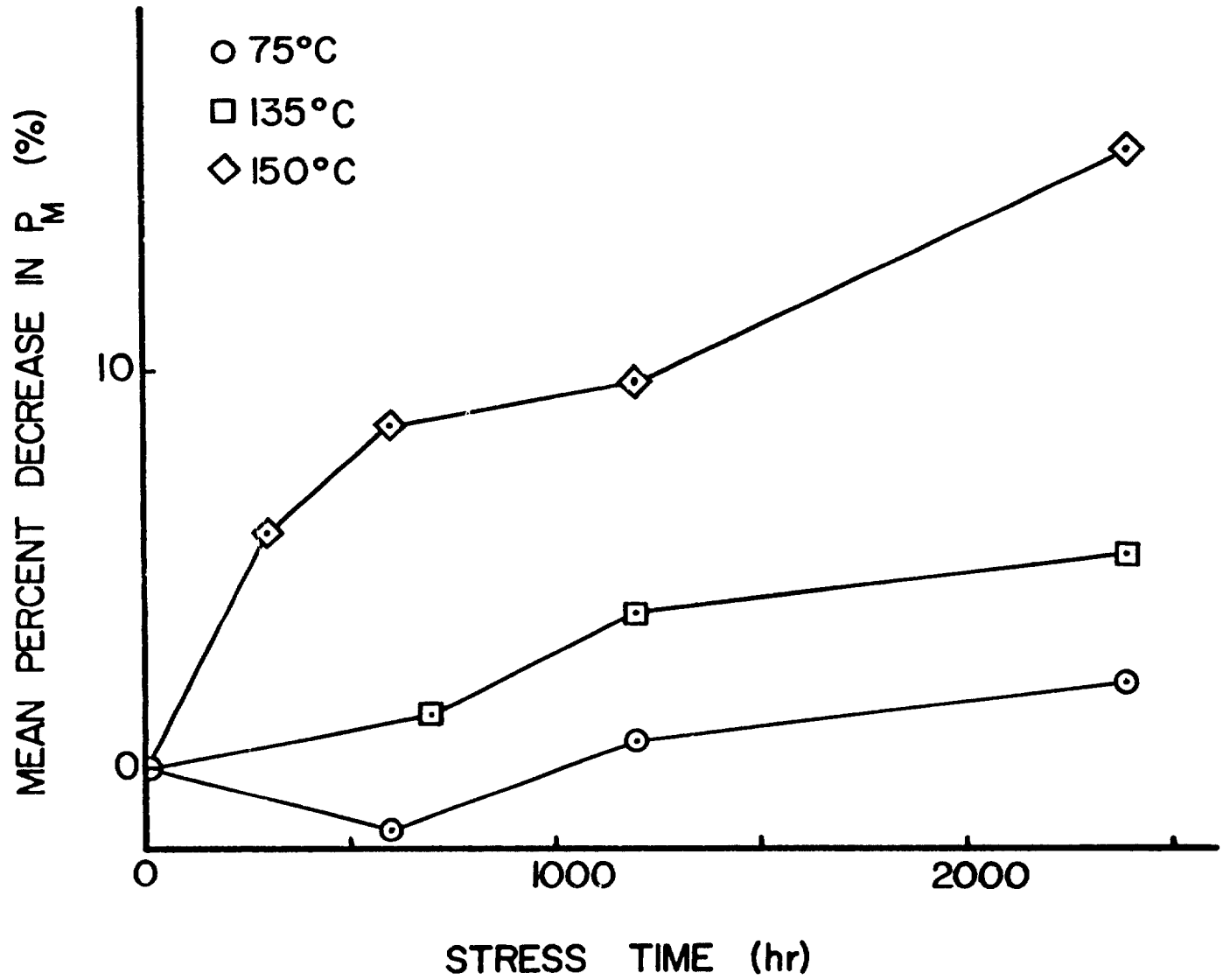

Figure 6.2. Mean Percent Decrease in P_m for Type F Cells, Bias-Temperature Stress Tests.

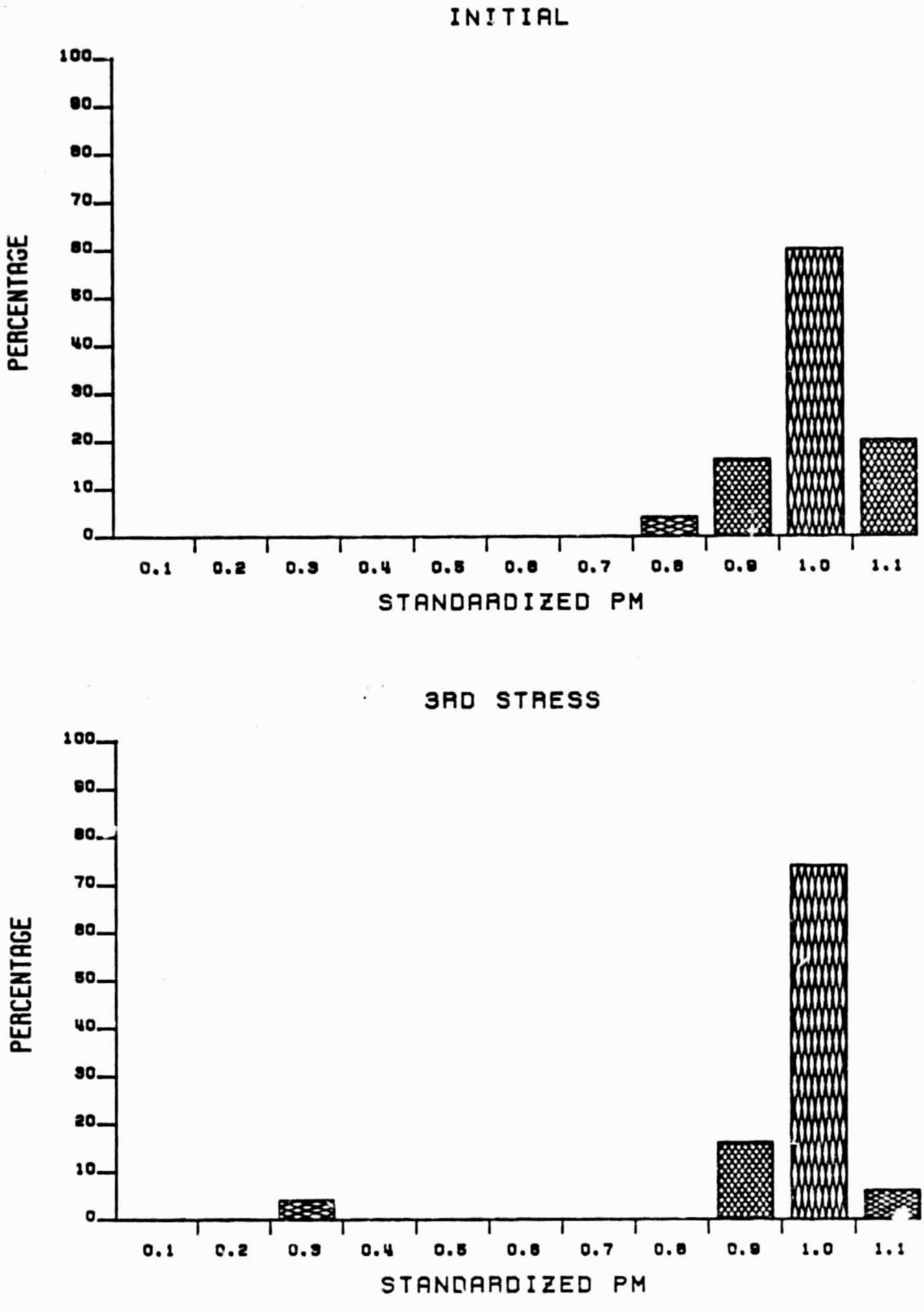

Figure 6.3. Type F Cell 75°C Bias-Temperature Stress Test Lot P_m Distribution, Prestress and After 2400 Stress Hours.

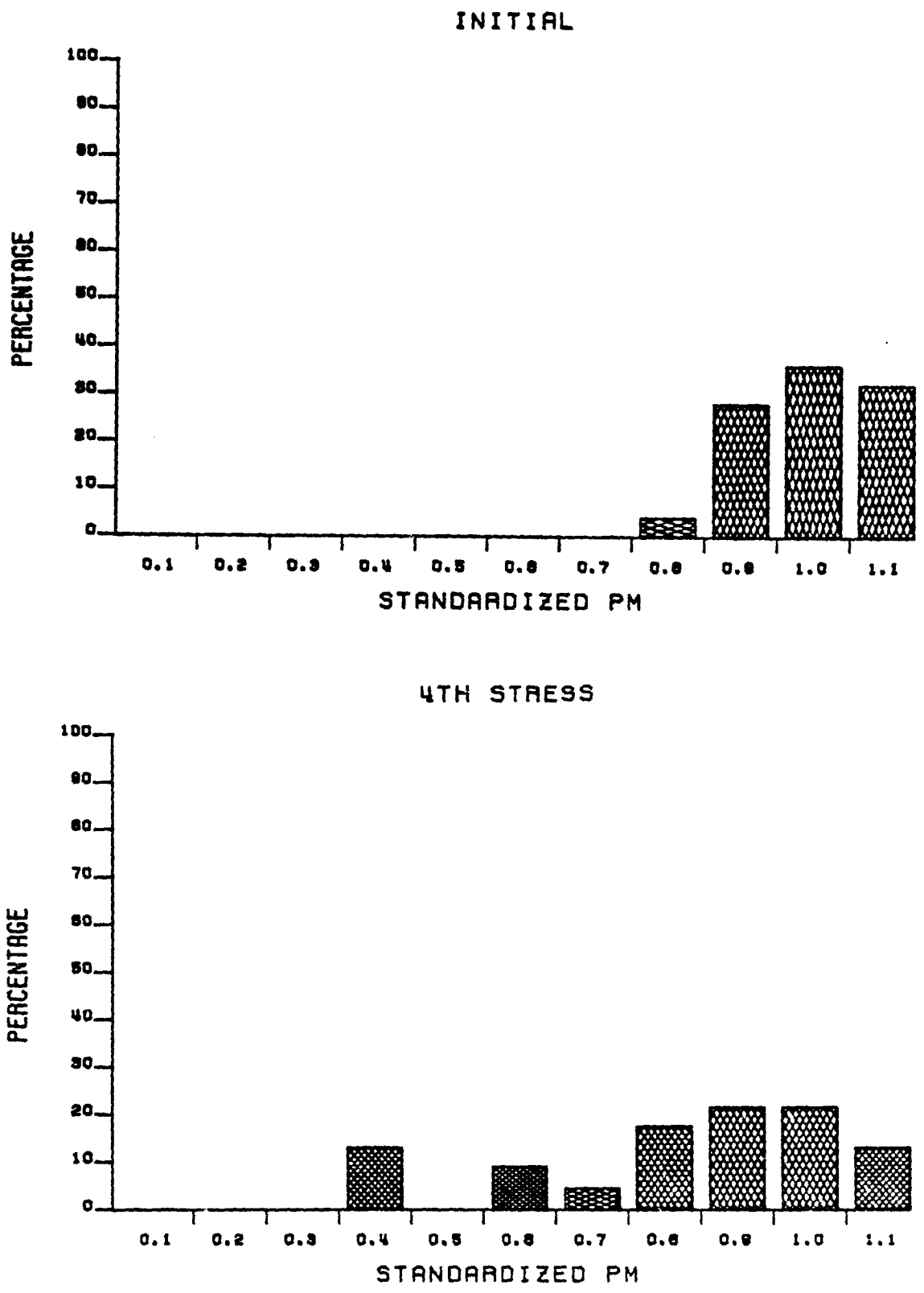

Figure 6.4. Type F Cell 150°C Bias-Temperature Stress Test Lot P_m Distribution, Prestress and After 2400 Stress Hours.

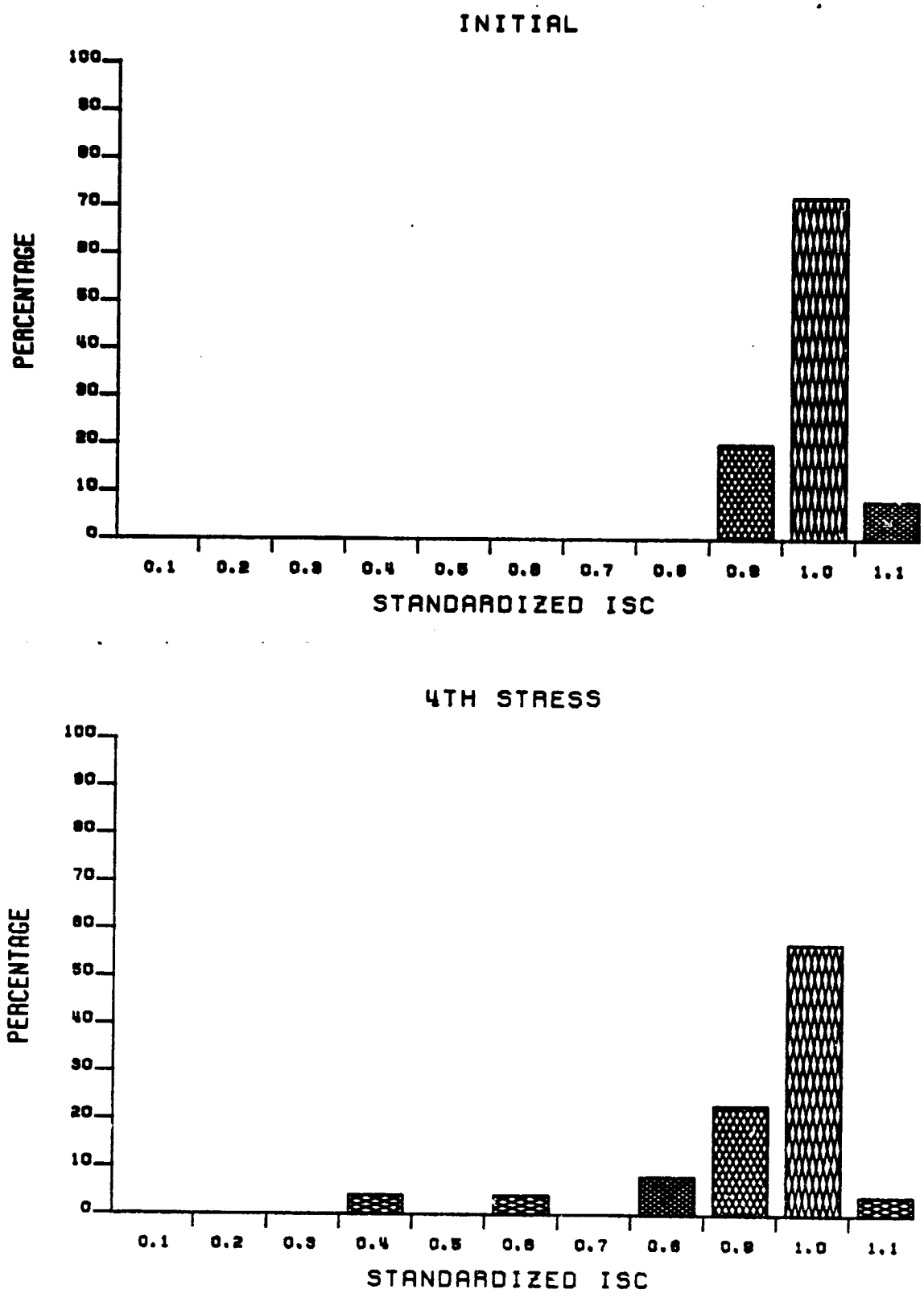

Figure 6.5. Type F Cell 150°C Bias-Temperature Stress Test Lot I_{sc} Distribution, Prestress and After 2400 Stress Hours.

frequency of the bubbles, for the F cells, was consistent with both time and temperature with all the 150°C test lot cells showing bubbles by the third downtime. In some instances the bubbles were fairly large (1/16" diameter). Other physical effects such as minor, infrequent peeling of the front metalization and partial failure of the AR coating (color change) were observed for type F cells. The AR coating failure was noted by the first downtime for many F cells and seemed to originate at the cell perimeter.

The mechanism for P_m and I_{sc} degradation of both the freak cells and, in the case of the 150°C stress test, the total population, is not clear. However, the correlation of the I_{sc} decrease with the P_m decrease, coupled with visual observations, leads to the tentative conclusion that degradation of the AR coating is responsible for both.

The behavior of the mean percent decrease in P_m due to B-T stress testing for type G cells is shown in Figure 6.6. Examination of detailed data for the type G B-T stress lots showed a somewhat different behavior for this cell type compared to type F cells. Populations from the 75°C and 135°C tests showed only general decreases in P_m, with small general downward trends in V_m , I_m , and I_{sc} with stress. From the decreases in the last three parameters, it appears that the decrease in P_m is due both to the decrease in I_{sc} and to the increase in series resistance (or decrease in shunt resistance). The 150°C B-T test population showed a slightly stronger general decrease in P_m stress, which was also due to a shift downward of the V_m , I_m , and I_{sc} distributions. Examples of this behavior are seen in Figures 6.7 and 6.8 which show the P_m and V_m distributions prestress and after 2400 stress hours. For this lot the mean I_{sc} decrease was slightly less than 4 percent over the stress test. Thus, as in the 75°C and 135°C

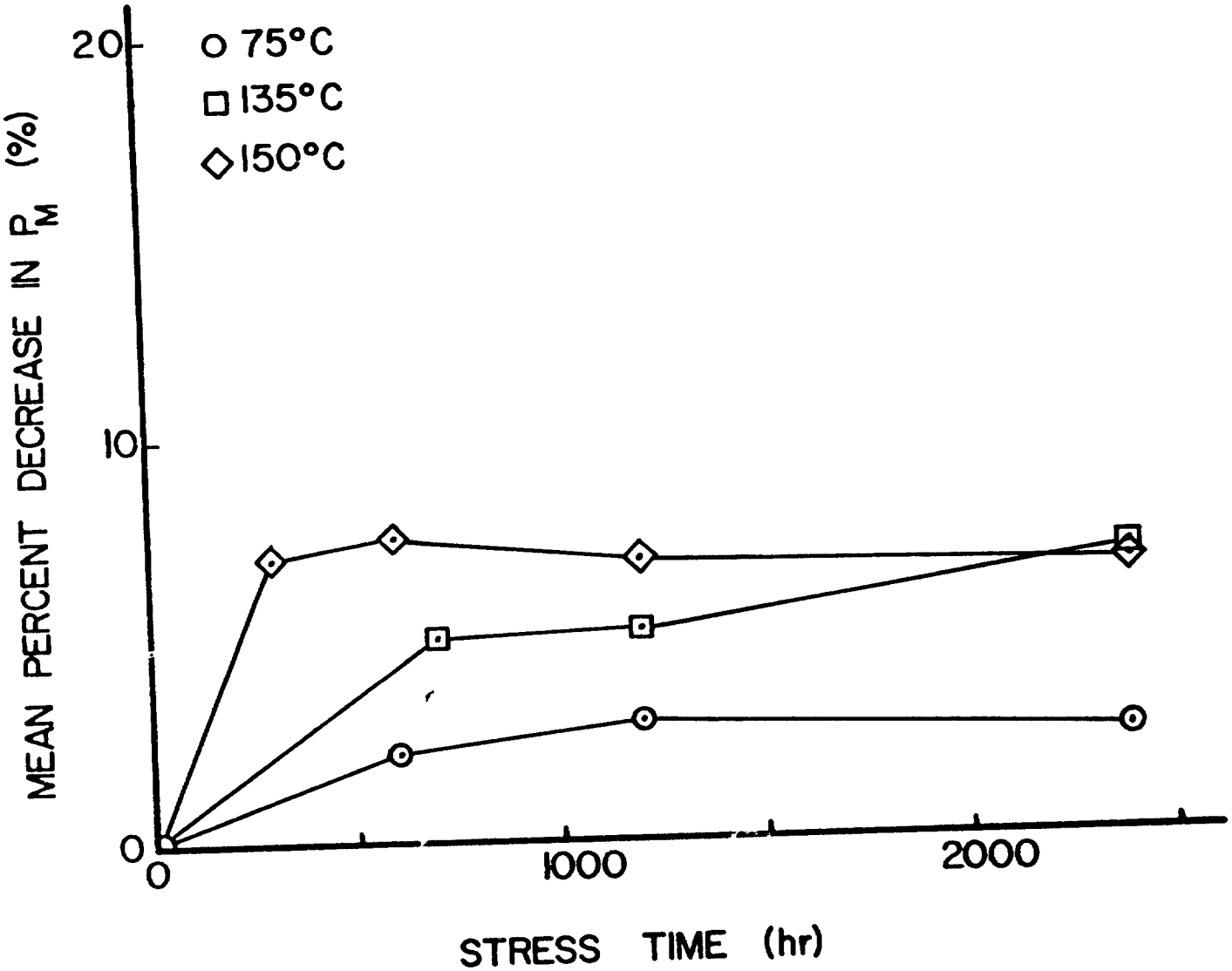

Figure 6.6. Mean Percent Decrease in P_m for Type G Cells, Bias-Temperature Stress Tests.

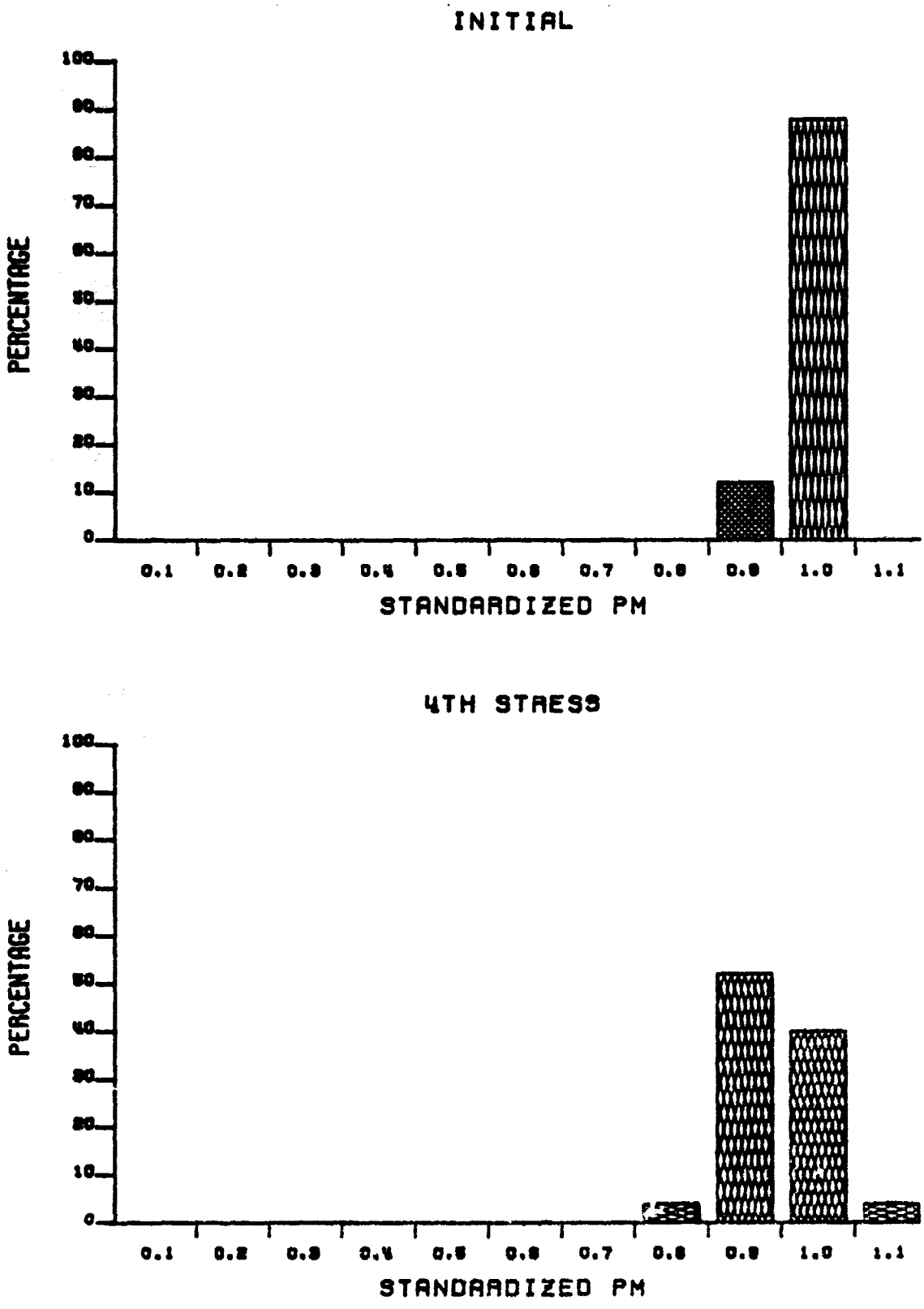

Figure 6.7. Type G Cell 150°C Bias-Temperature Stress Test Lot P_m Distribution, Prestress and After 2400 Stress Hours.

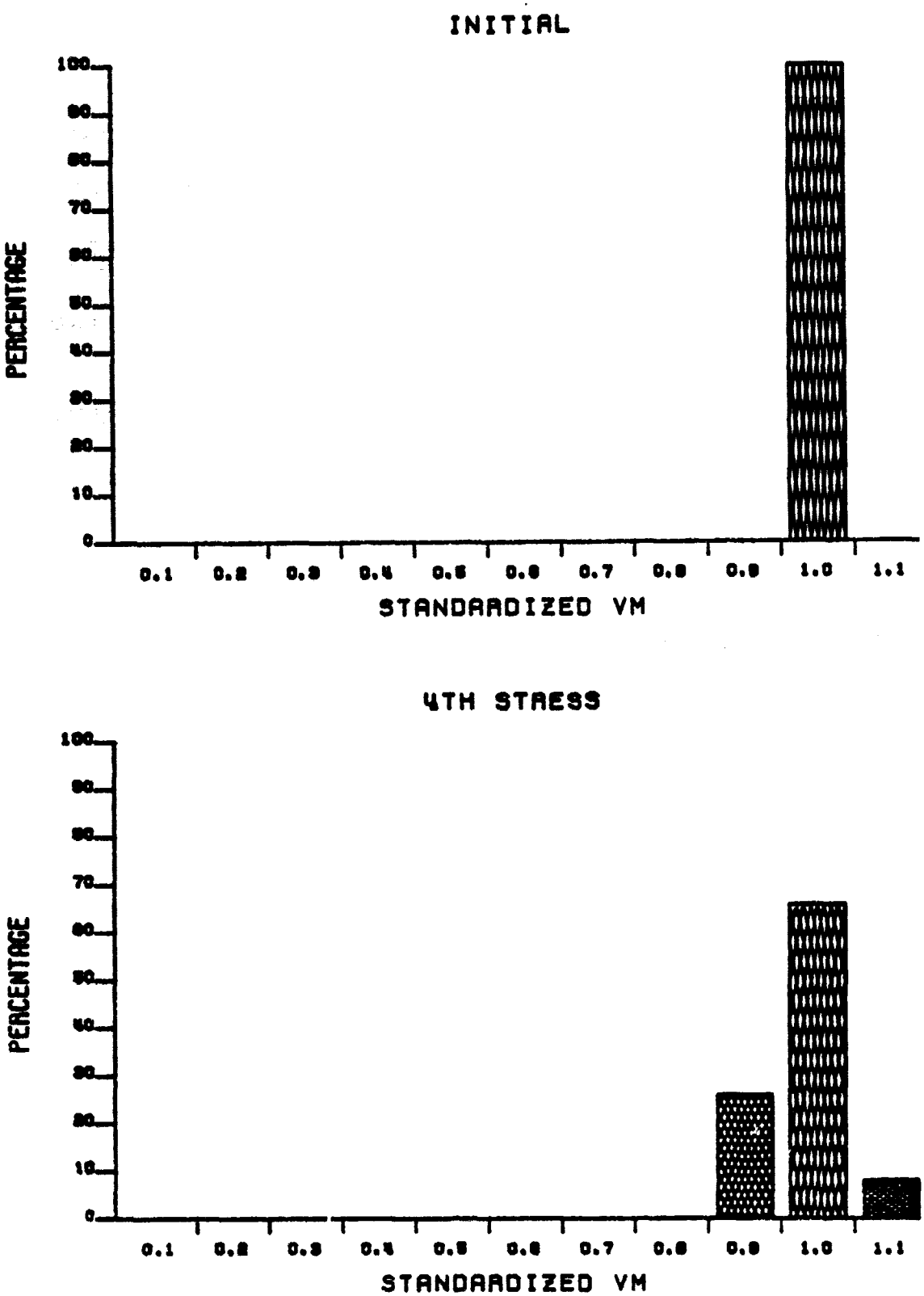

Figure 6.8. Type G Cell 150°C Bias-Temperature Stress Test Lot V_m Distribution, Prestress and After 2400 Stress Hours.

tests, the mechanisms for decrease in P_m appear to be the simultaneous decrease in I_{sc}, and an increase in series resistance, or decrease in shunt resistance. Cell illuminated I-V plots have not yet been analyzed to determine the extent of resistance change or which resistance is changing. From visual inspection, it was found that some type G cells exhibited bubbles of minute dimension. The bubble formation was observed for only a small percentage of the type G cells, regardless of the stress test temperature, and thus is not clearly correlated with degradation in P_m. No visible changes in the AR coating were observed, and the cause of the I_{sc} is not clear at this time. Note that no freak cells were found in the type G cell B-T stress test populations.

Type H cells subjected to B-T stress testing exhibited little or no significant response, except what might be considered an improvement in the 135°C B-T test population. This is shown in Figure 6.9. The response of mean P_m was correlated very closely to the response of I_{sc}. For example, the apparent 3.17% improvement in P_m shown for the 135° test lot at 700 hours was accompanied by a 2.6% improvement in I_{sc}; at 1200 hours, when the improvement in P_m was 2.7%, the improvement in I_{sc} was 1.92%. Physically, a few of the type H cells exhibited minor discoloration of the AR coating, beginning at the corners of the cells, and a discolaration (reddening) of the grid metal for 135°C test lot cells. In addition, the following tendency mentioned in an earlier report (1), most of type H B-T cells had lost one lead by the end of the tests, and remaining leads were barely adhering due to weld breakage. None of these visually observable effects can be correlated with cell improvement. Thus, the mechanism for the improvement, if in fact it is real and not an artifact of the measurement process, is not clear but must be internal to the device itself.

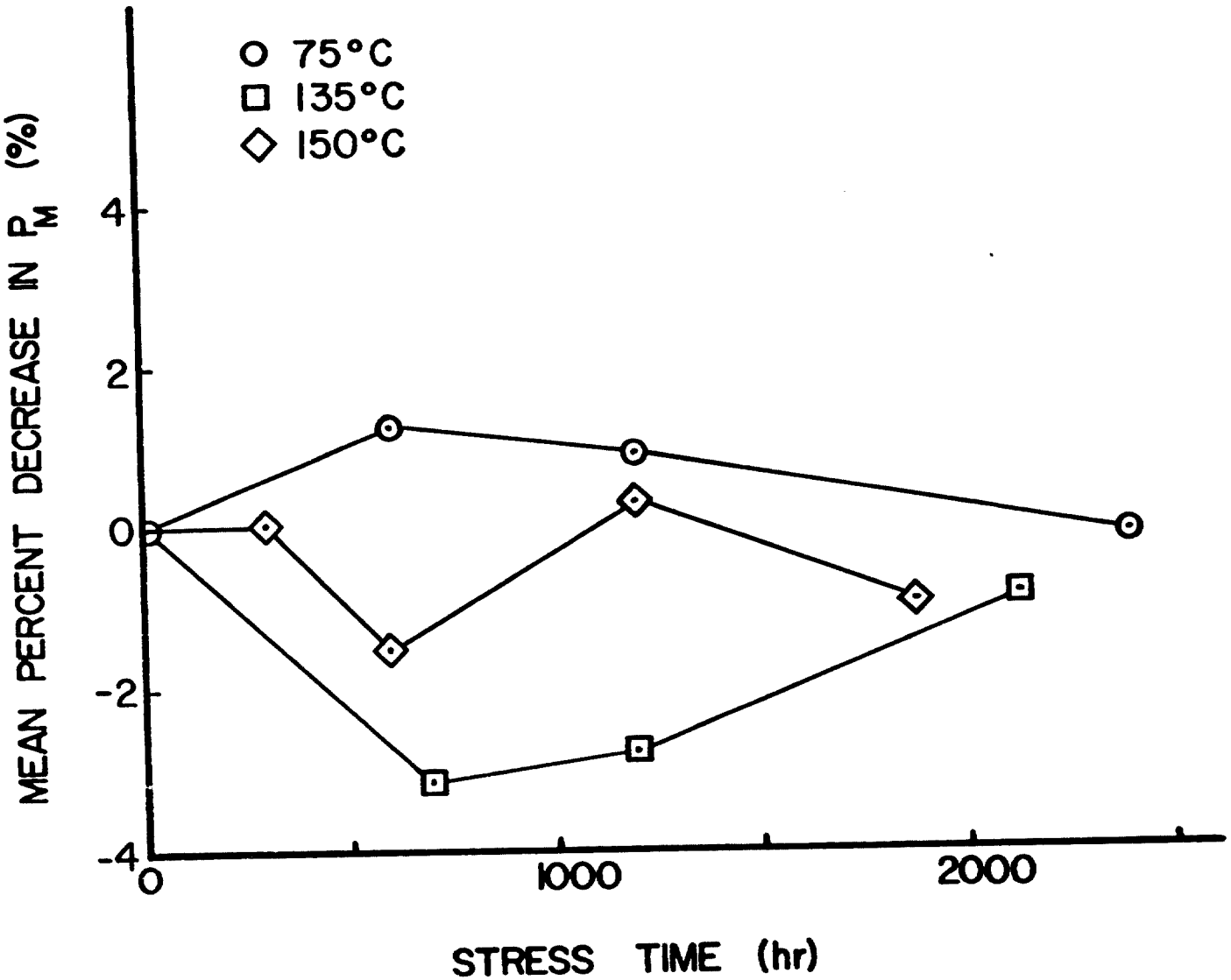

Figure 6.9. Mean Percent Decrease in P_m for Type H Cells, Bias-Temperature Stress Tests.

Sintering of the contacts might be considered as a possibility, but that should not result in improvement in I_{sc}, and so must be discarded as a mechanism.

6.3 Bias-Temperature-Humidity and Temperature-Humidity Stress Test Results

The behavior of the mean percent decrease in P_m for type F cells subjected to temperature-humidity stress testing, both with applied forward bias (B-T-H stress) and without applied forward bias (T-H stress), is shown in Figures 6.10 and 6.11. It was expected, and has in fact been observed in earlier work, that the pressure cooker stress test would show much more severe effects on the cells compared to the 85°C/85% R.H. test, for equivalent times. This was found to be true for type F cells. However, the difference between the degradation caused by the two different stress tests was not nearly as great as had been observed in the past. The mechanism leading to the P_m degradation for pressure cooker stress is primarily I_{sc} decrease not connected with severe series or shunt resistance change. Both biased and unbiased cells were similar in this respect. Figures 6.12 and 6.13 show the B-T-H (pressure cooker) lot P_m and I_{sc} distributions prior to stress and after 499 stress hours. The correlation between P_m and I_{sc} decreases is clear. Essentially no effect on the V_m distribution was observed with increasing stress test duration. Very similar behavior of the distributions was noted for the T-H (pressure cooker) stress test lot. Thus the active mechanism in the pressure cooker stress test is evidently not affected by applied bias. Some regions of AR coating, on most cells, were removed during the test, apparently due to condensation and dripping of pressure cooker water. This is the only ready explanation for the observed pattern of bleaching. A puzzling observation was the occurence of very large bubbles in the back metal of four (of 15) T-H test cells. In no other test, including B-T, was this effect observed.

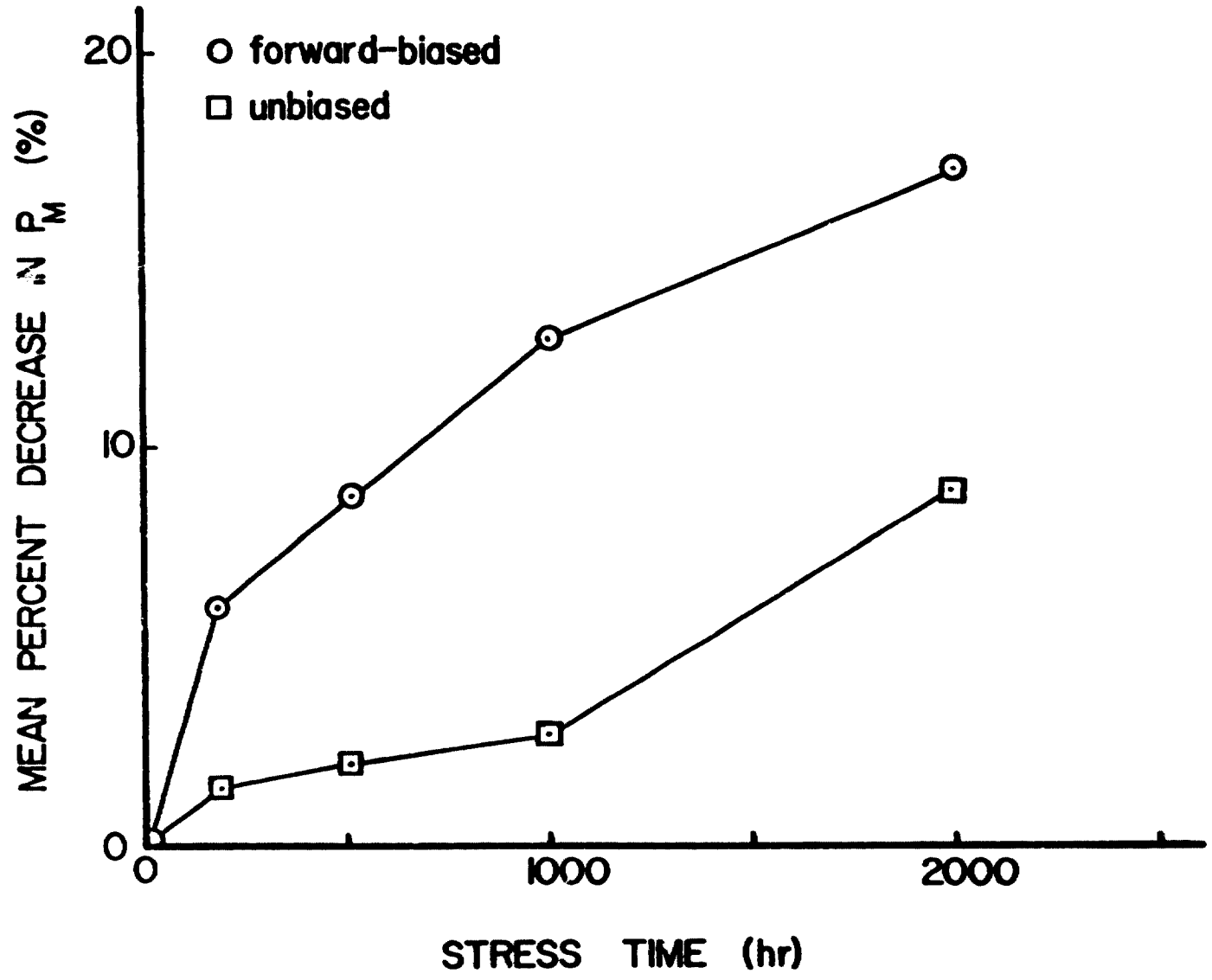

Figure 6.10. Mean Percent Decrease in P_m for Type F Cells, Temperature-Humidity (85°C/85%RH) Stress Test.

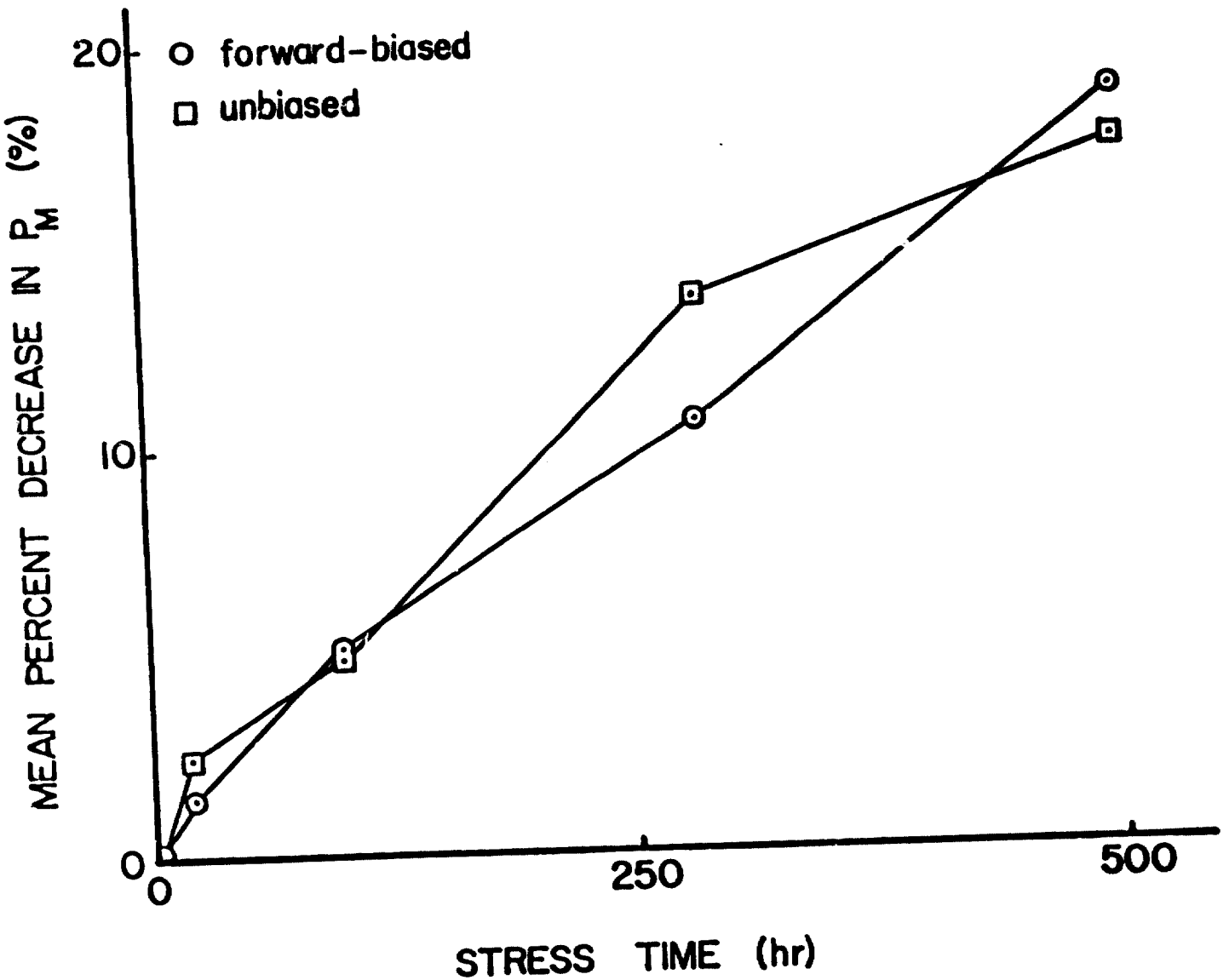

Figure 6.11. Mean Percent Decrease in P_m for Type F Cells, Temperature-Humidity (Pressure Cooker) Stress Test.

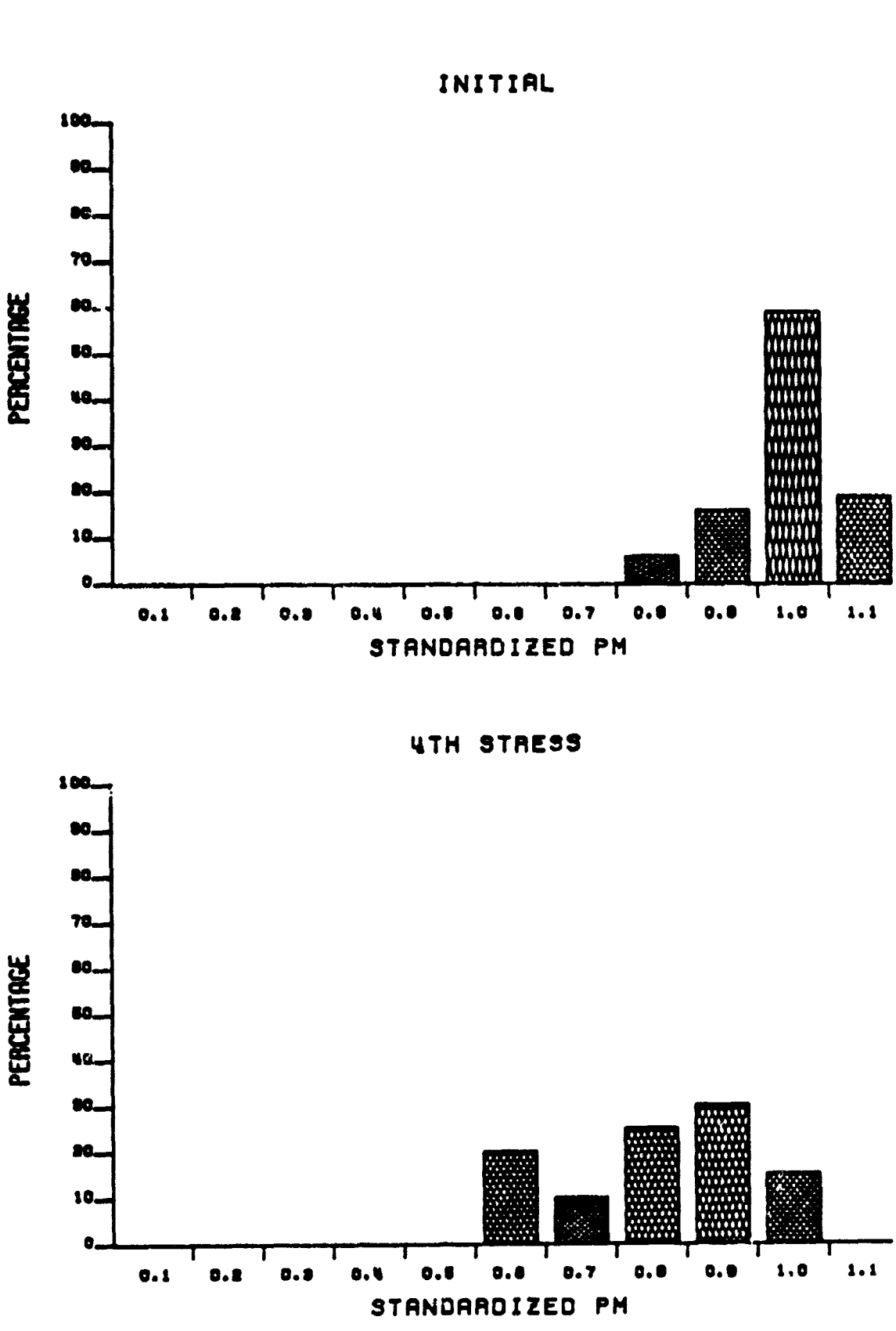

Figure 6.12. Type F Cell Bias-Temperature-Humidity (Pressure Cooker) Stress Test Lot P_m Distribution, Prestress and After 499 Stress Hours.

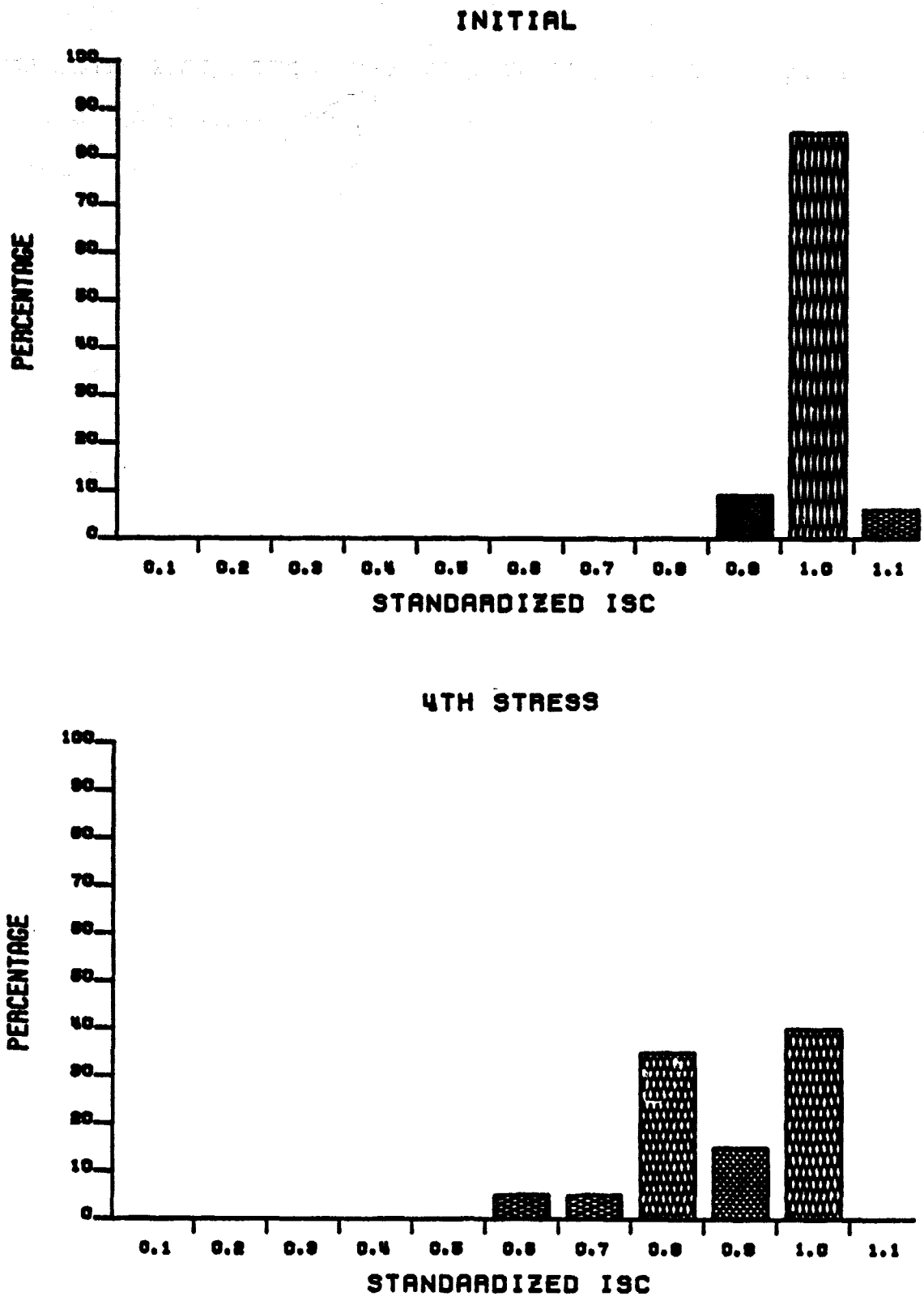

Figure 6.13. Type F Cell Bias-Temperature-Humidity (Pressure Cooker) Stress Test Lot I_{sc} Distribution, Prestress and After 499 Stress Hours.

The behavior of the type F cells subjected to 85°C/85% R.H. stress is different in some respects from the behavior of the pressure cooker lots. It is obvious from Figure 6.10 that the 85°C/85% R.H. B-T-H and T-H response of the cells was not the same. Examination of the parameter distributions showed that a large part of the difference was due to a few cells in the B-T-H population which exhibited anomalously large P_m and I_{sc} decreases. This odd behavior is clear in Figures 6.14 and 6.15, which show the P_m and I_{sc} distributions both prestress and after 2006 stress hours. The anomalous cells did not exhibit unusually low V_m, although I_m was expectedly low for these cells through correlation with I_{sc}. Thus the conclusion is that the freak behavior was probably not caused by shunt or series resistance effects. Only minor discoloration of the AR coating, and no massive bleaching of it was noted. The discoloration observed does not seem to be sufficient to cause the large I_{sc} effects shown in Figure 6.10. However, in the absence of other evidence, the AR coating effects are presumed to be the mechanism causing P_m and I_{sc} decrease. The T-H cells did show less discoloration than the B-T-H cells, and thus the correlation with bias exists.

The response of type G cells to B-T-H and T-H stress is shown in Figures 6.16 and 6.17. A slightly greater effect of applied bias is seen for pressure cooker stress with type G cells than was seen for type G cells, although the early truncation of the type G tests cloud the issue somewhat. For the 85°C/85% R.H. stress the response of the type G cells is similar to that of the type F cells, i.e., bias apparently does not provide acceleration of degradation. However, the severity of degradation in P_m is clearly less for both tests for the type G cells. Examination of the detailed parametric distributions showed that for the pressure cooker B-T-H test population there

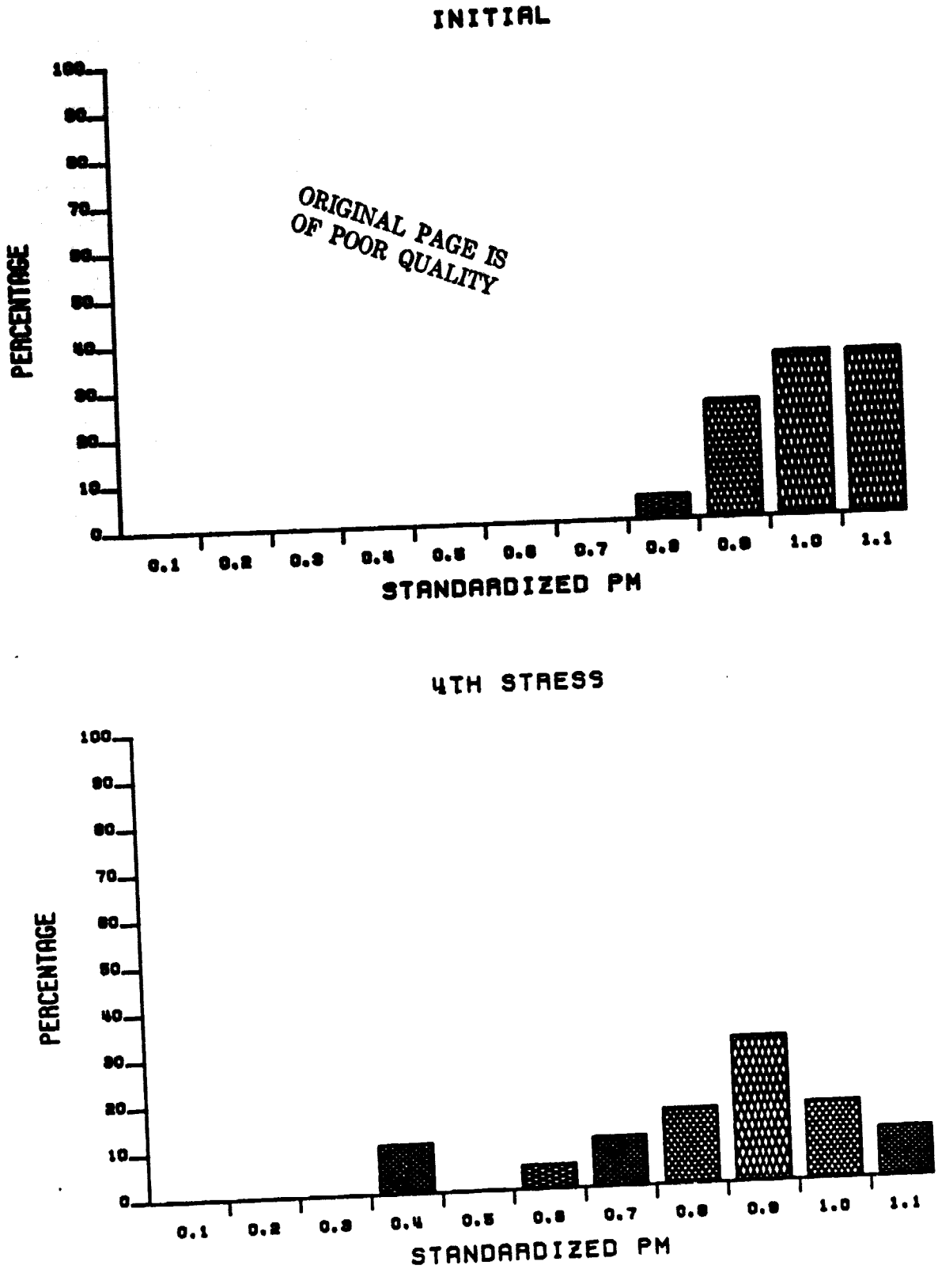

Figure 6.14. Type F Cell Bias-Temperature-Humidity (85°C/85%RH) Stress Test Lot P_m Distribution, Prestress and After 2006 Stress Hours.

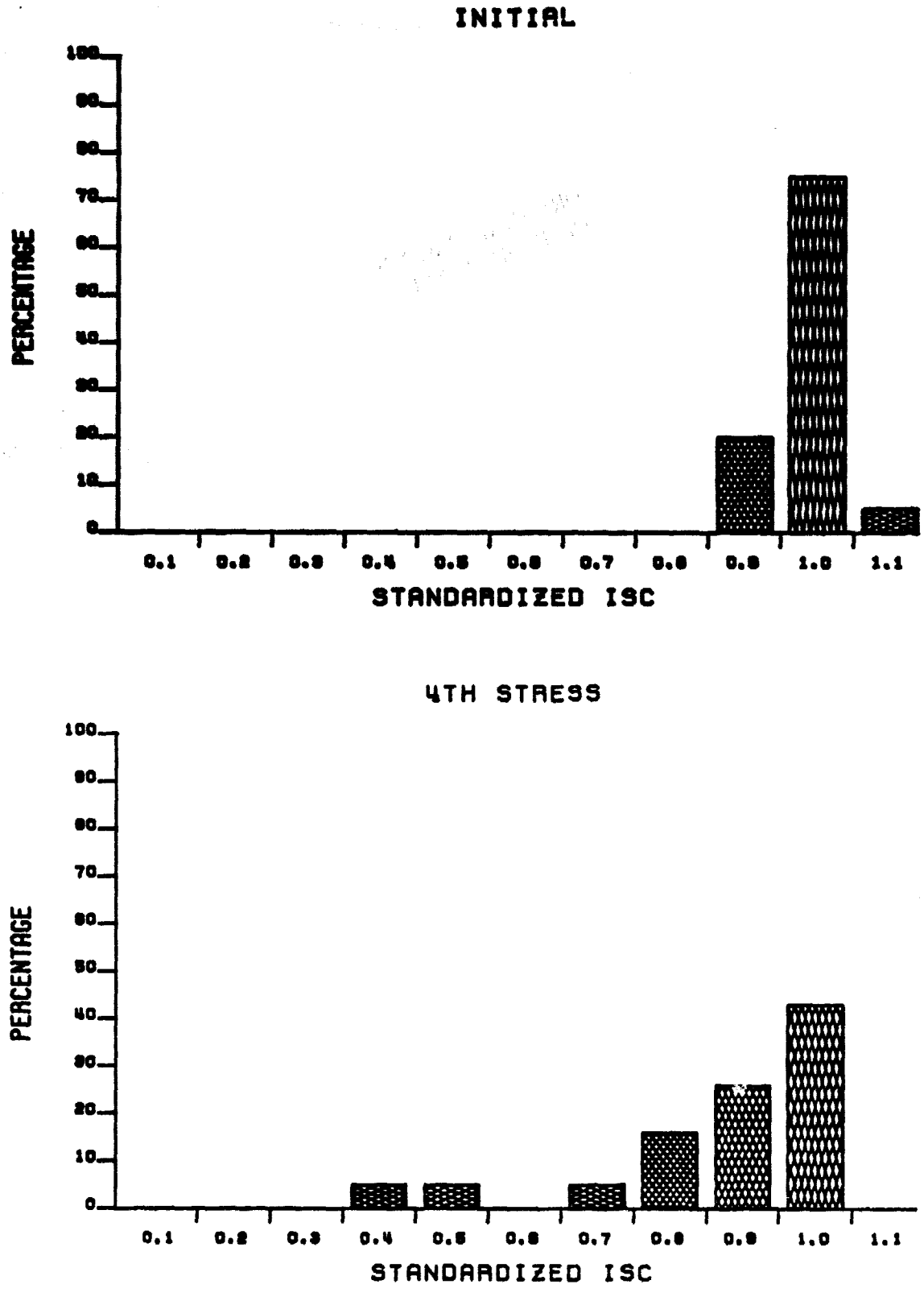

Figure 6.15. Type F Cell Bias-Temperature-Humidity (85°C/85%RH) Stress Test Lot I_{sc} Distribution, Prestress and After 2006 Stress Hours.

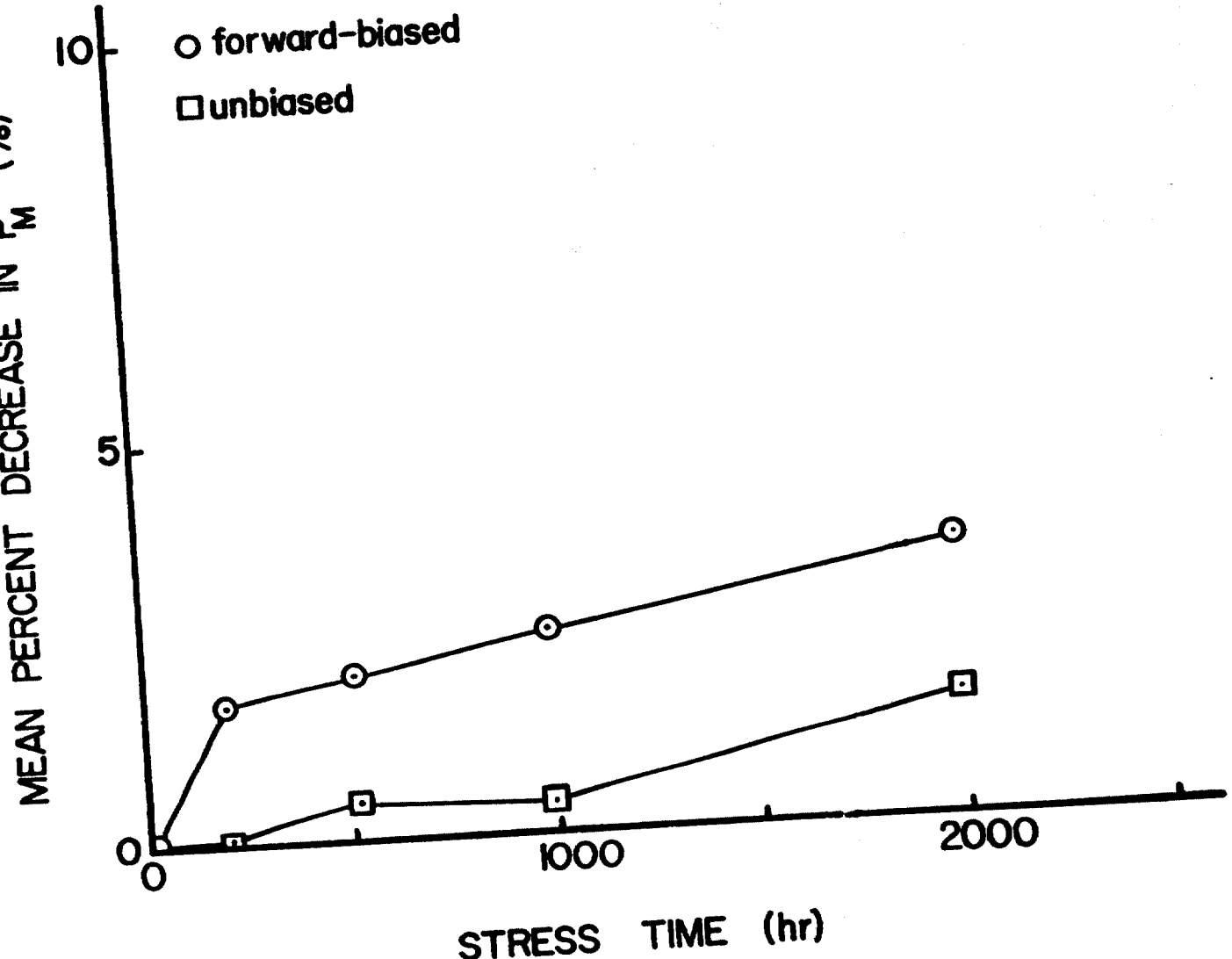

Figure 6.16. Mean Percent Decrease in P_m for Type G Cells, Temperature-Humidity (85°C/85%RH) Stress Test.

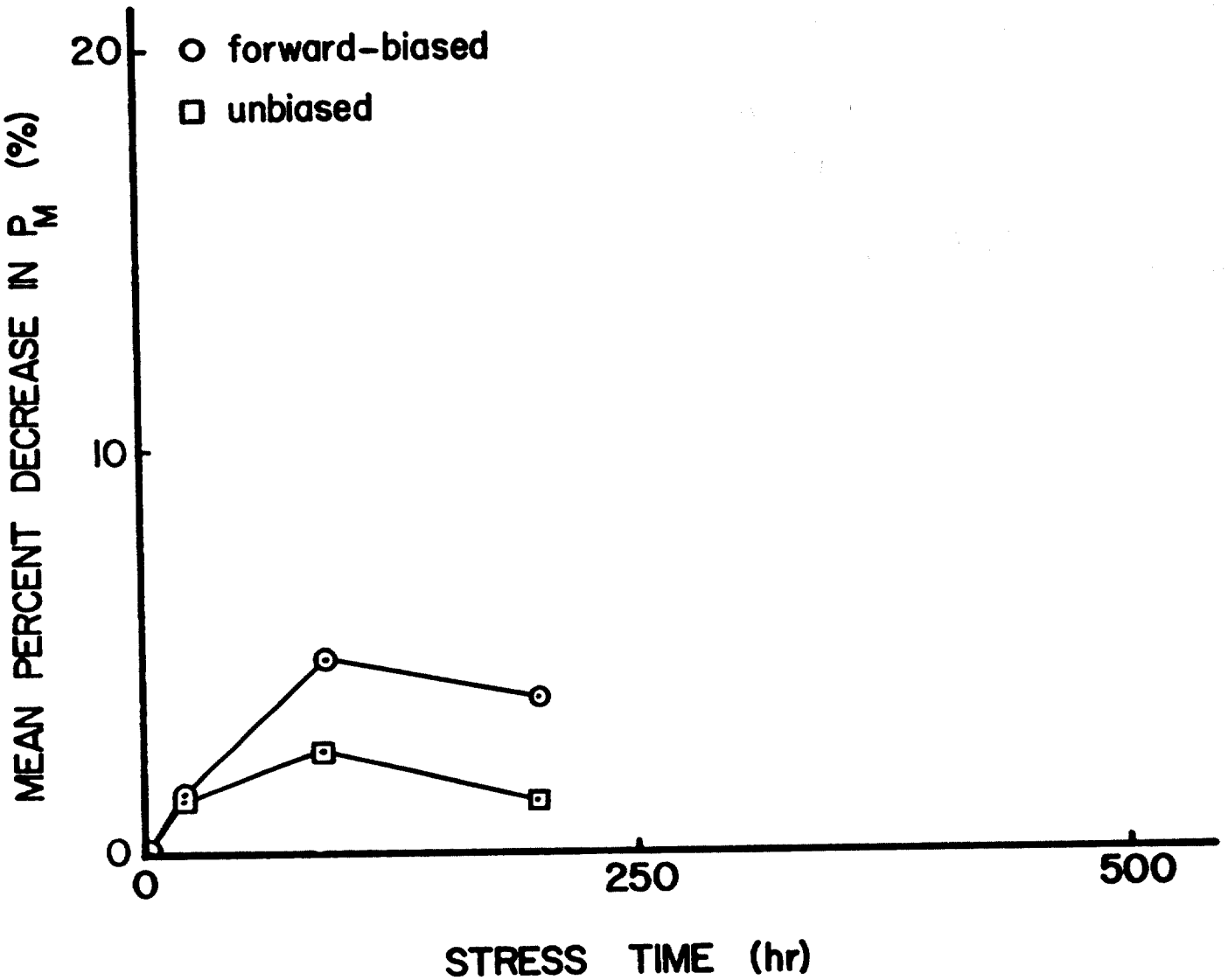

Figure 6.17. Mean Percent Decrease in P_m for Type G Cells, Temperature-Humidity (Pressure Cooker) Stress Test.

was a general downward trend in the P_m, I_{sc}, and I_m distributions, with no discernable stress effect on V_{oc} and V_m and with no freak units appearing under stress. The same was generally true of the pressure cooker T-H test population, although with the small size of the parametric decreases for this lot, definite pronouncements on distribution shifts are more difficult. The behavior of the P_m and I_{sc} pressure cooker B-T-H population distributions are shown in Figurec 6.18 and 6.19, which exhibit the general, small downward trend in paramters and the lack of freak units. For the 85°C/85% R.H. and T-H test lots the effect of stress on the parameter distributions was also seen as (small) general shifts downward of the P_m, I_{sc}, and I_m distributions, with no freak units evident. Thus at this point no T-H metalization/contact problems for type G cells are evident from the electrical data. All effects seem to be attributable to I_{sc} decreases. Results of visual inspection are in general agreement with the electrical results. Minor discoloration of the AR coating was observed for both B-T-H and T-H pressure cooker cells, but no observable metal effects were noted for either T-H test beyond the appearance of a golden haze on the back metal of some cells. No clear visual difference was observed between biased and unbiased cells; however, the electrical effects were so small that this is not surprising.

The response of type H cells to B-T-H and T-H stress is shown in Figures 6.20 and 6.21. Short supply of cells prevented unbiased 85°C/85% R.H. testing of type H cells. Analysis of the details of the 85°C/85% R.H. test data showed that the primary source of P_m decrease was decrease in I_{sc} and I_m with little or no decrease in V_m. Little or no discoloration of the AR coating was observed, while severe peeling of the grid lines was noted. The loss of grid lines apparently did not increase series resistance enough to show up as a significant decrease in V_m.

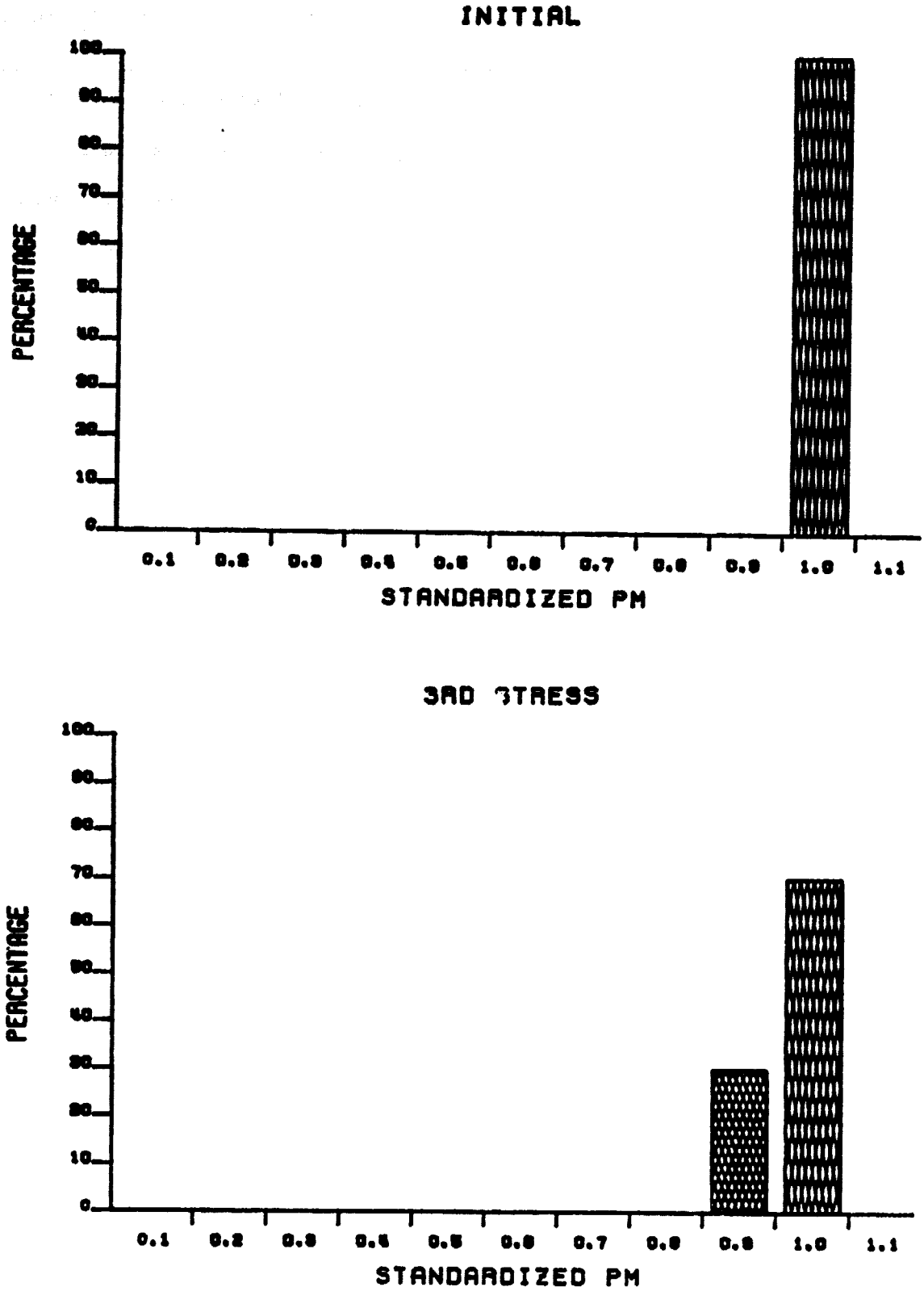

Figure 6.18. Type G Cell Bias-Temperature-Humidity (Pressure Cooker) Stress Test Lot P_m Distributions, Prestress and After 204 Stress Hours.

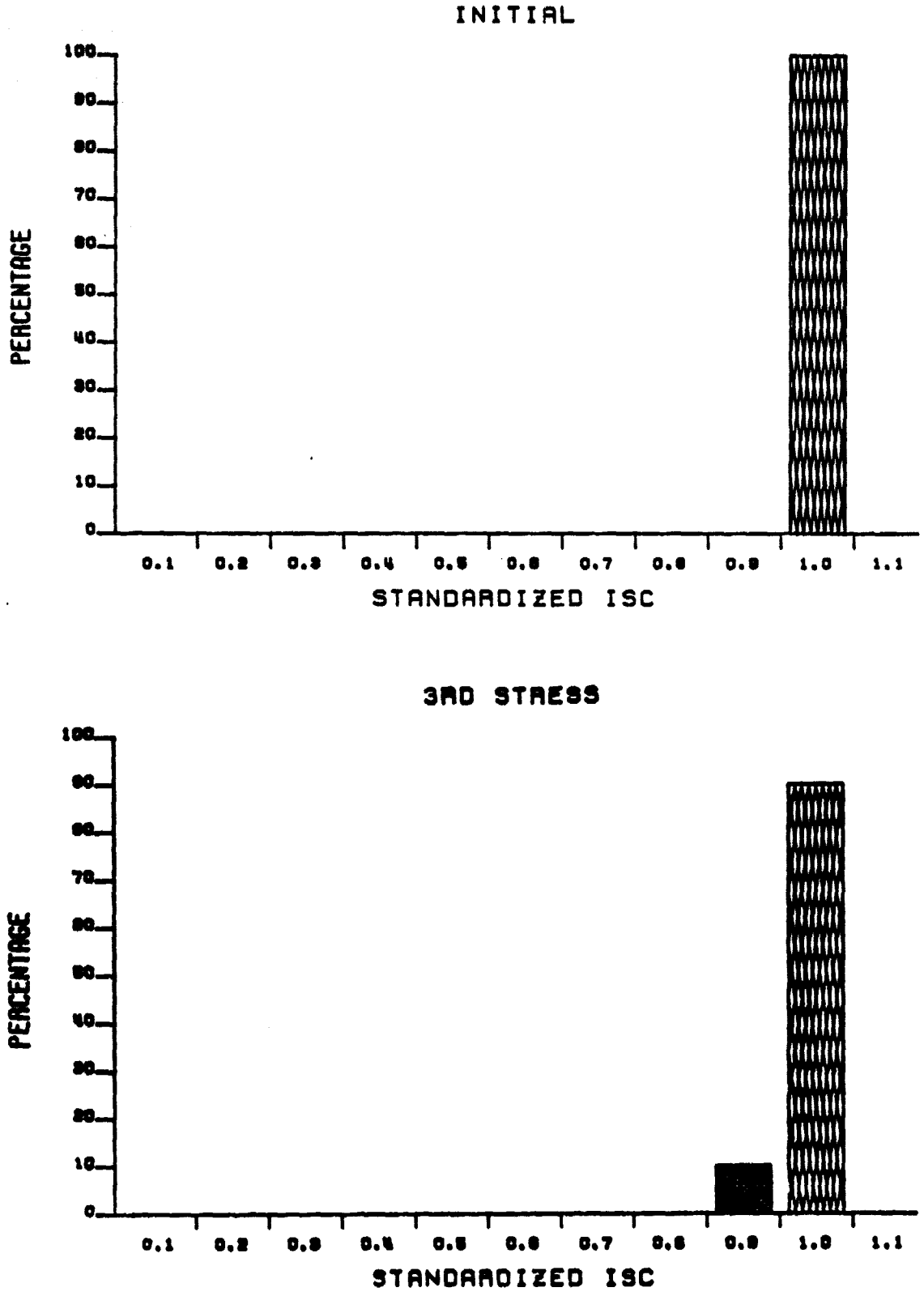

Figure 6.19. Type G Cell Bias-Temperature-Humidity (Pressure Cooker) Stress Test Lot I_{sc} Distributions, Prestress and After 204 Stress Hours.

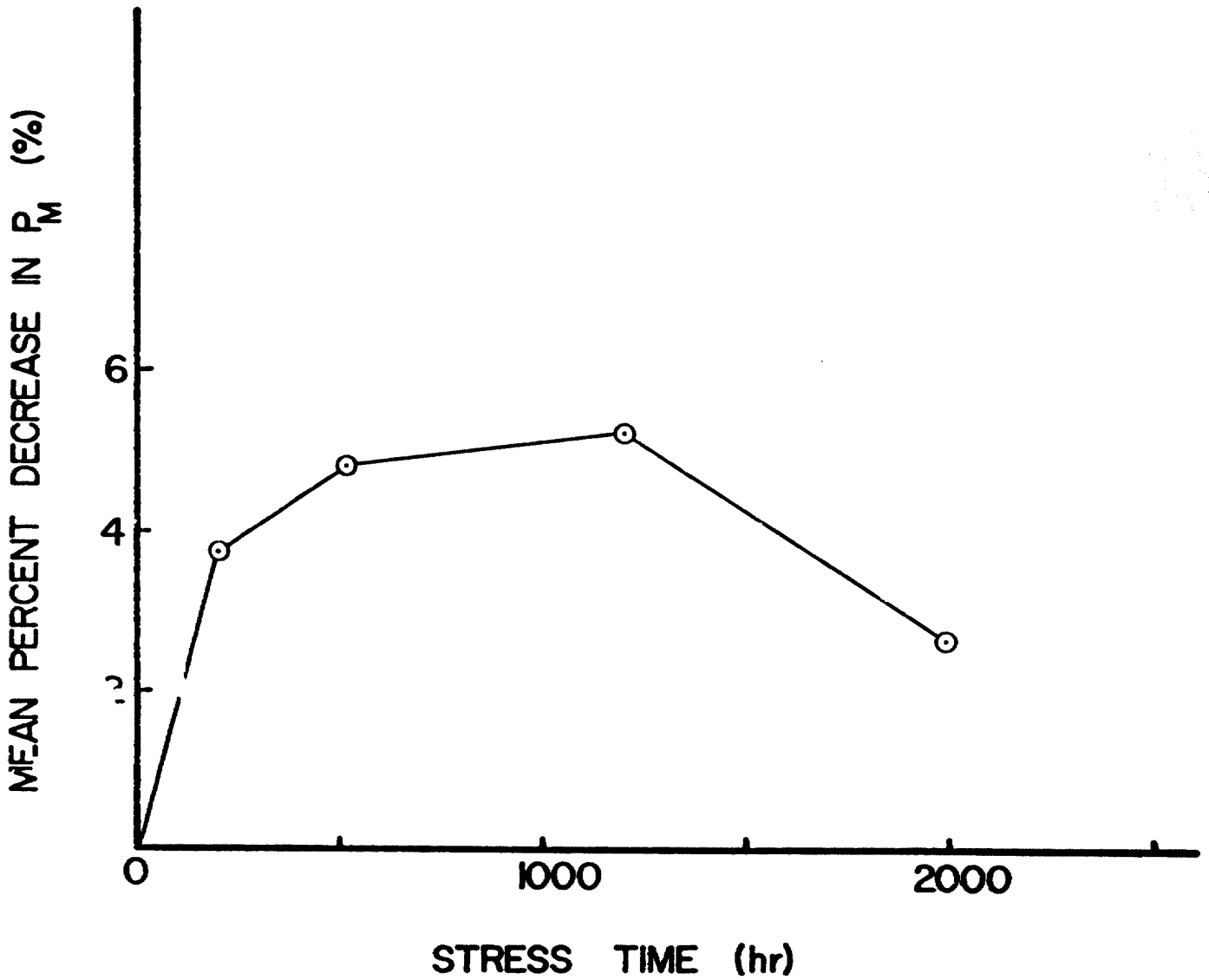

Figure 6.20. Mean Percent Decrease in P_m for Type H Cells, Bias-Temperature-Humidity (85°C/85%RH) Stress Test.

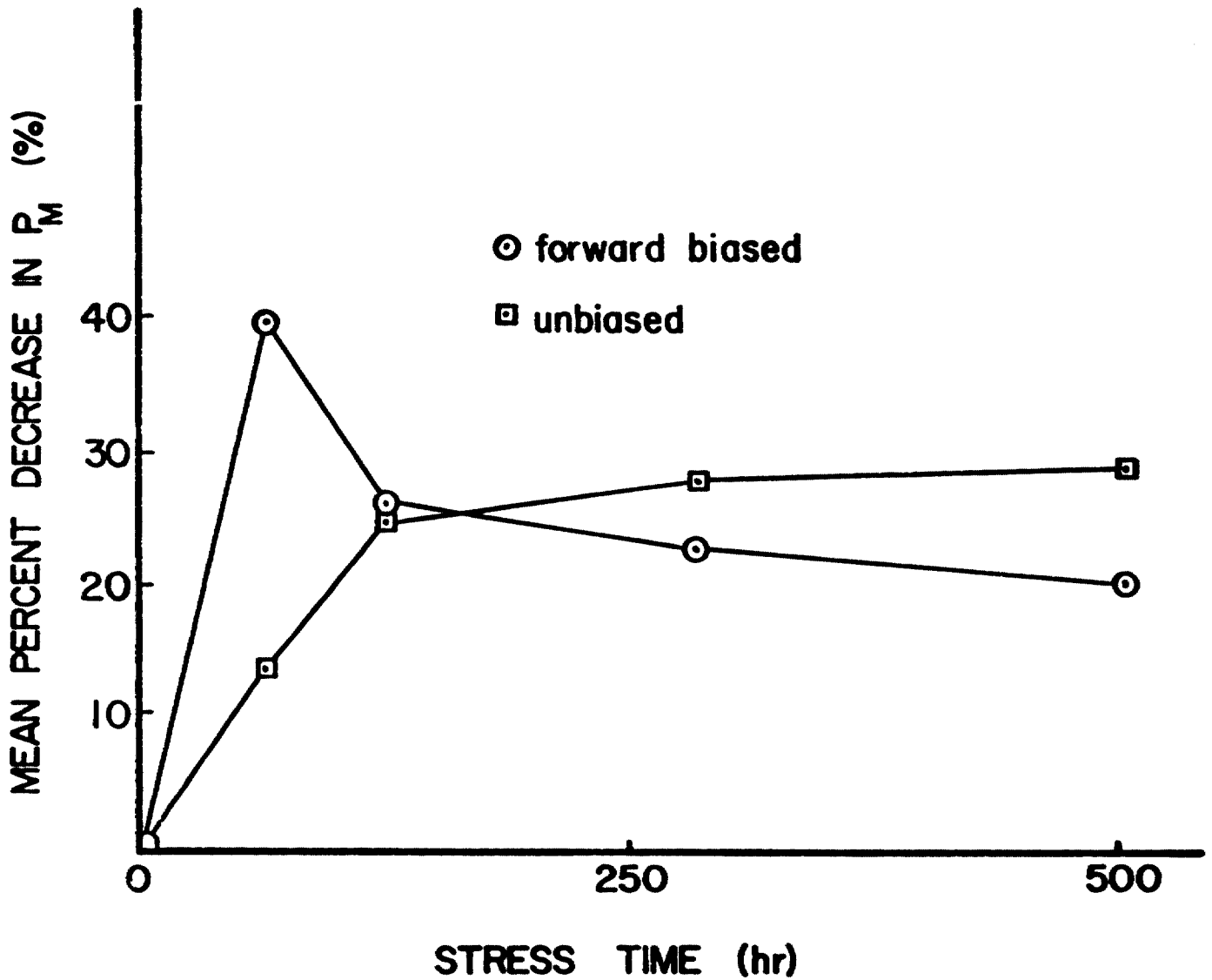

Figure 6.21. Mean Percent Decrease in P_m for Type H Cells, Temperature-Humidity (Pressure Cooker) Stress Test.

The severe P_m effects due to pressure cooker B-T-H and T-H stress, shown in Figure 6.21, were clearly due to I_{sc} decrease The behavior with stress of the P_m distribution and the I_{sc} distribution for the biased pressure cooker stress test lot are shown in Figures 6.22 and 6.23 respectively. In considering the data of Figures 6.21 through 6.23 some consideration should be given to the fact that the pressure cooker lot sizes were only 6 (biased) and 4 (unbiased). However, the effects of the stress were clear cut: P_m and I_{sc} decreased in a correlated manner, with V_{oc} and V_m being essentially unaffected by stress. I_m naturally followed I_{sc}. The large decrease in P_m seen at the 65 hour downtime for the biased pressure cooker lot (see Figure 6.21) was caused by anomalously low values of I_m from two cells. Subsequent measurements, at 130 hours and 285 hours, showed these two cells to be very similar to the other cells, i.e., not anomalously low in P_m and I_m. Examination of the first quadrant I-V plots indicates low R_{sh} for these two cells at the first downtime, but not subsequently. Shunting due to fine metallic deposits is suspected as the cause of the observed behavior. Metallic deposits such as that shown in Figure 6.24 were observed, particularly for the biased pressure cooker stress lots. Severe attack of the AR coating was also noted for both biased and unbiased stress lots. The AR coating effects apparently are the cause of the decreases in I_{sc} for both lots. The metal dissolution/ deposition phenomenon is similar to behavior seen for other cell types in earlier work. It is, however, unique to type H cells in this years contract work, and is definitely a potential problem from the standpoint of both R_{sh} and R_s. Finally, while it appears from most of the data of Figure 6.21 that the response of the cells to biased and unbiased stress testing was very similar, the occurrence of the metal dissolution phenomenon in the biased tests does point up the existence of differing potential degradation

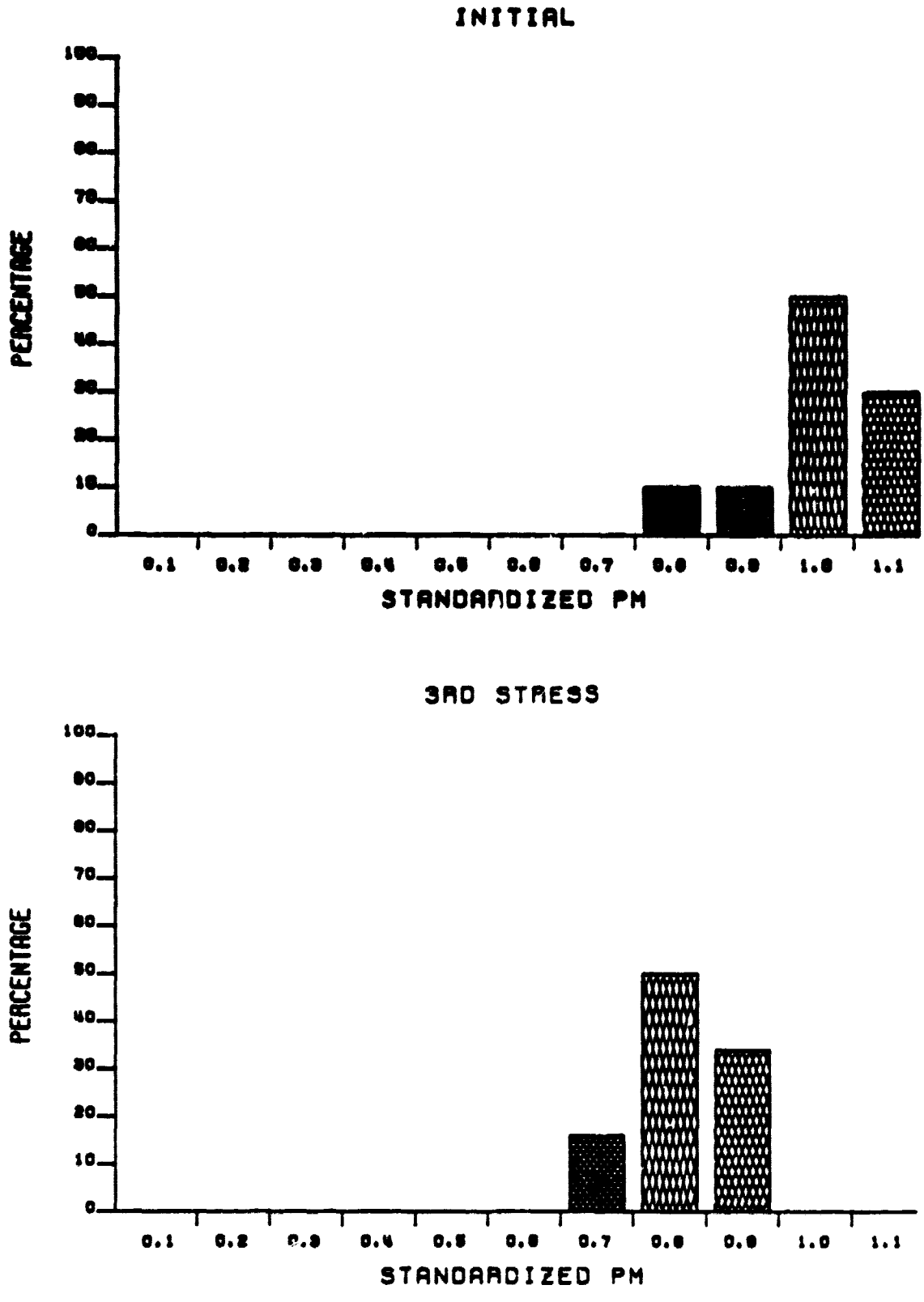

Figure 6.22. Type H Cell Bias-Temperature-Humidity (Pressure Cooker) Stress Test Lot P_m Distributions, Prestress and After 285 Hours.

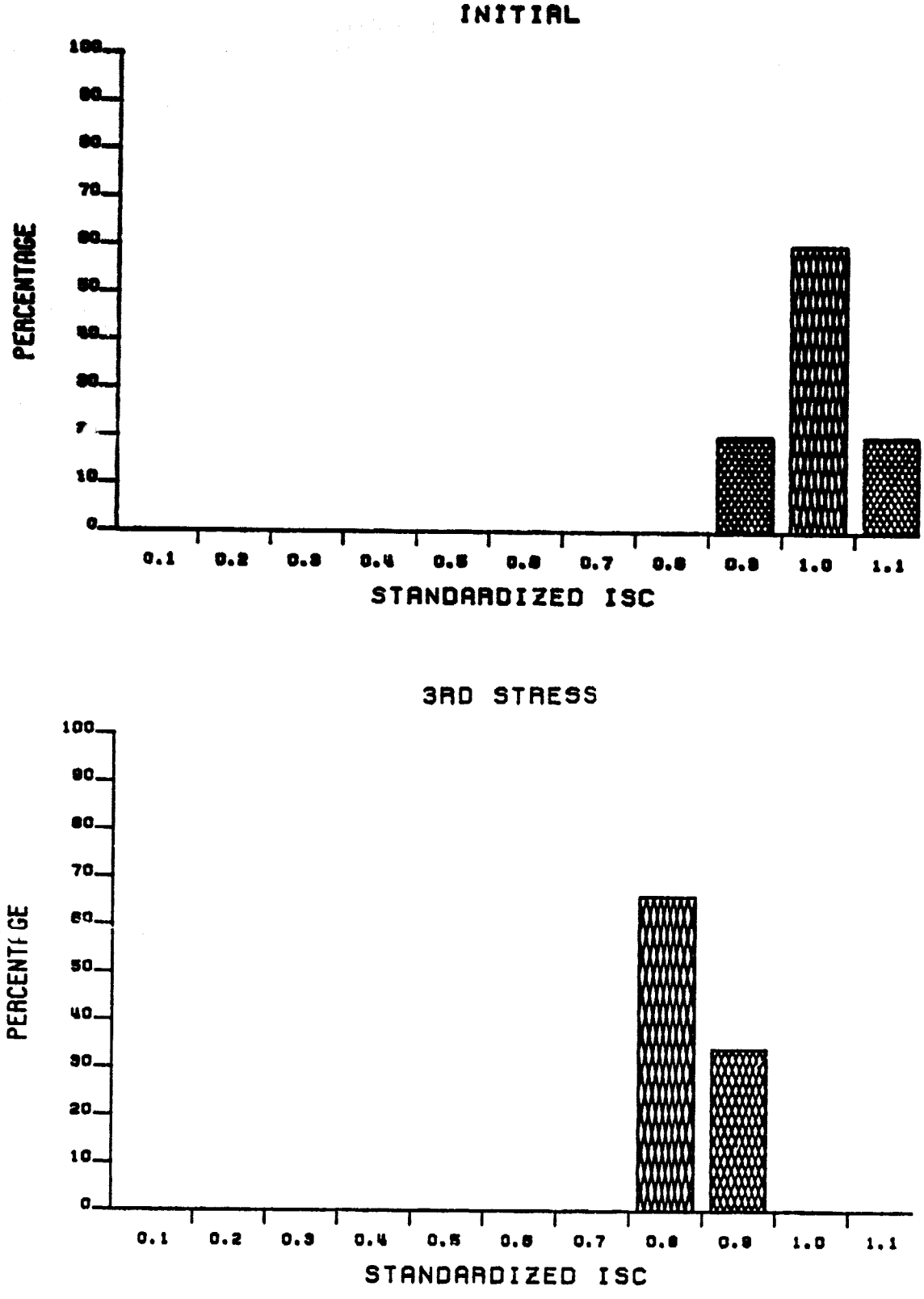

Figure 6.23. Type H Cell Bias-Temperature-Humidity (Pressure Cooker) Stress Test Lot I_{sc} Distributions, Prestress and After 285 Stress Hours.

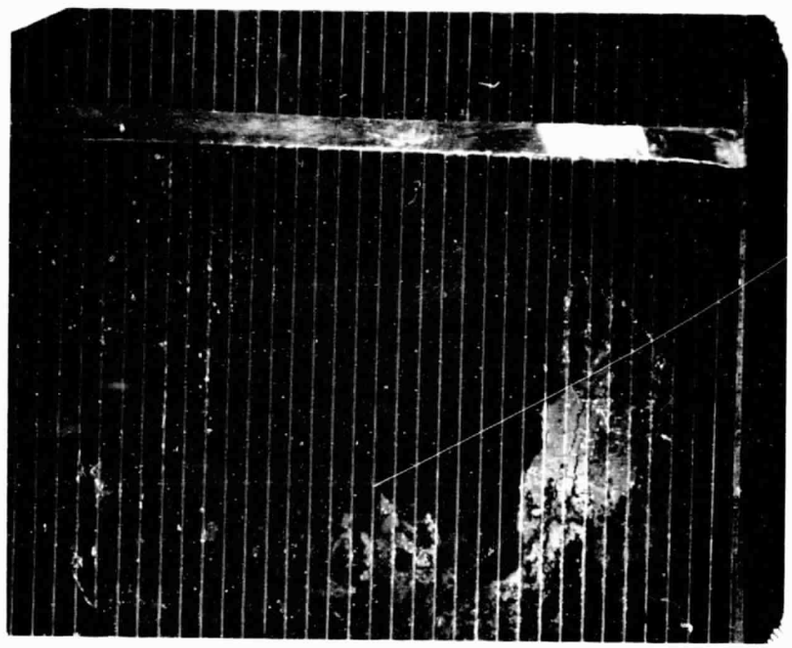

Figure 6.24. Example of Metallic Deposit on Type H B-T-H Pressure Cooker Cells.

modes in the two tests. Thus the effects of bias do exist for this cell type.

6.4 Thermal Cycle/Thermal Shock Stress Test Results

The behavior of the mean percent decrease in P_m for types F, G and H cells subjected to -65°C to +150°C thermal cycle and thermal shock are shown in Figures 6.25, 6.26 and 6.27. The data shown in these figures is somewhat misleading because only the surviving cells are included in the averages at each downtime; cells removed from the test lots due to true catastrophic failure (e.g., breaking in half) are not included. Tables 6.5, 6.6 and 6.7 show the cumulative percent of thermal shock and thermal cycle populations which experienced catastrophic failure during the tests. "Catastrophic failure" in this case means a physical effect which, in a module, would probably cause the cell to exhibit serious electrical degradation. Minor effects, such as the occurrence of a small conchoidal fracture, were not included in the tables.

Typical types of effects seen for type F cells are shown in Figure 6.28. No conchoidal fractures under metal were observed for this cell type, although in two cases conchoidal fractures oriented along the long axis of the cells, not associated with metal, were observed. Figure 6.29 shows a typical conchoidal fracture under metal, associated with tabs, for a type G cell subjected to thermal shock. This was the usual type break for type G cells, occurring in 13 of 16 cells for which serious effects were seen. Figure 6.30 shows physical effects observed for type H cells. The back metal delamination was the most common effect, occurring in 5 of 6 cells exhibiting serious effects; the sixth cell was the broken cell shown in Figure 6.30. In addition, nearly all tabs came off during the tests and during storage, prestress, for type H cells and so is not specifically associated with thermal shock or cycling.

Number of Cycles, Cumulative	Cumulative % Cells Removed, Thermal Cycle	Cumulative % Cells Removed, Thermal Shock
1	0	0
10	14.3	28.6
20	35.7	50
40	42.9	71.4

Table 6.5 Cumulative Percent Type F Cells Exhibiting Catastrophic Failure in Thermal Cycle and Thermal Shock Tests

Number of Cycles, Cumulative	Cumulative % Cells Removed, Thermal Cycle	Cumulative % Cells Removed, Thermal Shock
1	0	0
10	0	30.8
20	38.5	61.5
40	61.5	61.5

Table 6.6 Cumulative Percent Type G Cells Exhibiting Catastrophic Failure in Thermal Cycle and Thermal Shock Tests

Number of Cycles, Cumulative	Cumulative % Cells Removed, Thermal Cycle	Cumulative % Cells Removed, Thermal Shock
1	25	50
10	25	50
20	25	50
40	25	50

Table 6.7 Cumulative Percent Type H Cells Exhibiting Catastrophic Failure in Thermal Cycle and Thermal Shock Tests

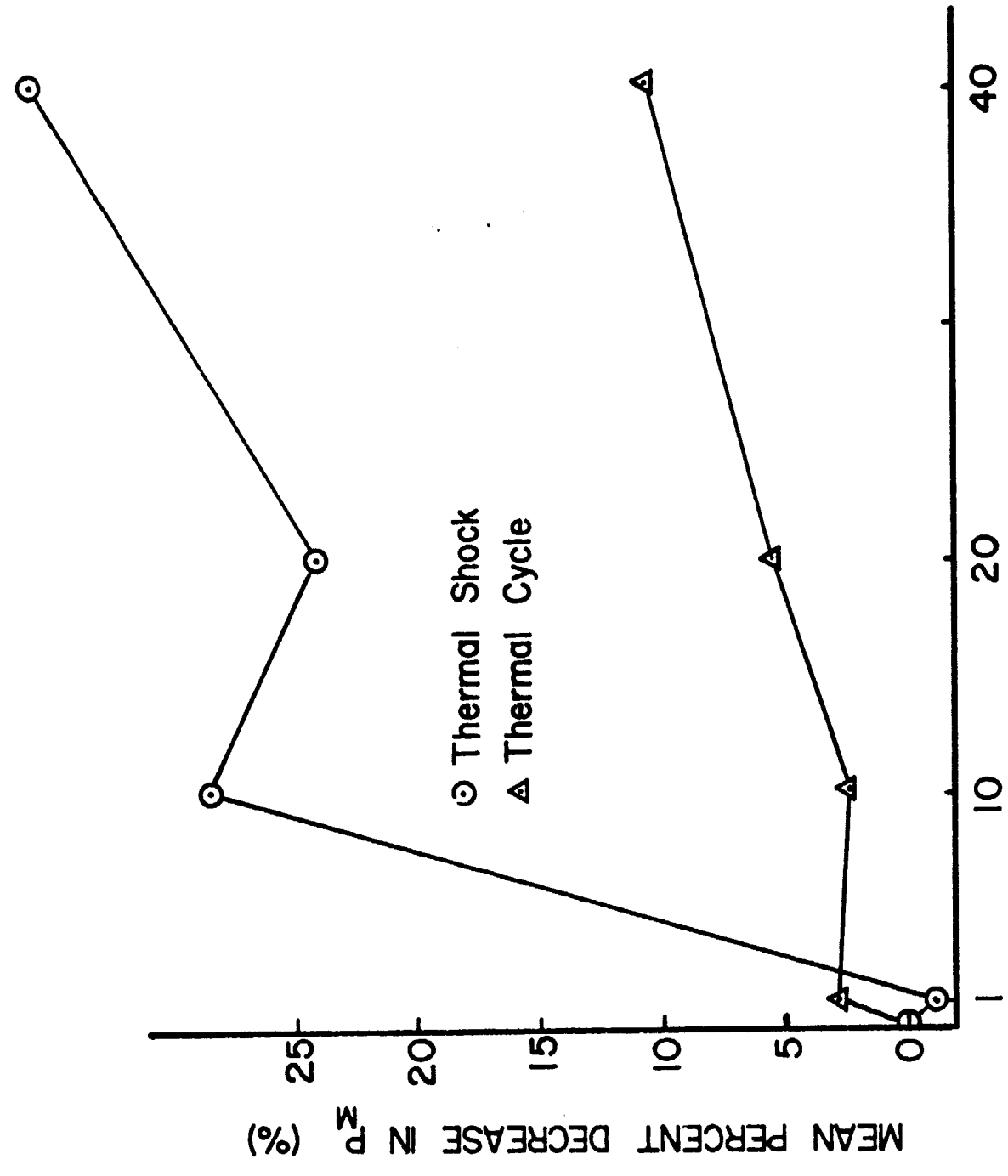

Figure 6.25. Mean Percent Decrease in P_m for Type F Cells, Thermal Cycle and Thermal Shock Stress Tests.

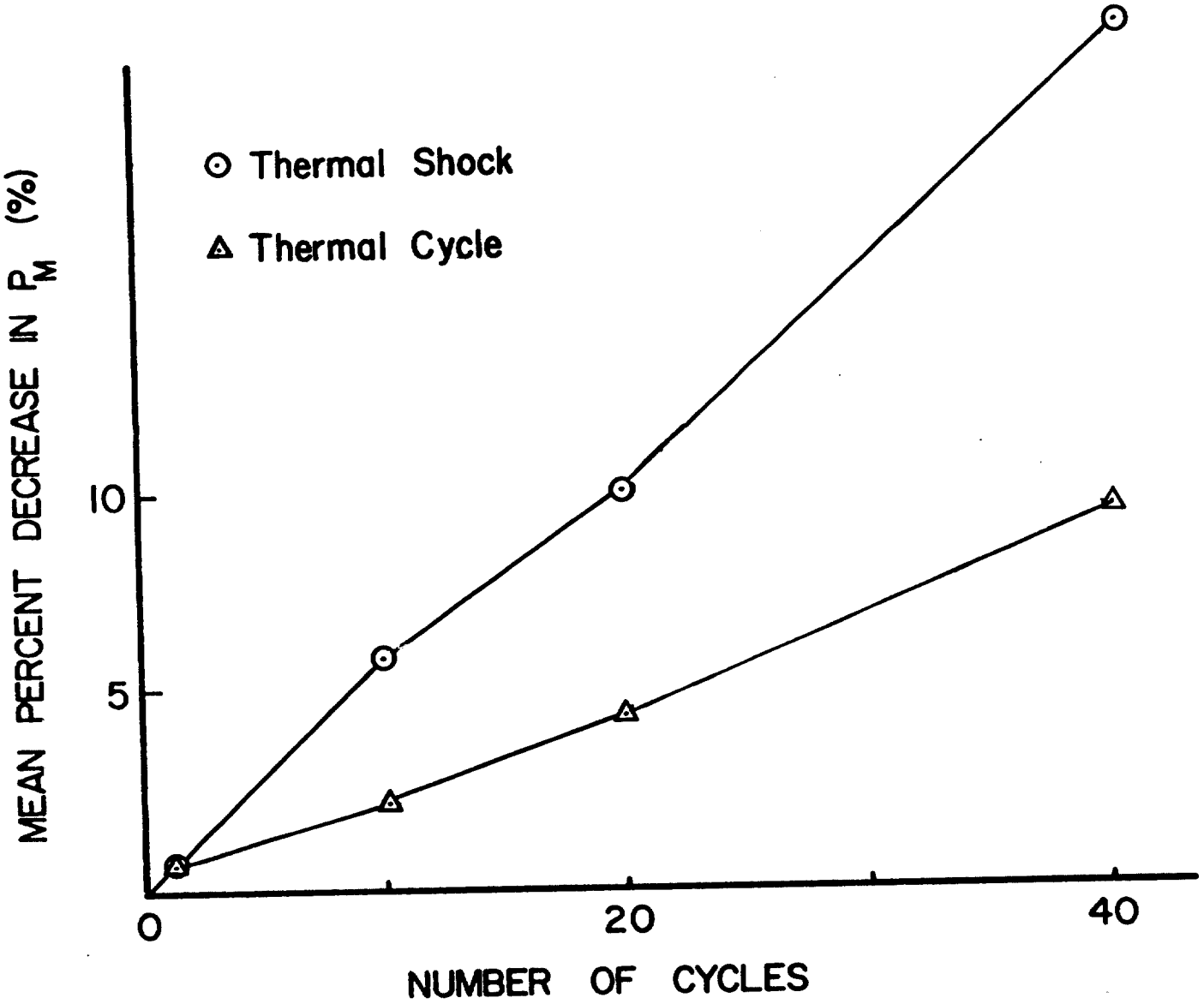

Figure 6.26. Mean Percent Decrease in P_m for Type G Cells, Thermal Cycle and Thermal Shock Stress Tests.

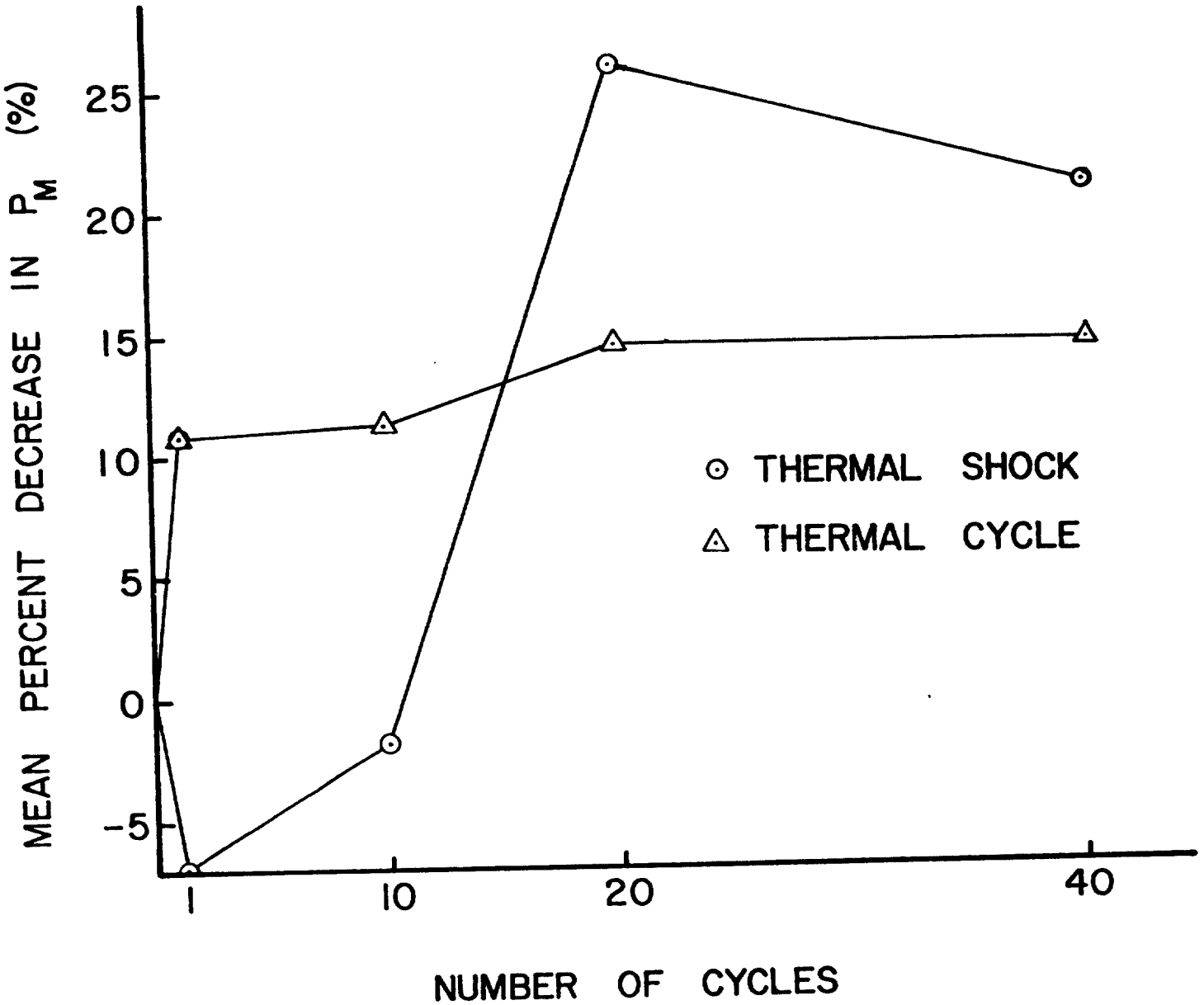

Figure 6.27. Mean Percent Decrease in P_m for Type H Cells, Thermal Cycle and Thermal Shock Stress Tests.

ORIGINAL PAGE IS
OF POOR QUALITY

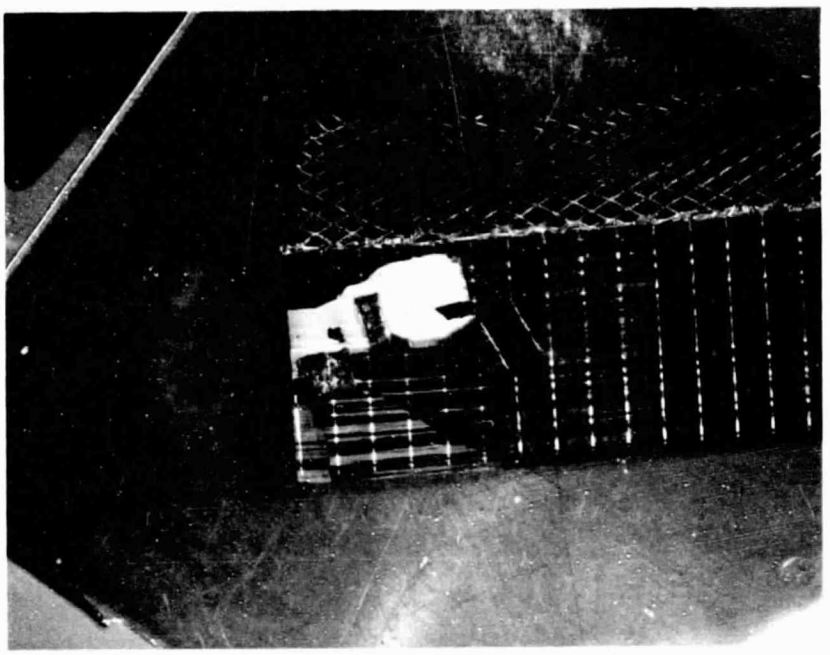

(a)

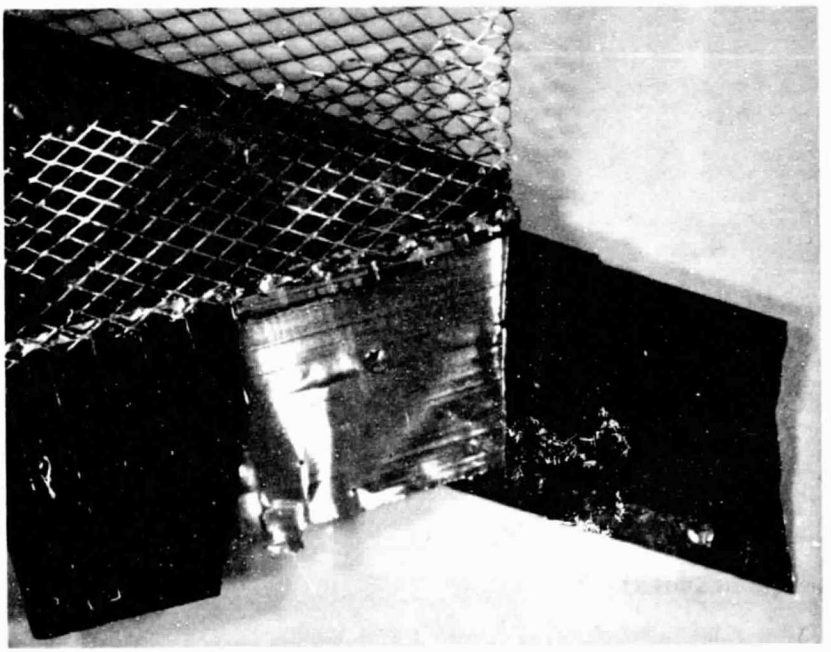

(b)

Figure 6.28. Typical Physical Effects of Thermal Shock/Thermal Cycle on Type F Cells.

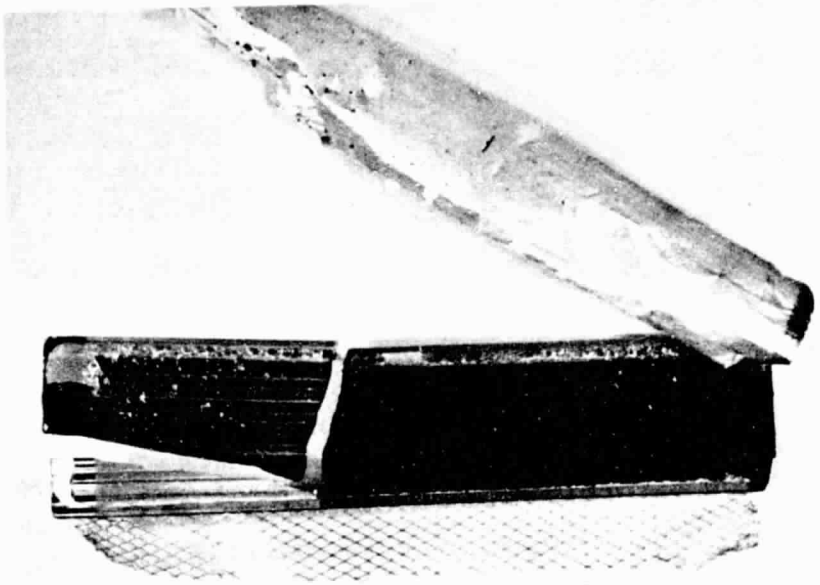

(c)

Figure 6.28. (Continued)

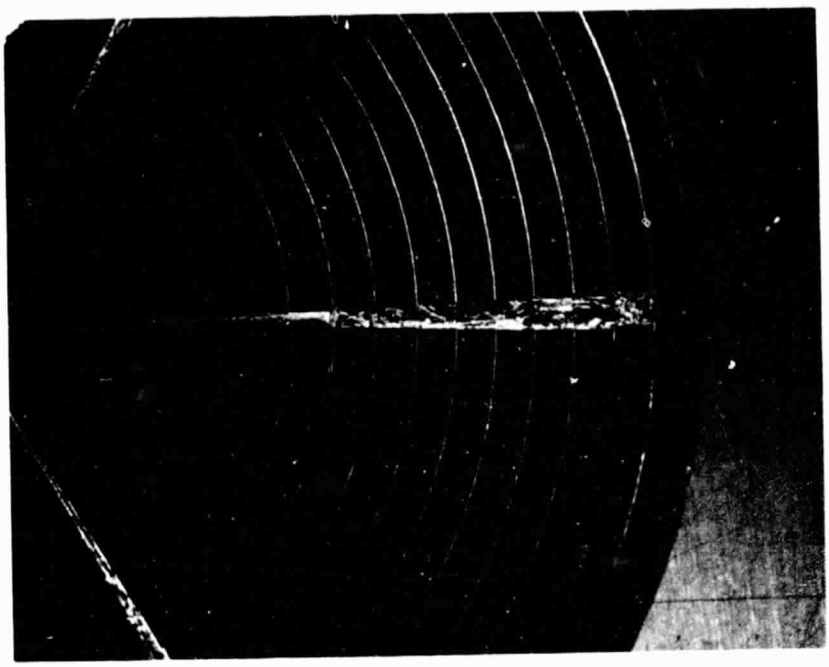

Figure 6.29. Typical Conchoidal Fracture Caused by Thermal Shock, Type G Cell.

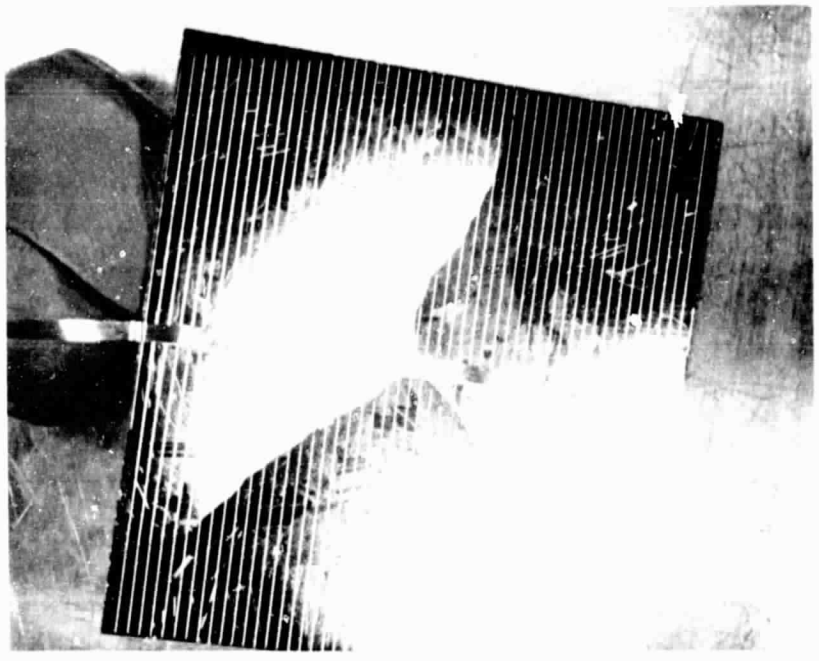

(a)

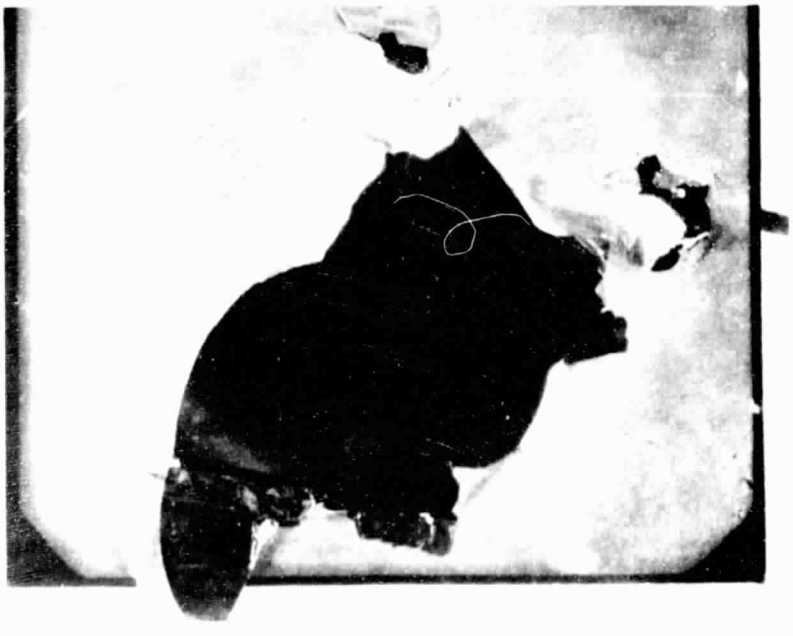

(b)

Figure 6.30. Typical Physical Effects of Thermal Cycle/Thermal Shock on Type H Cells.

7.0 CONCLUSIONS

7.0 CONCLUSIONS

1. A preliminary look at a limited number of cells has verified the thermal nature of the second quadrant characteristics. Three operating ranges have been identified: a region of uniform temperature in excess of ambient, but less that 170°C (solder melting temperature); a region of uniform temperature in excess of 170°C, but less than the temperature at which the base becomes intrinsic (approximately 300°C); and a region of non-uniform temperature in which hot spots in excess of 300°C appear. This third region is one with positive thermal feedback and unless the current is externally limited melting of silicon can result with catastrophic results.

Breakdown in the second quadrant has been traditionally defined by the knee of the characteristic. Since the temperature of the knee is roughly the temperature at which the base becomes intrinsic, independent of whether the knee occurs at a low voltage or a high voltage, a cell with a high breakdown should be able to survive second quadrant operation better than a cell with a low breakdown, all other characteristics being equal.

2. Extended B-T testing of the A, B, C, and E cells illustrated the value of long term testing. Continuation of these cells to 9000 hours "uncovered" an enhanced rate of degradation in E cells at 135°C, similar to that seen earlier at 165°C. The extended tests thus confirmed that the 165° effect was not anomalous and at the same time was able to supply information concerning the effect's activation energy. The 135°C data, when combined with the 165°C data, however, is not sufficient to yield an accurate estimate of the activation energy - - data at an additional temperature is required. For this reason the 75°C cells (as well as the 135°C cells) are being continued on test in hopes they too will show an enhanced rate of degradation at a later date.

3. Figure 7.1 summarizes the relative effect on P_m of the various stress tests for the three cell types investigated. In this figure, the darkest square signify a degradation which was progressive with stress test duration, and significantly above the "noise" of the measurement technique. The lightest squares signify no discernable effect after stressing. "Medium" squares denote cases between the two extremes. Obviously subjective judgement was required in formulating the figure.

It can be seen from an examination of the columns of this figure that F cells showed appreciable degradation in all stress test whereas G and H cells showed only moderate to no degradation in many of the stress categories. It should be pointed out again, as it was in the first annual report, that while these conclusions demonstrate the applicability and potential usefulness of the technique, they should not be interpreted at this time as a quantitative measure of field degradation rates. It is felt that the technique is capable of such prediction, but considerable additional stress testing and field degradation analysis will be required before conclusive evidence can be demonstrated.

4. Breakage during thermal cycle/thermal shock continued to be a major problem. Cell type F, which utilized EFG material, showed severe breakage (shattering mode) after only 10 thermal cycles or shocks. It is felt that this problem is probably due to the unique nature of the material rather than the cell structure. Type G cells, which utilized Czochralski material, were also susceptible to thermal cycle/thermal shock, but damage was limited to small conchoidal fractures, usually under contact points, and a greater number of cycles were required for development. Type H cells, manufactured from Wacker polycrystalline materials, were reasonably insensitive to breakage, although there was a tendency for the entire back contact to lift off.

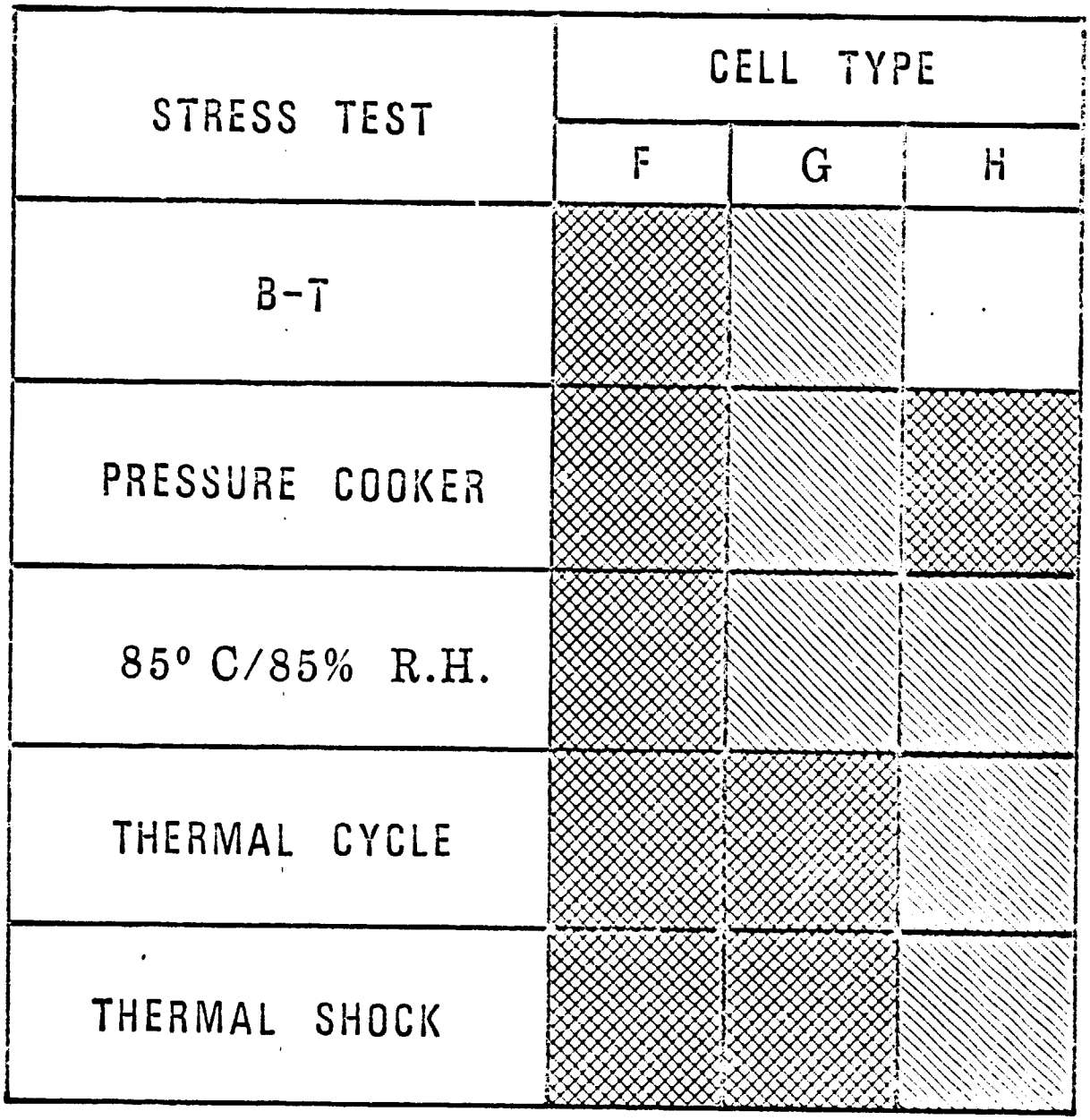

Figure 7.1 Relative Effects of Accelerated Stress Tests on P_m.

5. Although it is not apparent from the summary figure, difficulty was experienced with the manufacturer's attached leads of type H cells. These leads were attached by welding, and were often either over-welded so that the ribbon was burned through, or under-welded so that the ribbon fell off prior to stress.

6. Also not discernable from the summary-type data of Figure 7.1 is the occurrence of infant mortality or "freak" failures in the F cells. This type of failure had been predicted, but had not previously been observed. It should be pointed out, however, that only a few infant mortalities were observed and it would not be economically feasible to institute any type of burn-in procedure as routinely performed on integrated circuits.

7. Differences in the response of cells to both the pressure cooker and the 85/85 temperature-relative humidity tests indicate that both types of tests need to be continued, at least for the present. Similarity of the biased and unbiased pressure cooker tests leads to the conclusion that it may not be necessary to bias cells during pressure cooker stressing. Bias is required in 85/85 testing, however.

8.0 RECOMMENDATIONS

8.0 RECOMMENDATIONS

1. It is recommended that the preliminary reliability qualification test schedule for reliability monitoring described in the first annual report be modified to eliminate the need for bias in connection with pressure cooker tests.

2. It is recommended that quantities of F, G, and H cells be continued on bias-temperature stress to obtain additional degradation vs. time data similar to that being obtained on A, B, C, and E cell types.

3. In light of the unusual response of F cells to thermal cycle/thermal shock stress (shattering), it is recommended that a program to ascertain the cause be initiated.

4. As a consequence of the unexplained test results encountered with H cells on thermal cycle/thermal shock testing it is recommended that a program be initiated to better understand why some cells simultaneously showed an increase in P_m and a peeling of backside metalization.

5. Further investigation into second quadrant effects should be performed. Items to be covered include thermal modeling, additional data to permit statistical characterization of electrical data, and pulse response measurements.

6. It is recommended that the possibility of using forced second quadrant operations as a part of the stress test schedule be investigated.

9.0 NEW TECHNOLOGY

9.0 NEW TECHNOLOGY

Two items of new technology which have been submitted to the appropriate NASA legal office are the electrical measurement jig, described in Section 4 and the new stress test fixture, described in Section 3.

APPENDICES

APPENDIX A: Electrical Parameter Distributions of Type F, G, and H Solar Cells

In this Appendix the prestress distributions of the five primary cell electrical parameters are shown for types F, G, and H cells. The distributions were obtained by measurement of the parameters of 180 type F cells, 188 type G cells, and 77 type H cells. These cells constitute the total stress test populations for this phase of the program.

Cell Type	Total Units Measured	Mean P_m (W)	Standard Deviation (W)
F	186	.198	.015
G	194	.603	.020
H	82	.211	.028

Table A-1. Mean P_m and Standard Deviation for Prestress Cell Population

Cell Type	Total Units Measured	Mean I_{sc} (A)	Standard Deviation (A)
F	186	.506	.021
G	194	1.343	.021
H	82	.566	.064

Table A-2. Mean I_{sc} and Standard Deviation for Prestress Cell Population

Cell Type	Total Units Measured	Mean V_{oc} (V)	Standard Deviation (V)
F	186	.547	.010
G	194	.589	.040
H	82	.520	.012

Table A-3. Mean V_{oc} and Standard Deviation for Prestress Cell Population

Cell Type	Total Units Measured	Mean I_m (A)	Standard Deviation (A)
F	186	.444	.025
G	194	1.223	.033
H	82	.498	.055

Table A-4. Mean I_m and Standard Deviation for Prestress Cell Population

Cell Type	Total Units Measured	Mean V_m (V)	Standard Deviation (V)
A	186	.445	.011
B	194	.494	.007
C	82	.423	.020

Table A-5. Mean V_m and Standard Deviation for Prestress Cell Population

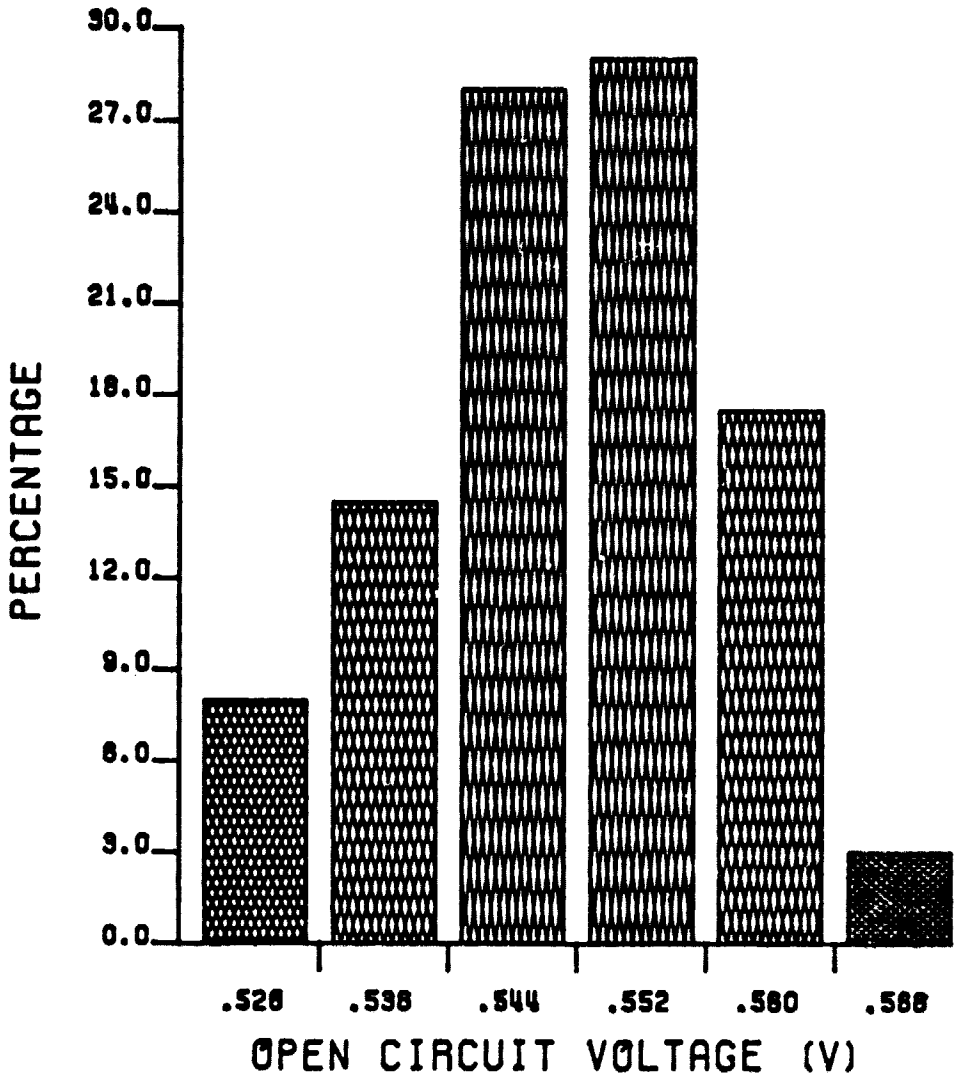

Figure A-1. Prestress Distribution of V_{oc}, Type F.

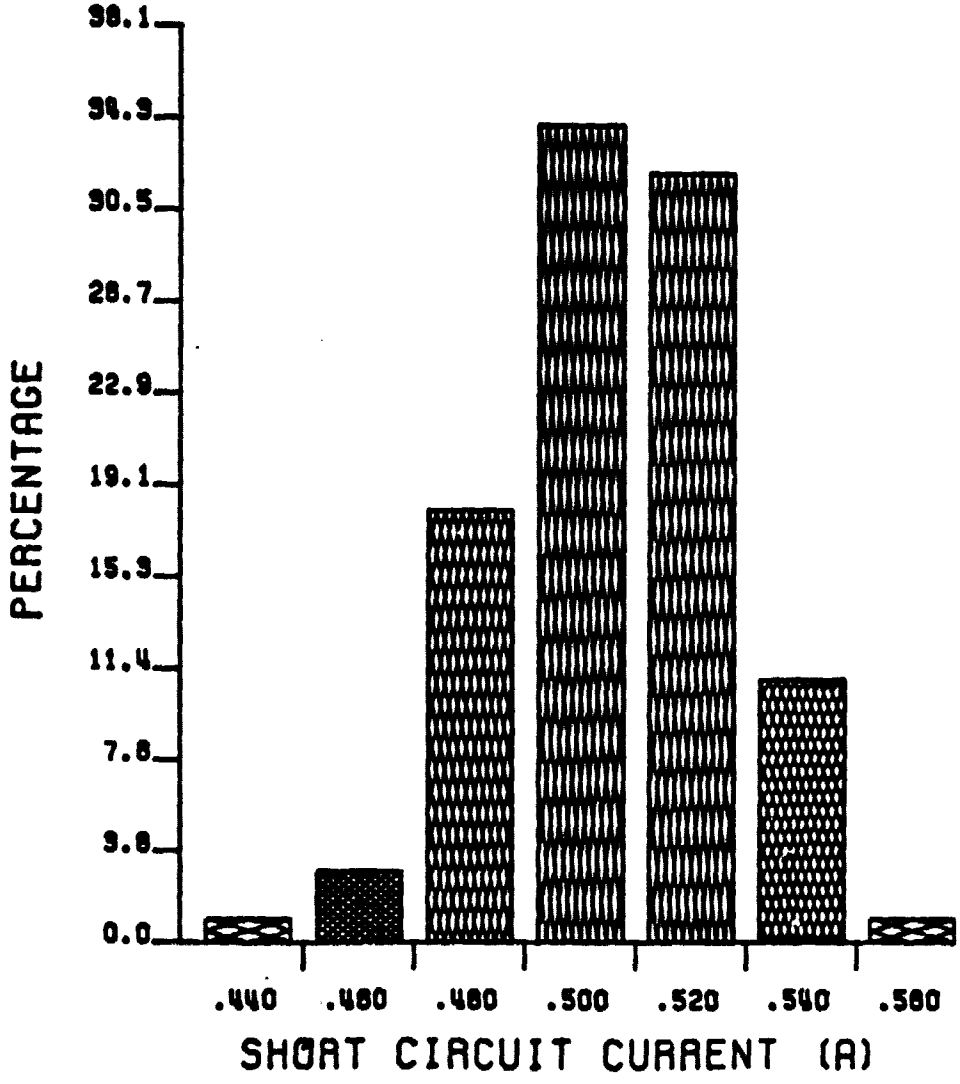

Figure A-2. Prestress Distribution of I_{sc}, Type F.

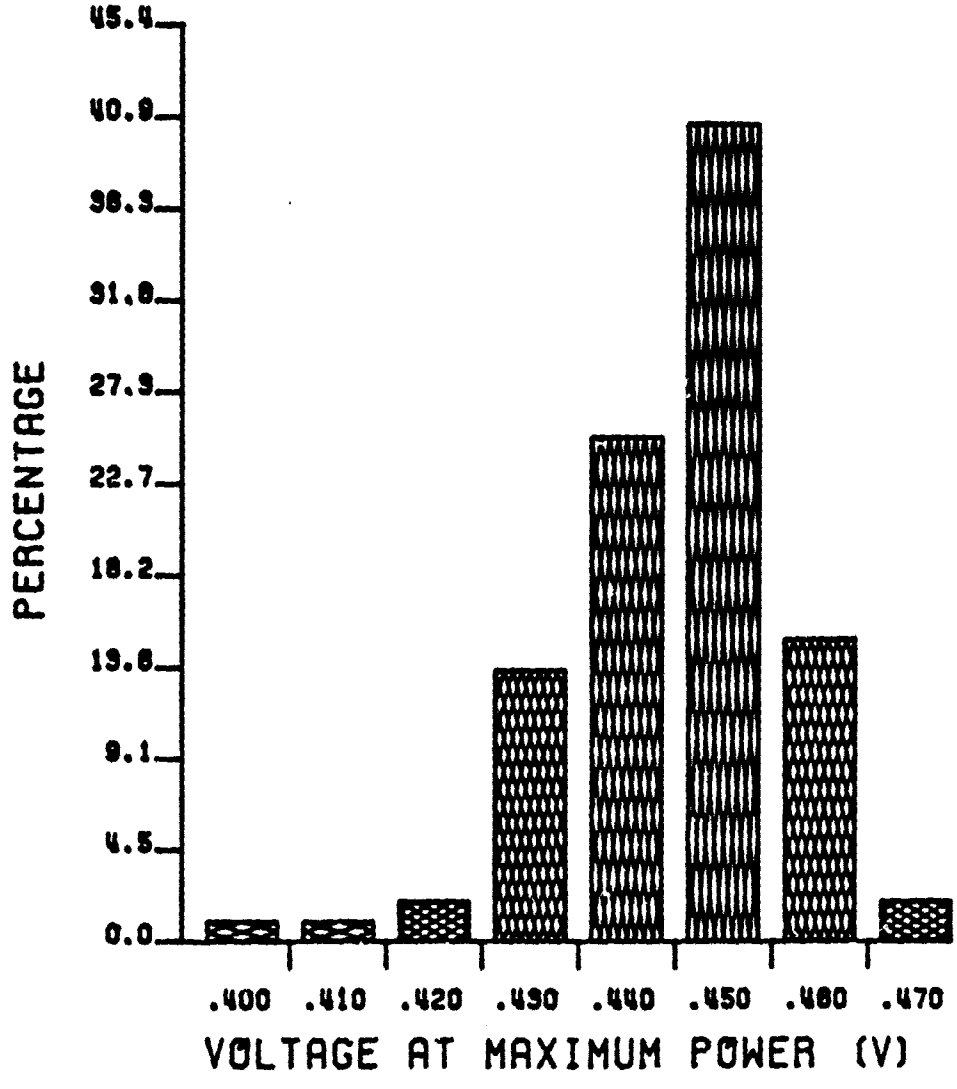

Figure A-3. Prestress Distribution of V_m, Type F.

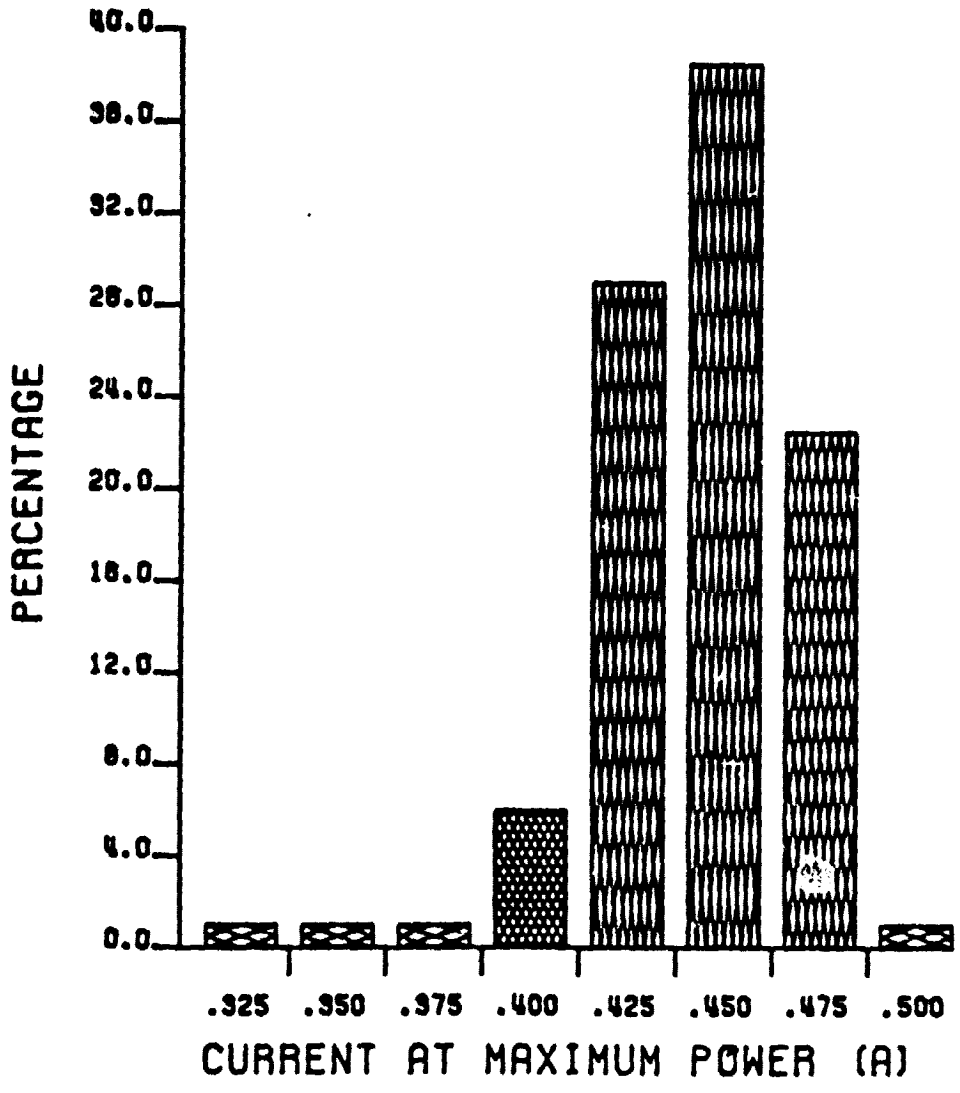

Figure A-4. Prestress Distribution of I_m, Type F.

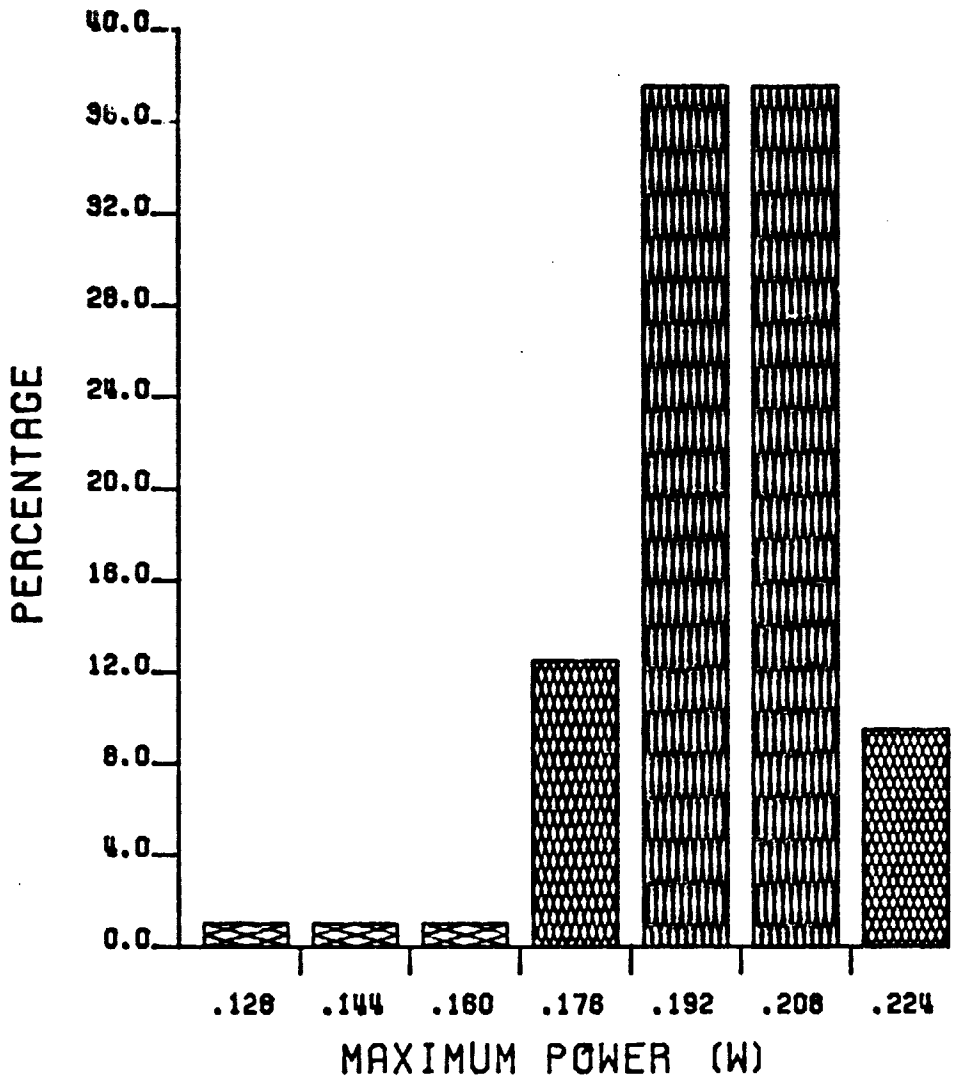

Figure A-5. Prestress Distribution of P_m, Type F.

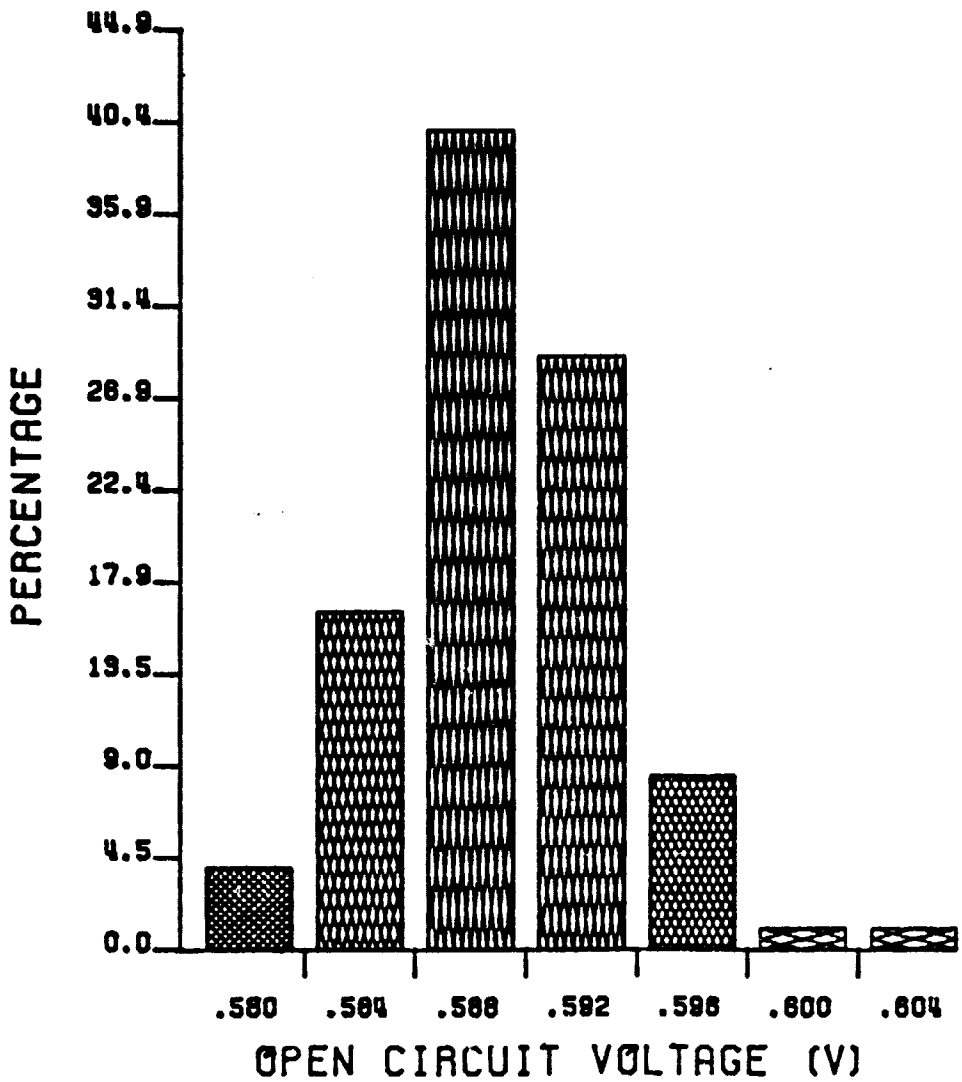

Figure A-6. Prestress Distribution of V_{oc}, Type G.

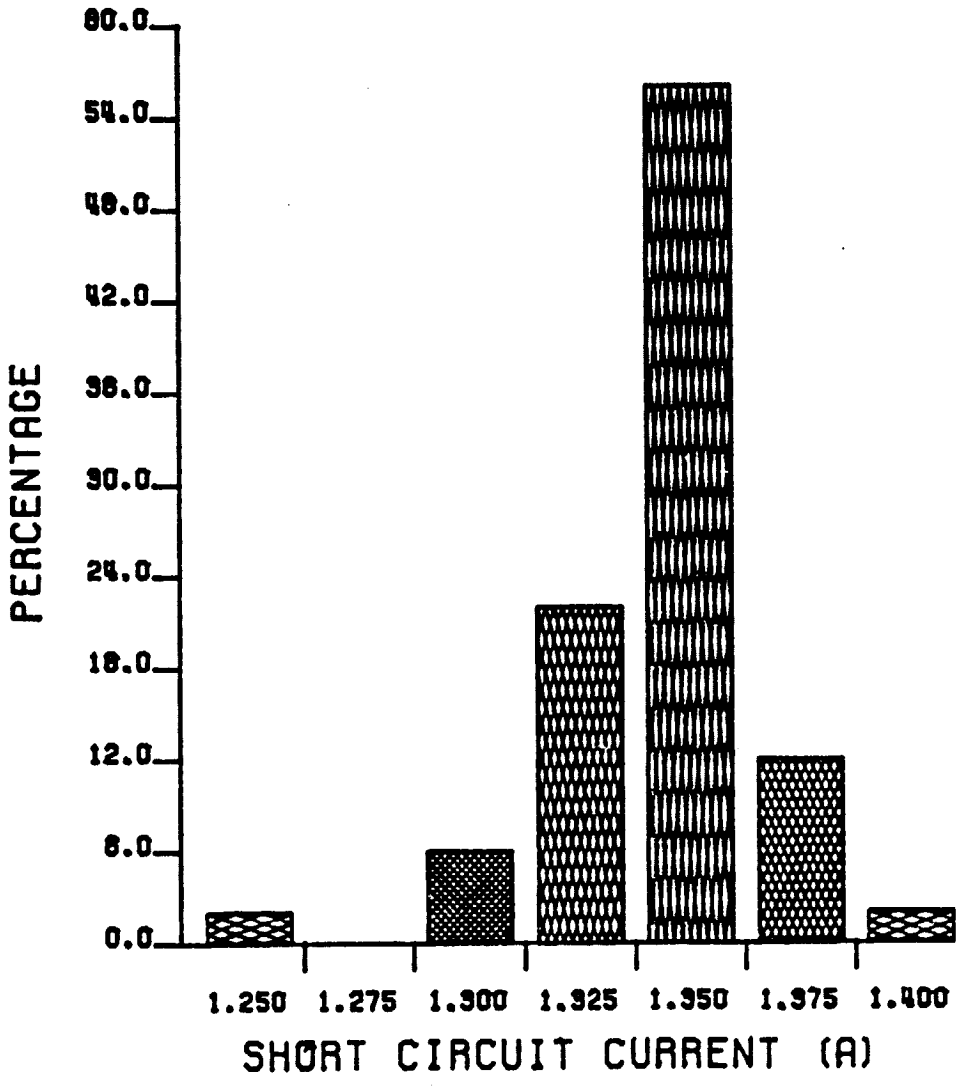

Figure A-7. Prestress Distribution of I_{sc}, Type G.

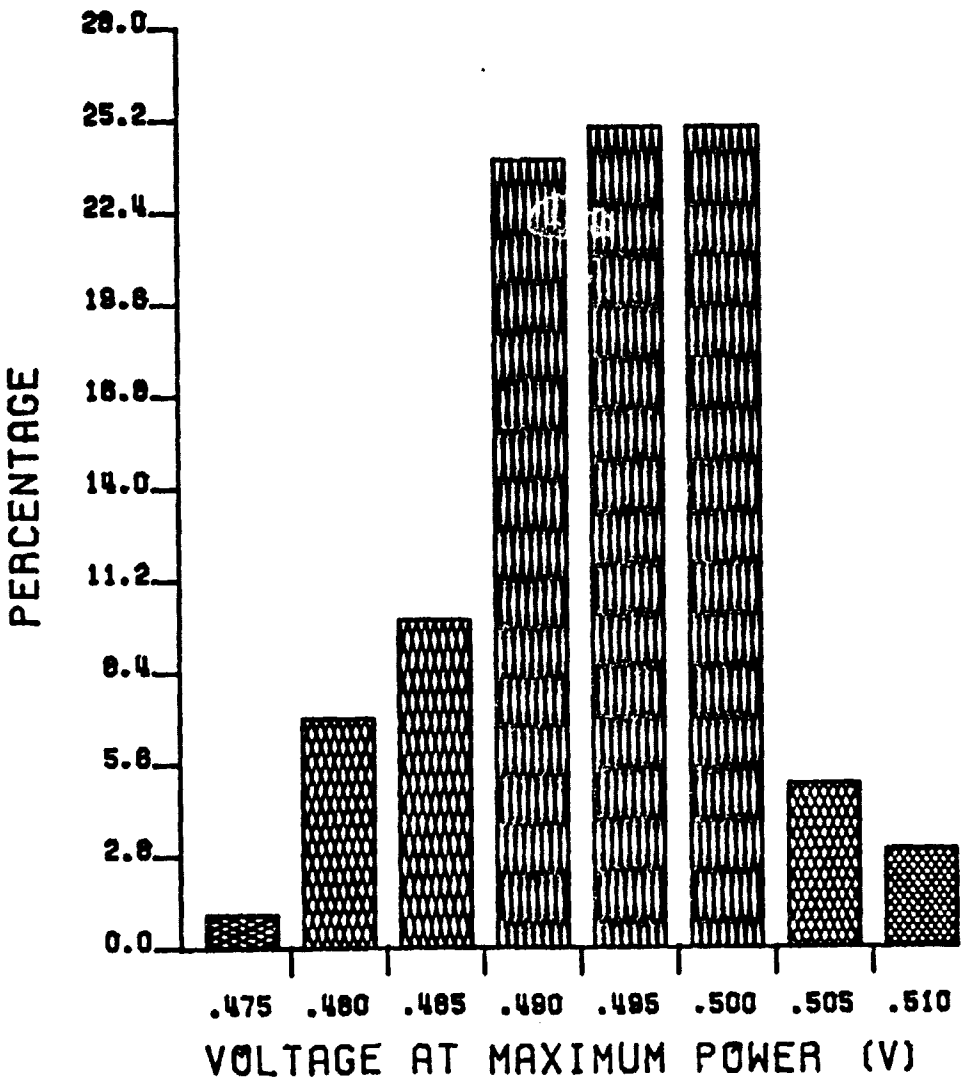

Figure A-8. Prestress Distribution of V_m, Type G.

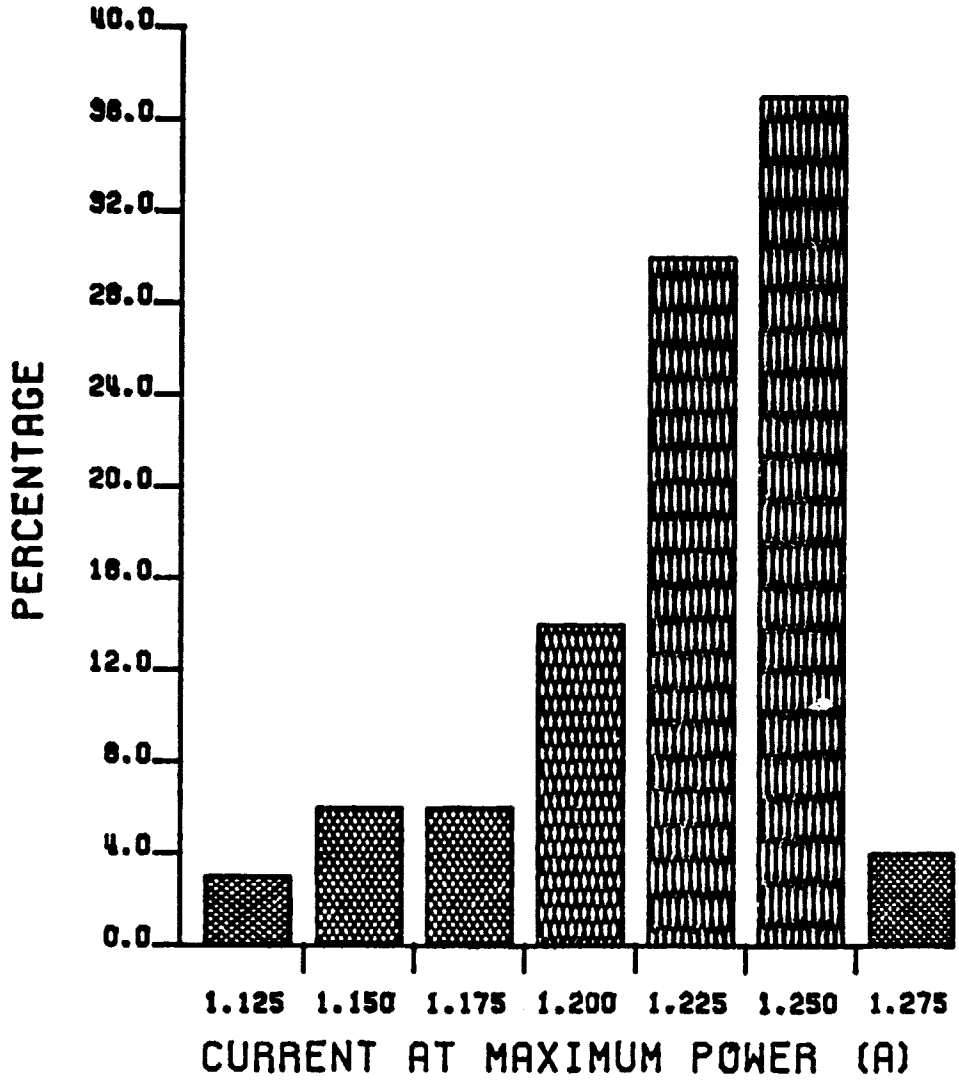

Figure A-9. Prestress Distribution of I_m, Type G.

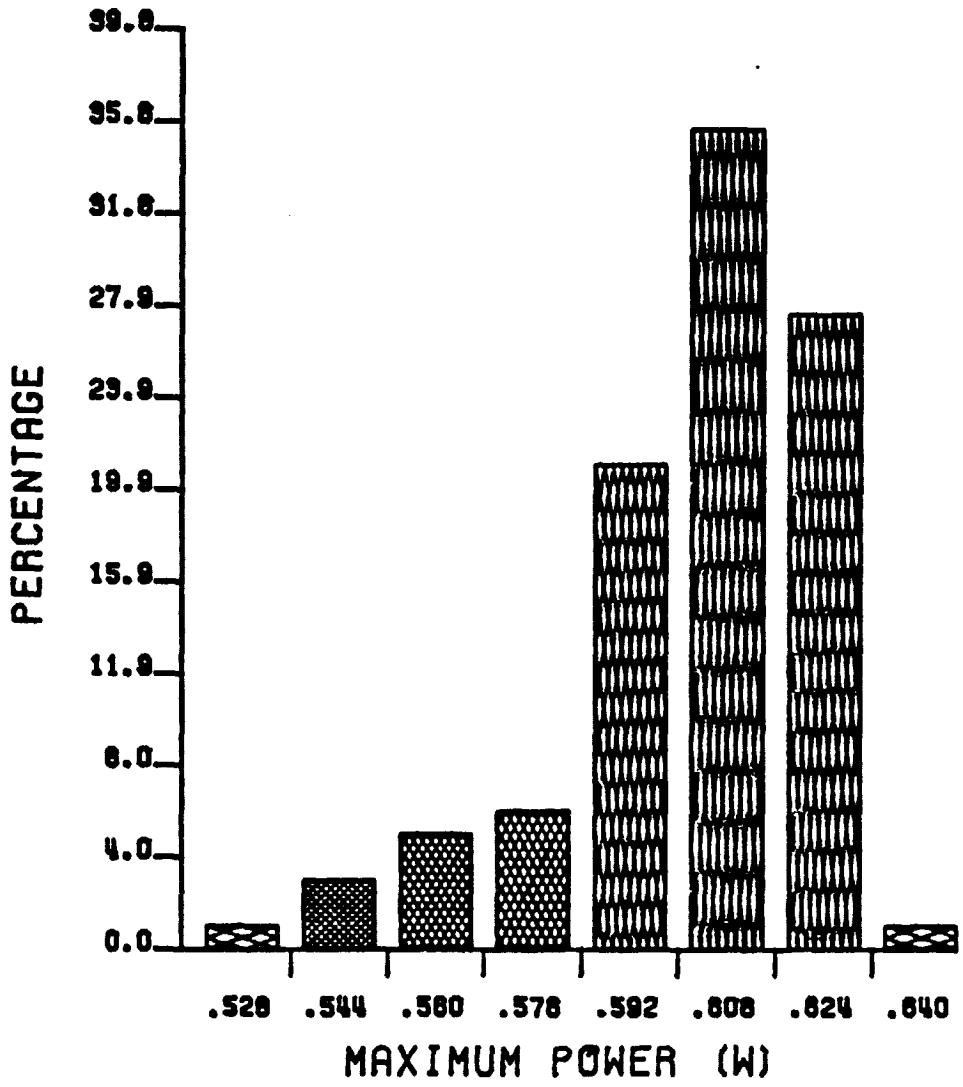

Figure A-10. Prestress Distribution of P_m, Type G.

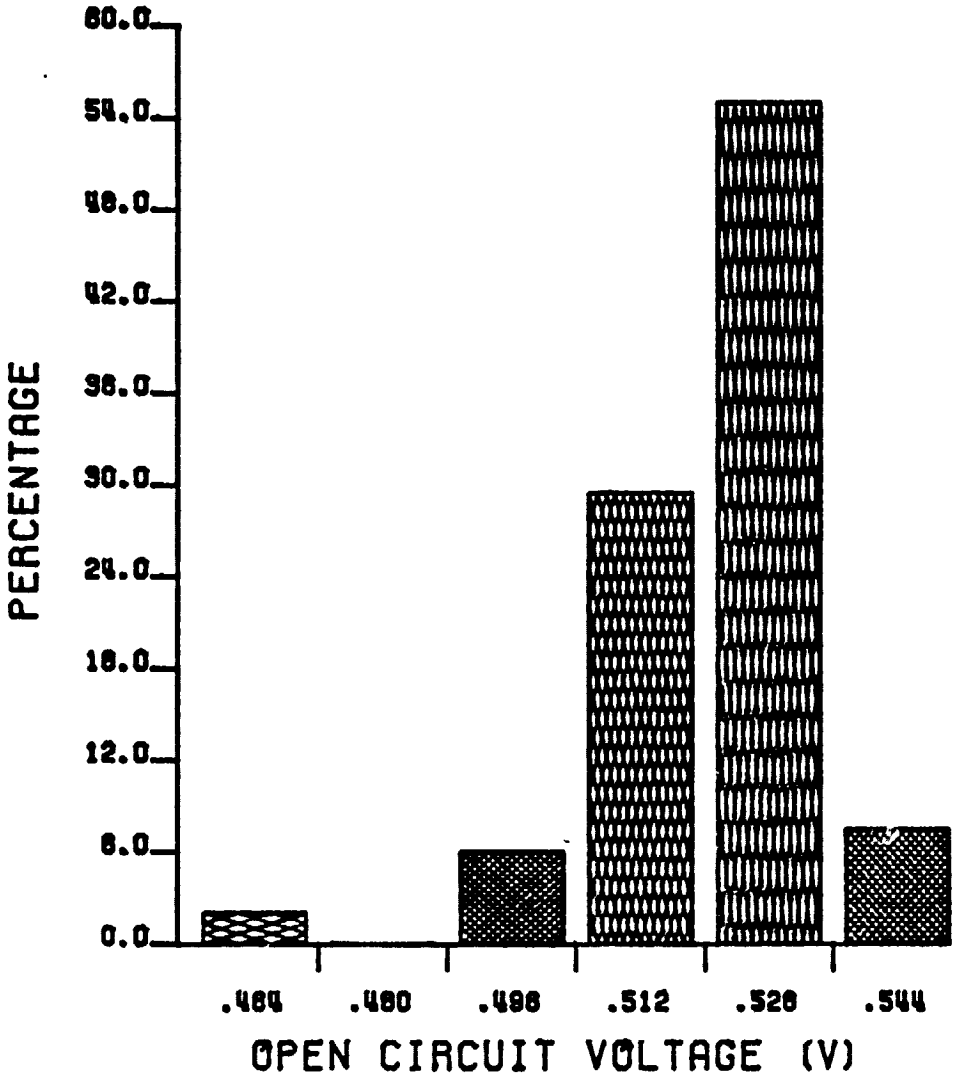

Figure A-11. Prestress Distribution of V_{oc}, Type H.

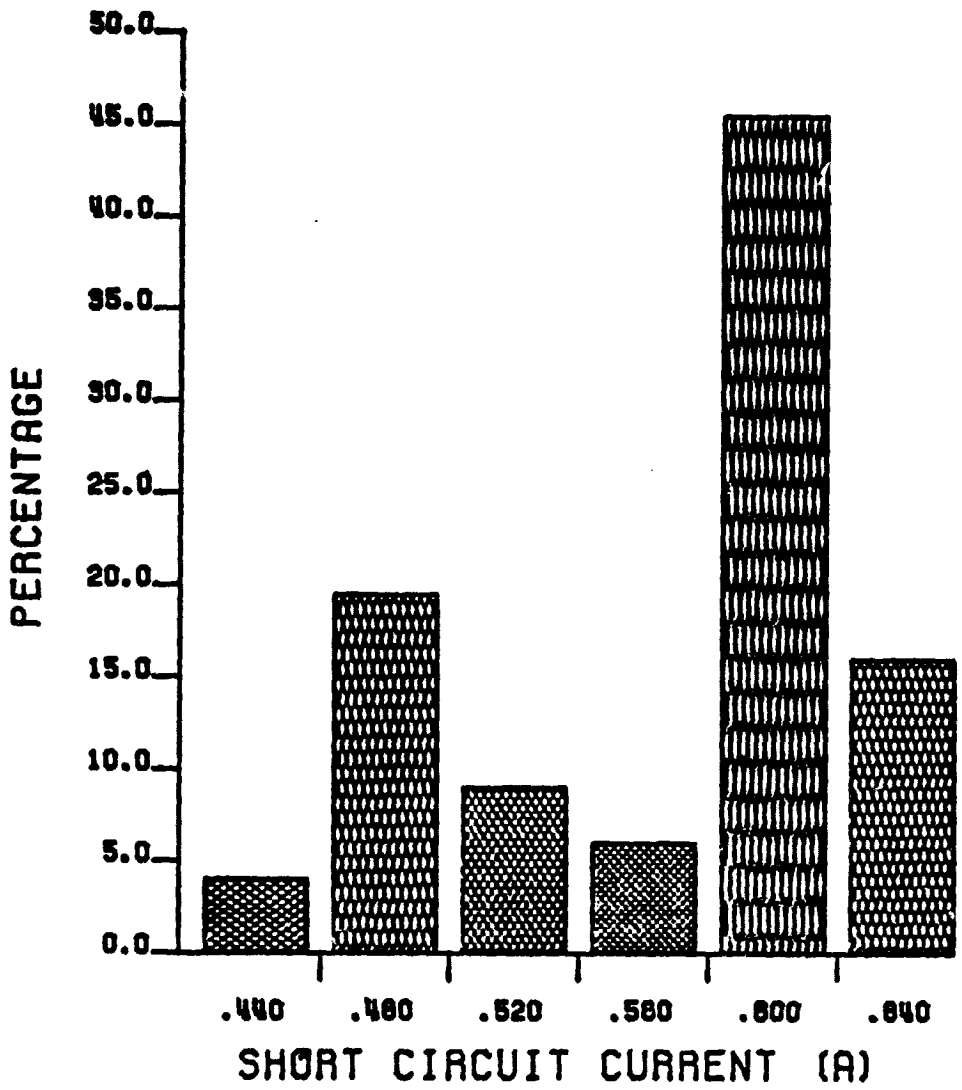

Figure A-12. Prestress Distribution of I_{sc}, Type H.

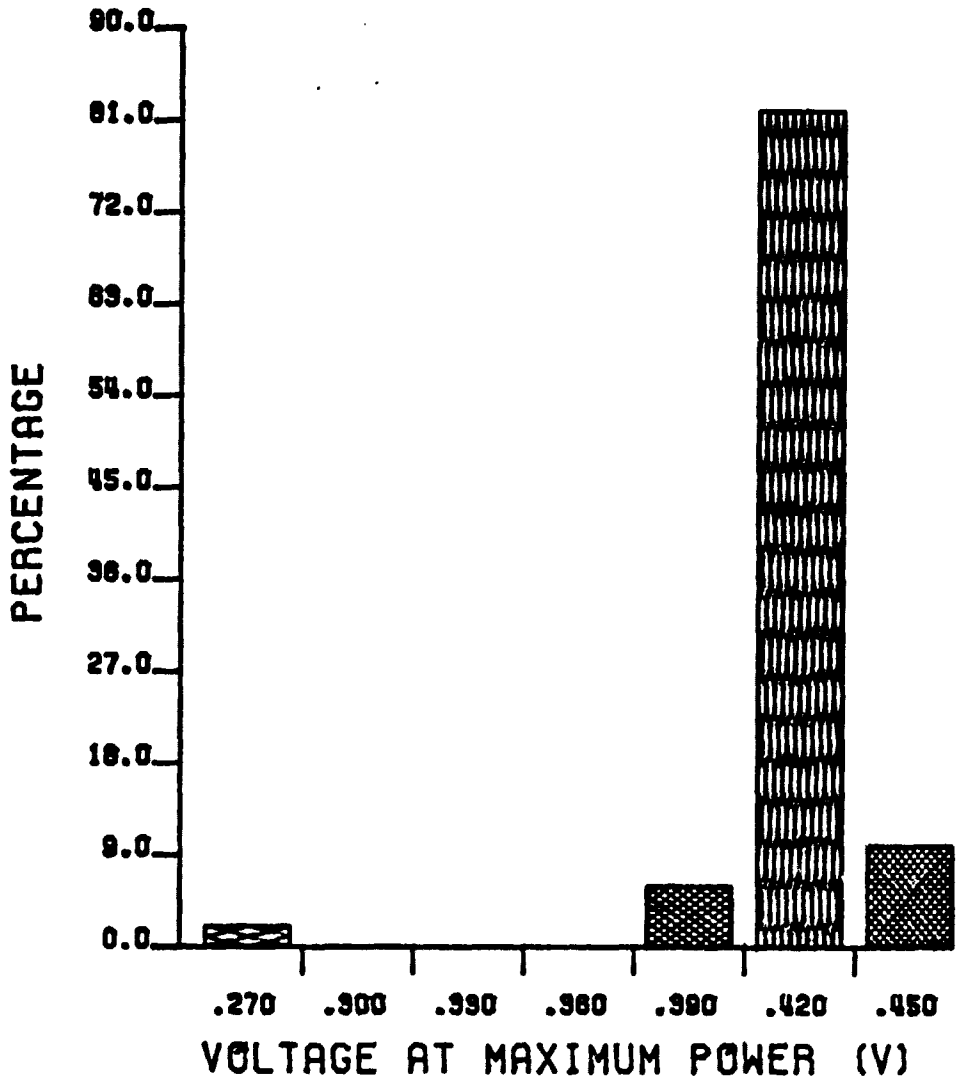

Figure A-13. Prestress Distribution of V_m, Type H.

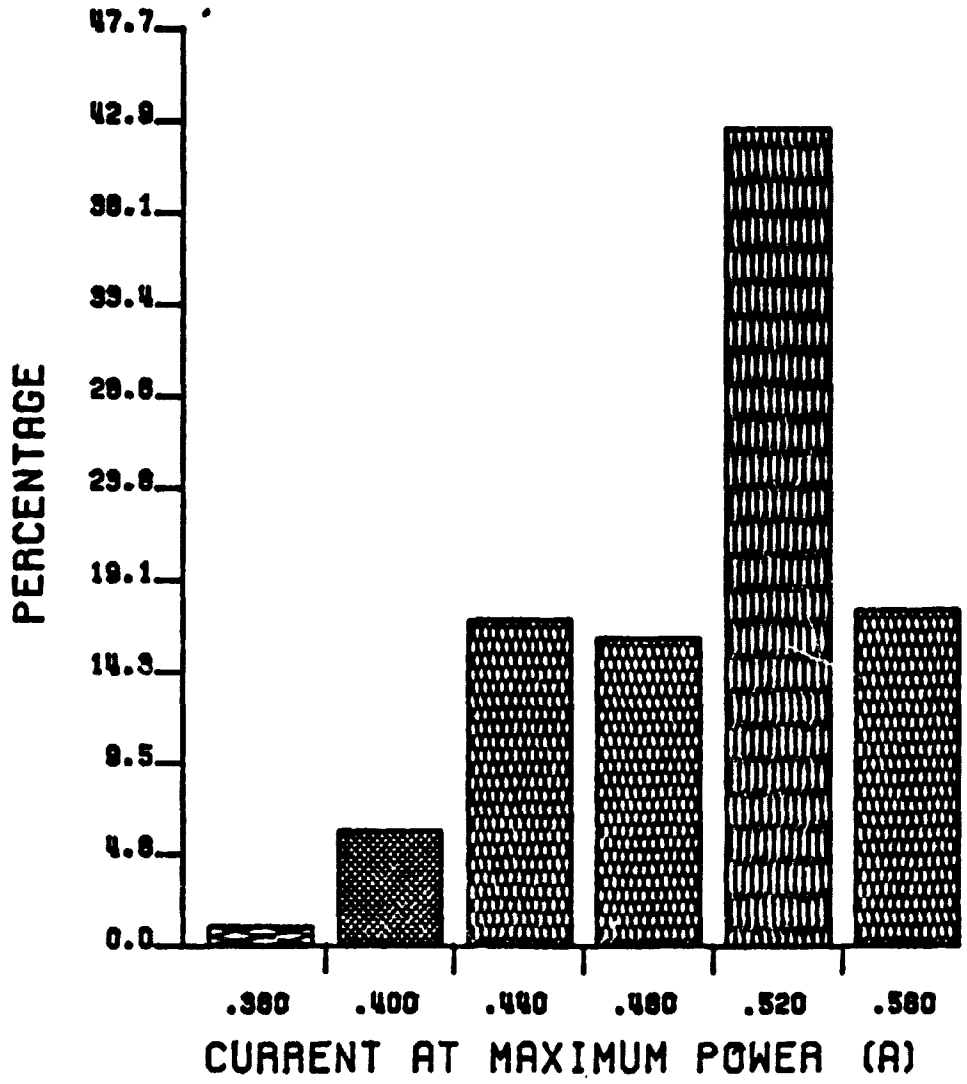

Figure A-14. Prestress Distribution of I_m, Type H.

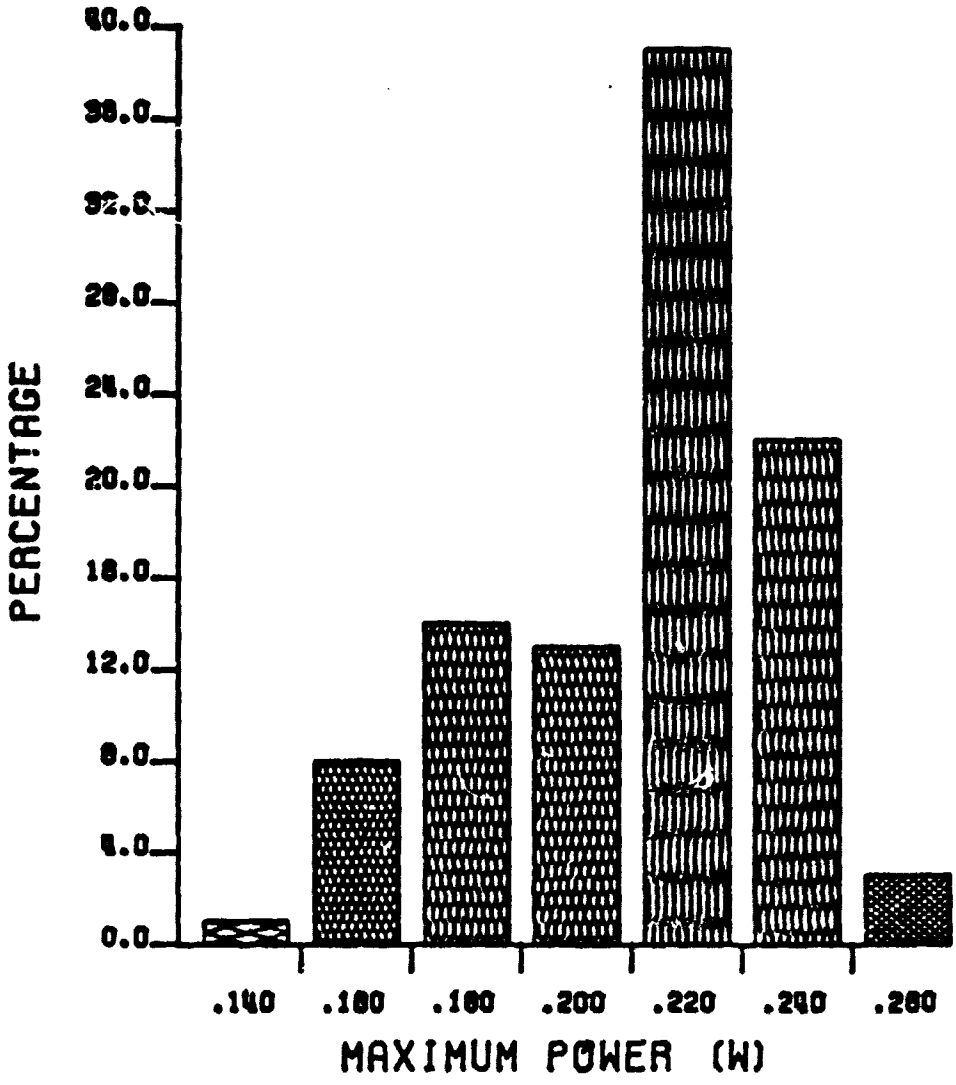

Figure A-15. Prestress Distribution of P_m, Type H.

APPENDIX B. VARIATION OF CELL ELECTRICAL PARAMETERS WITH TEMPERATURE

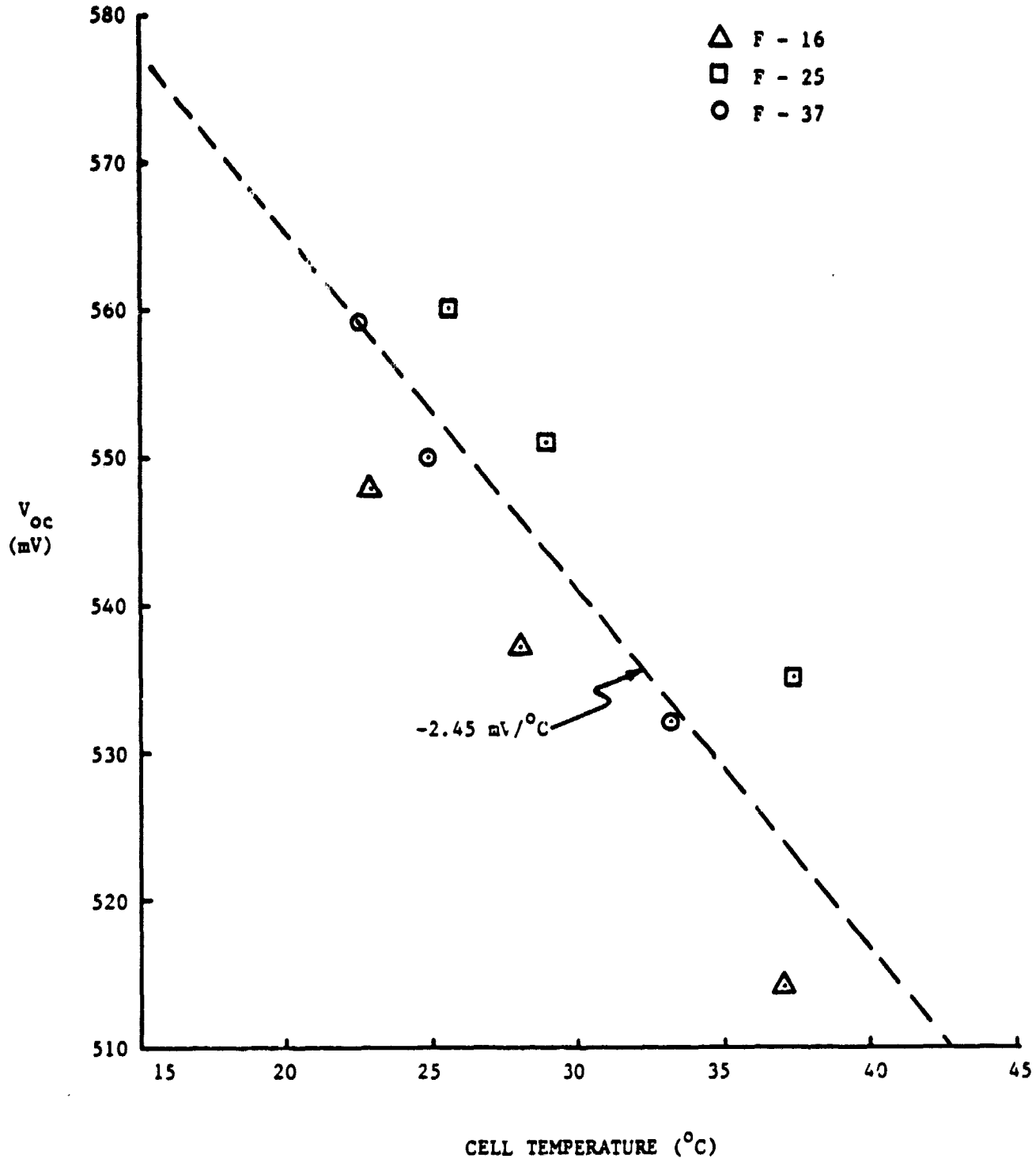

Figure B-1. V_{oc} vs. T for F-Cells Showing Average Slope.

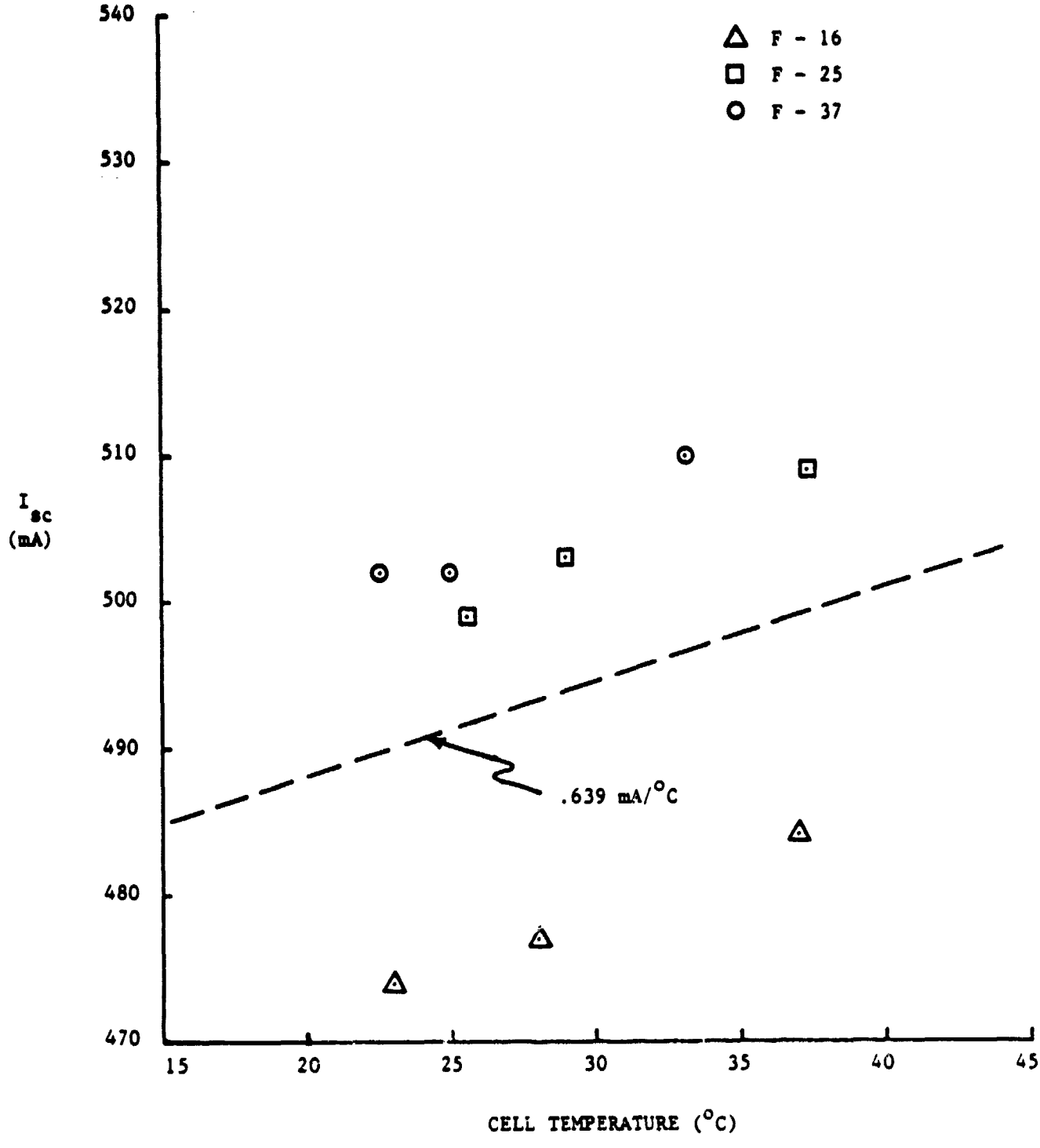

Figure B-2. I_{sc} vs. T for F-Cells Showing Average Slope.

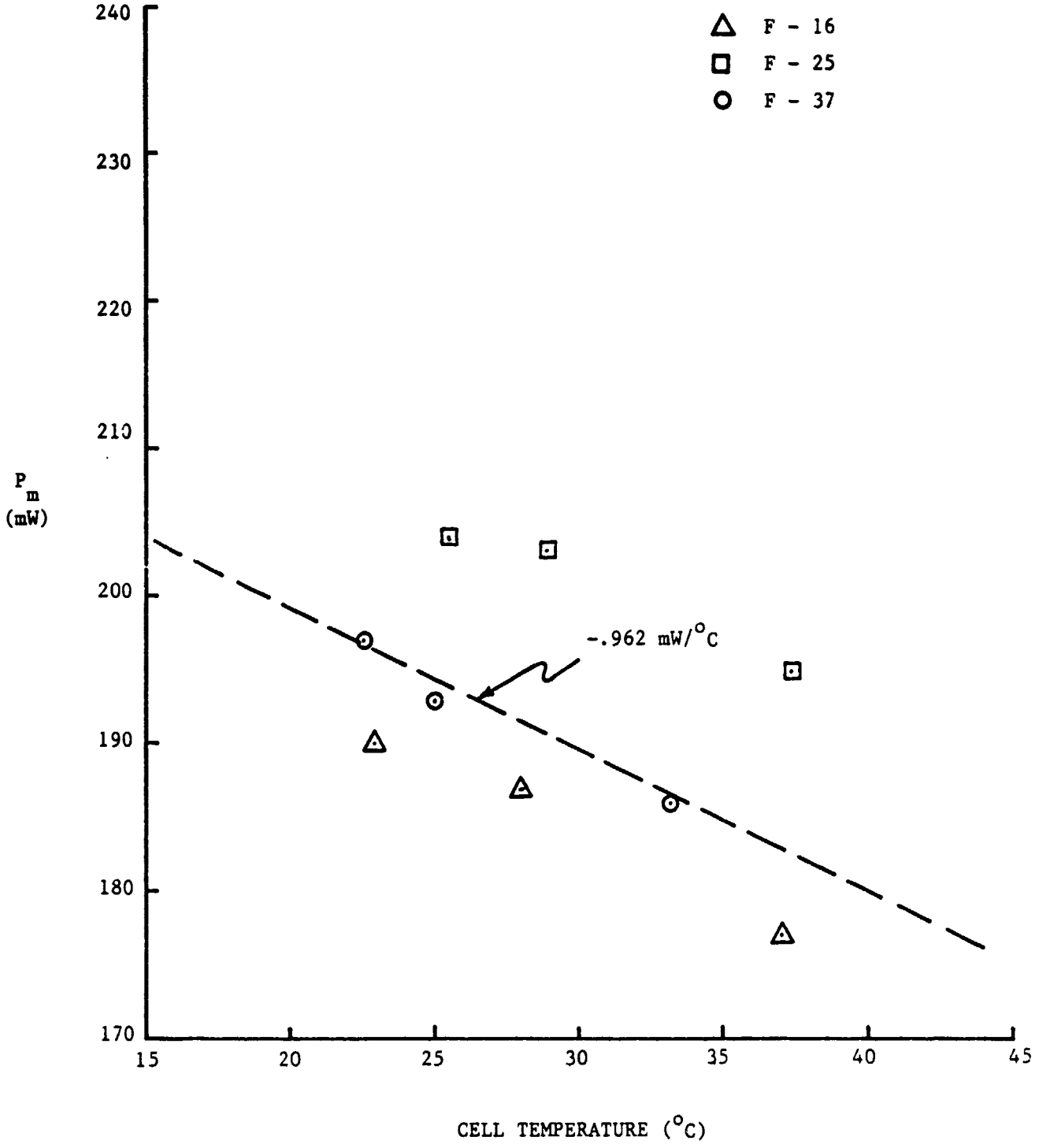

Figure B-3. P_m vs. T for F-Cells Showing Average Slope.

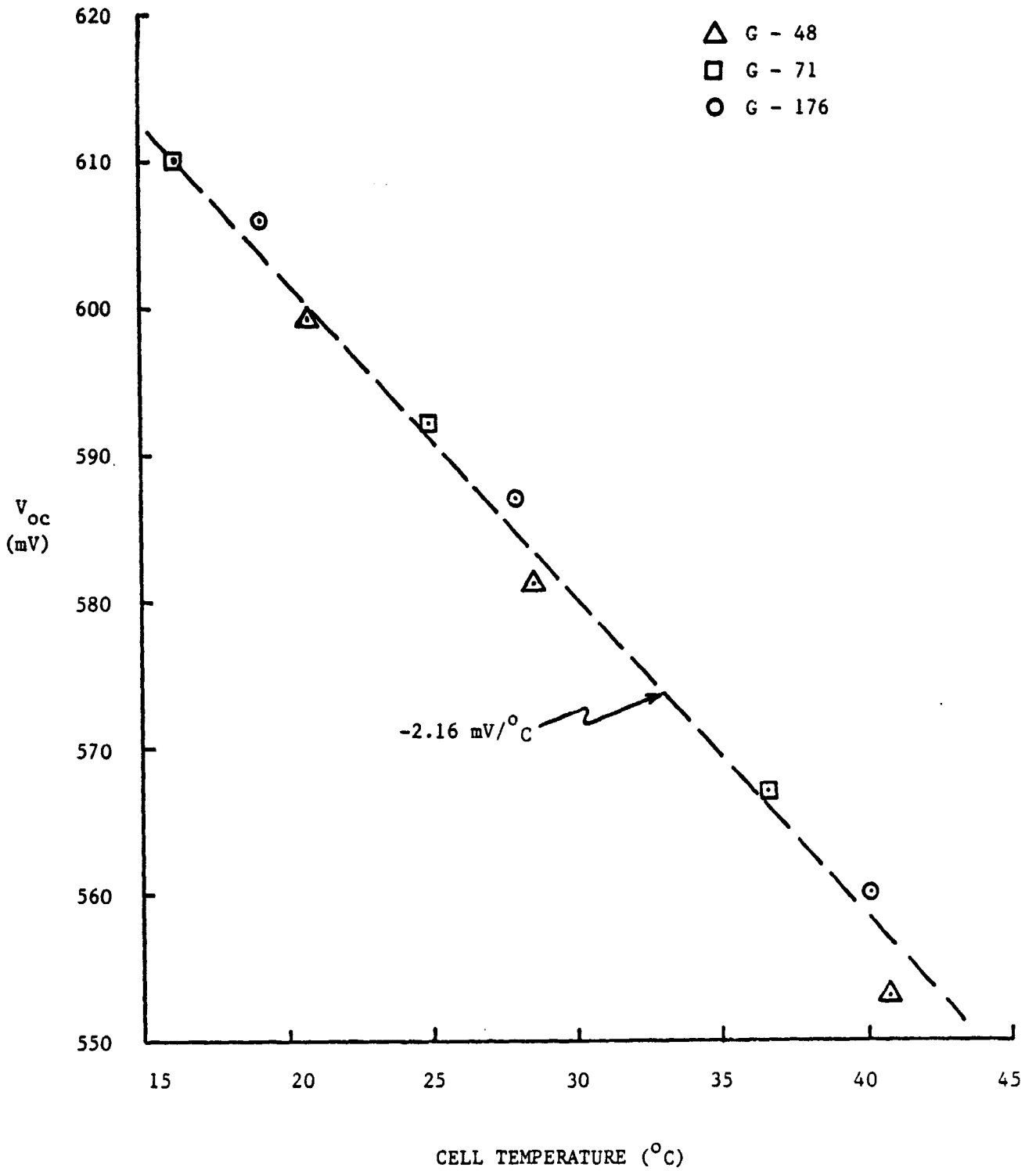

Figure B-4. V_{oc} vs. T for G-Cells Showing Average Slope.

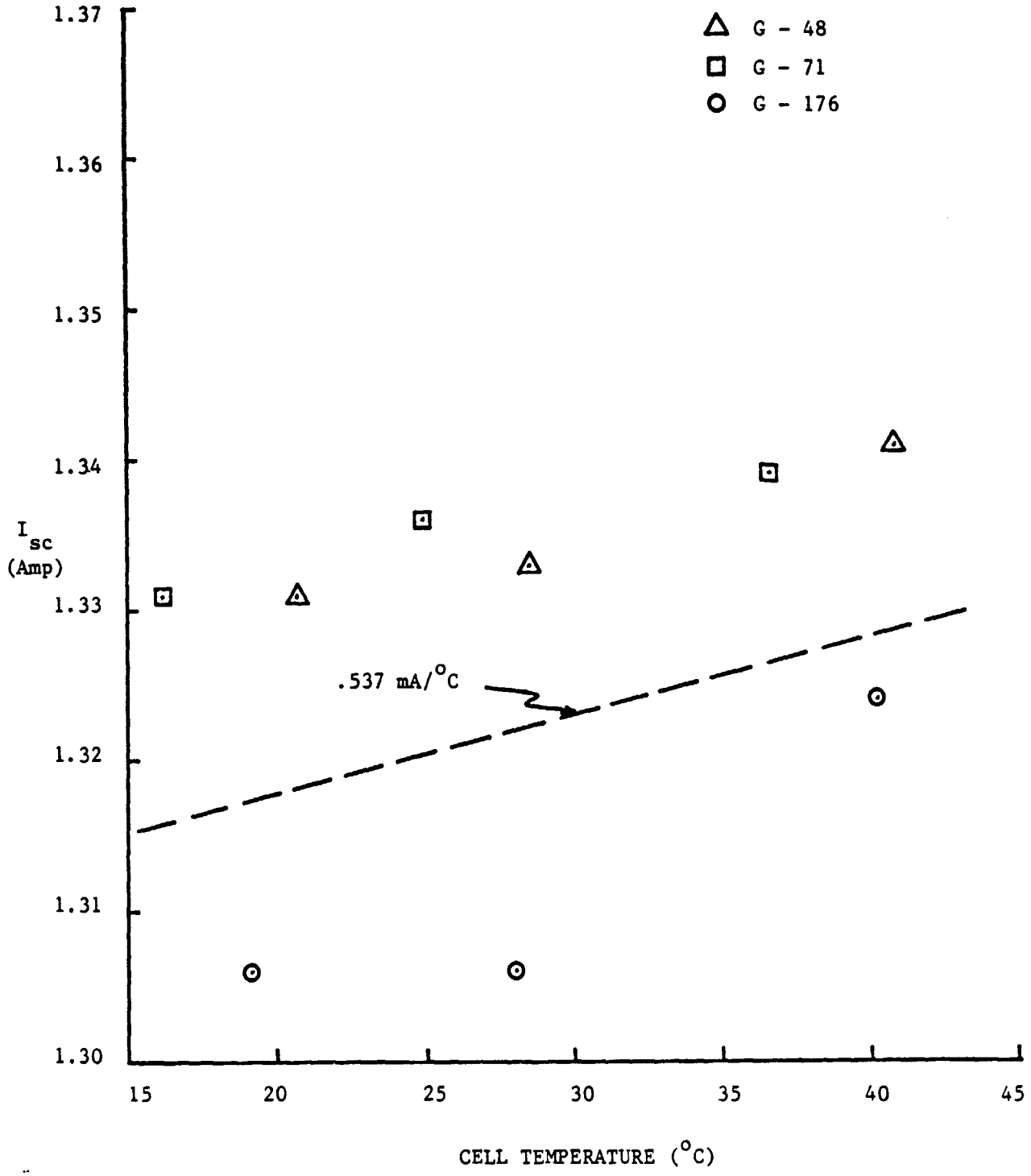

Figure B-5. I_{sc} vs. T for G-Cells Showing Average Slope.

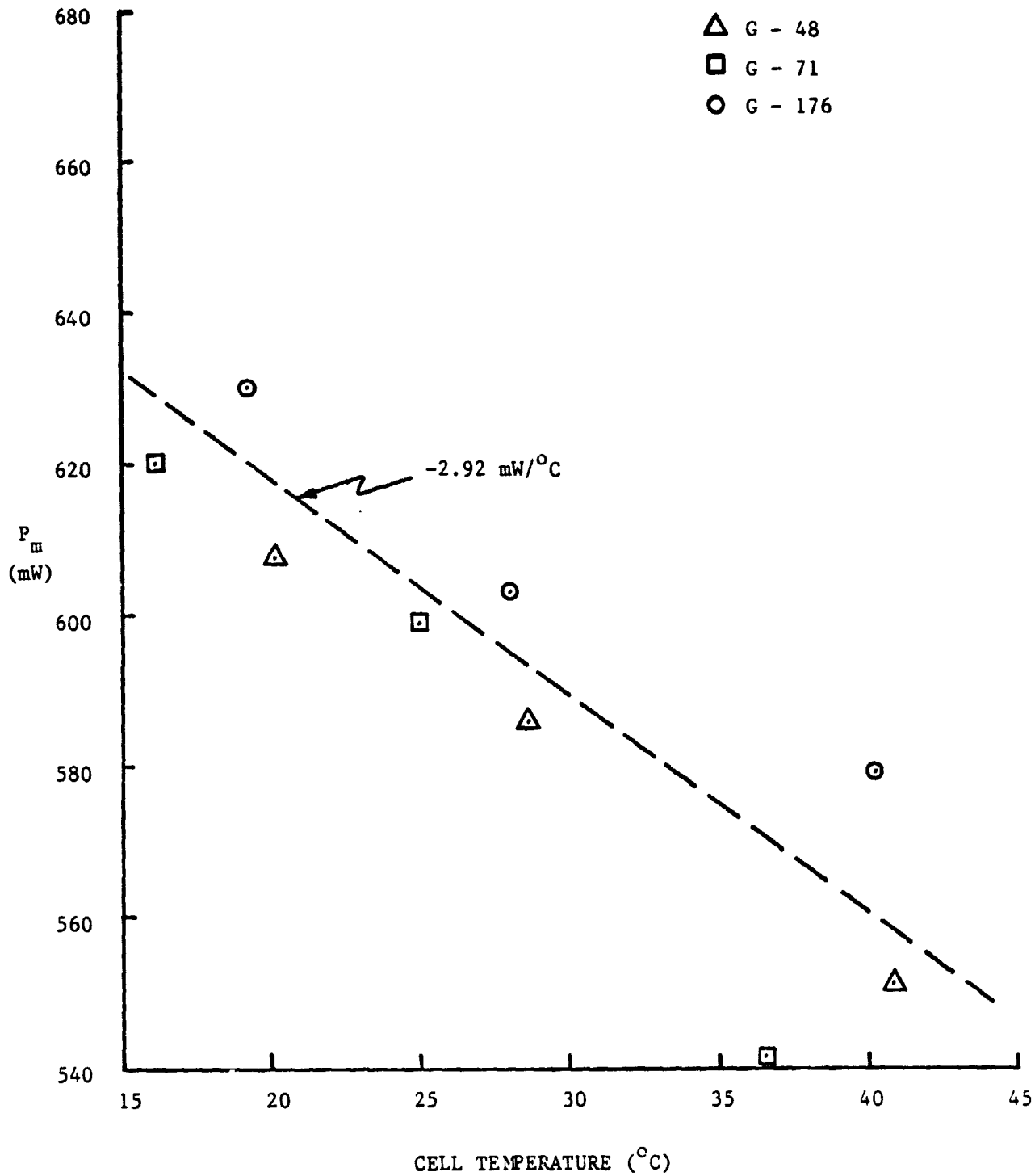

Figure B-6. P_m vs. T for G-Cells Showing Average Slope.

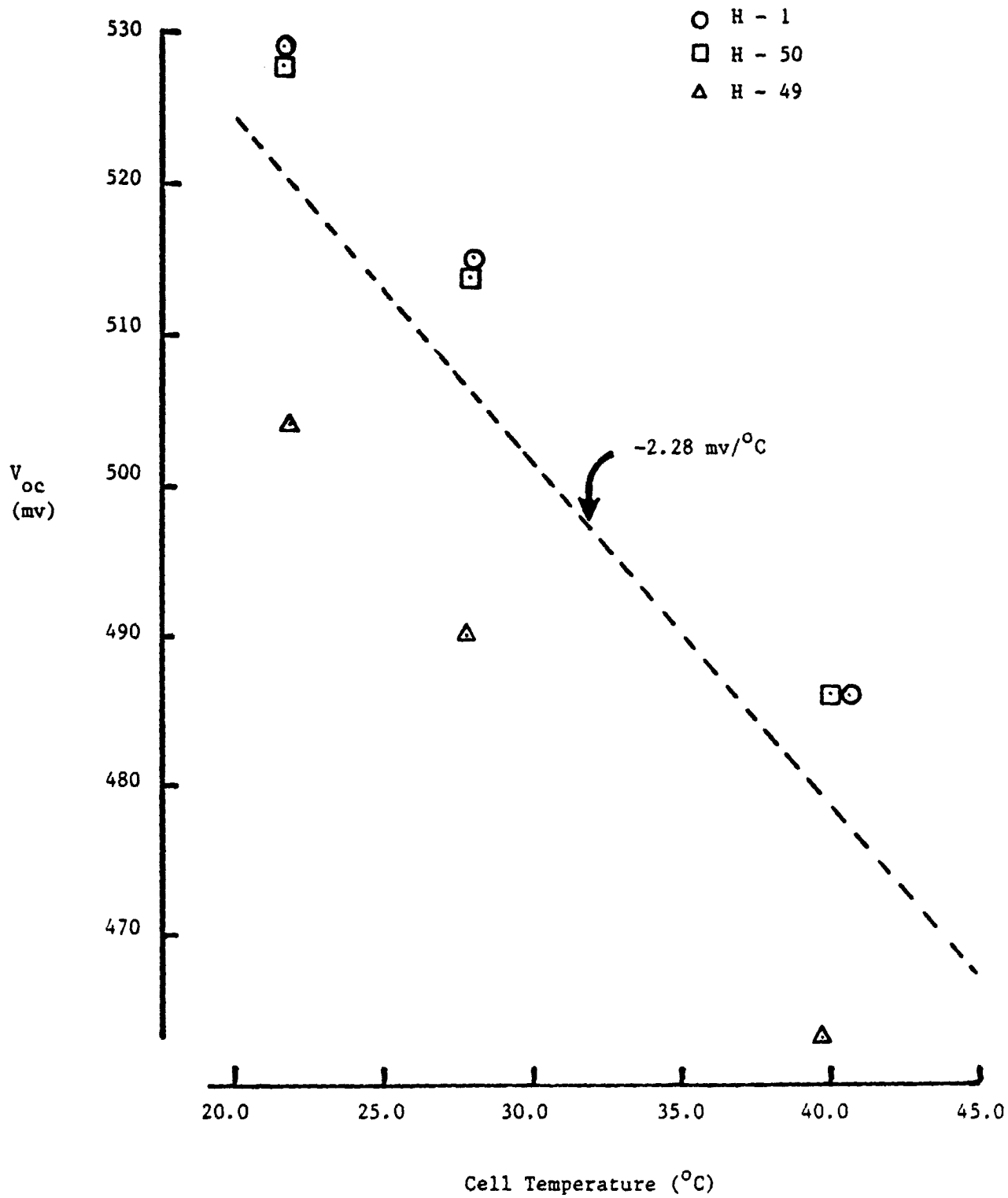

Figure B-7. V_{oc} vs T for Type H Cells Showing Average Slope

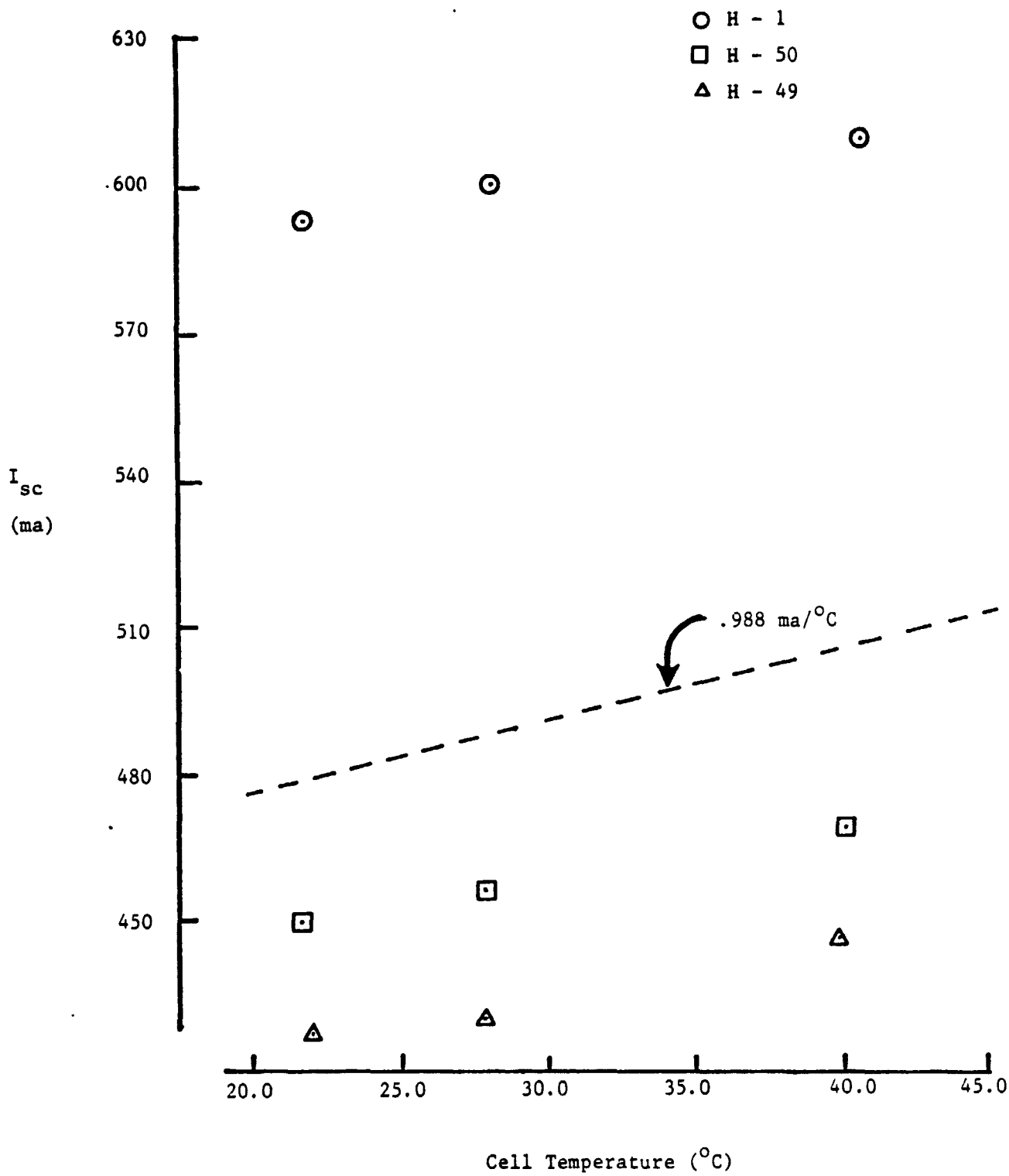

Figure B-8. I_{sc} vs T for Type H Cells Showing Average Slope

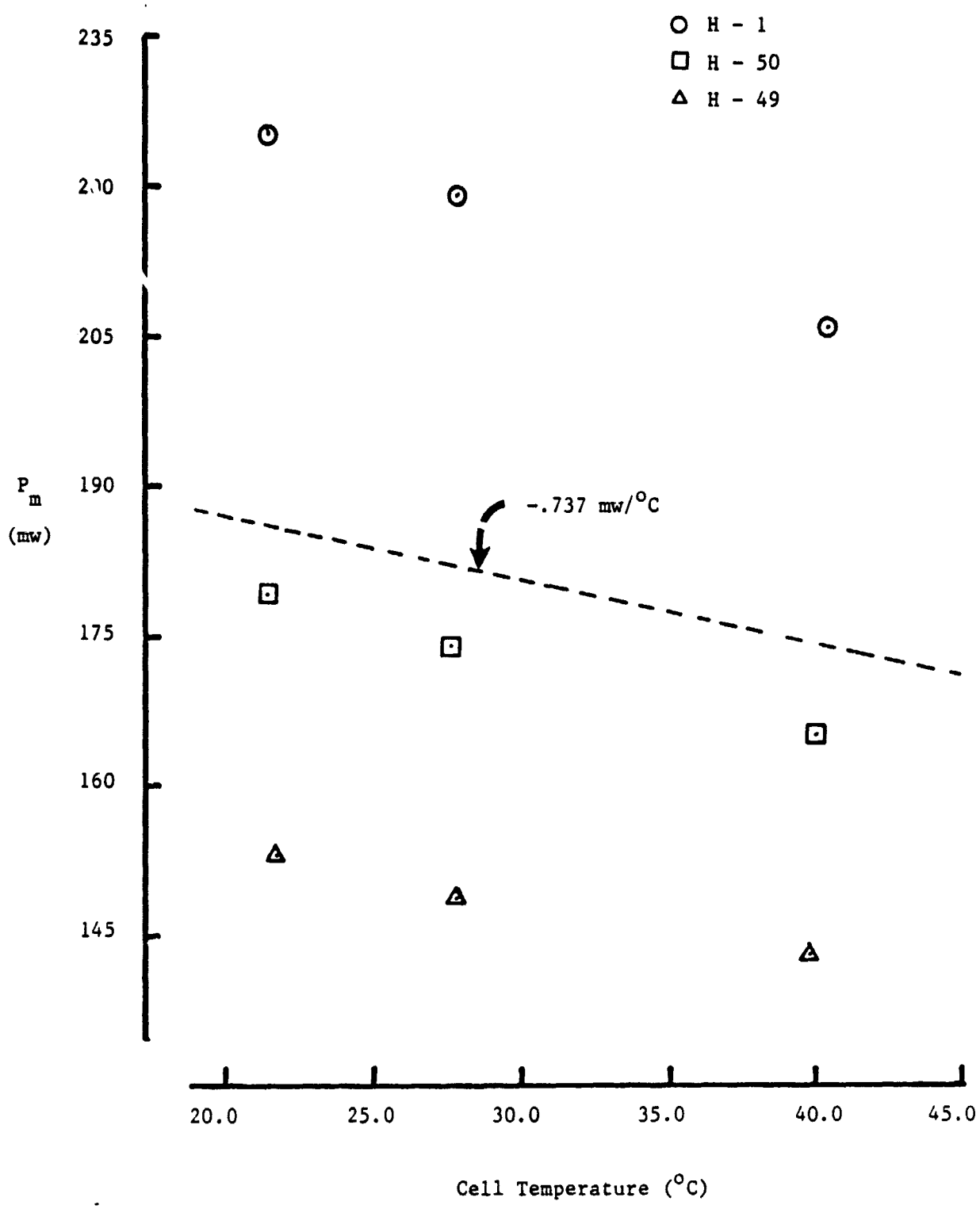

Figure B-9. P_m vs T for Type H Cells Showing Average Slope

APPENDIX C. TEMPERATURE SENSITIVE PHOSPHOR INFORMATION

Fluorescence Thermography

By W. H. Byler and F. R. Hays
U. S. Radium Corporation
Morristown, New Jersey

INTRODUCTION

Thermography is a method for visualizing, measuring, or recording surface temperatures, especially surface temperature differentials, by means of temperature-sensitive luminescent materials (phosphors). Phosphors are crystalline inorganic materials which are generally excited by ultraviolet radiation and emit in the visible range. It is not unusual for phosphors to show variation of efficiency with temperature, but thermographic phosphors are designed to exhibit large change of brightness per unit change of temperature or per unit of incident thermal radiation flux. Also, they are made in the form of fine-grain powder which is favorable for application to surfaces by spray, brush, etc., and for preparation of tape, sheets, and screens.

The thermographic method originated with Dr. Franz Urbach and his associates at Eastman Kodak Research Laboratories. They have discussed applications under two headings: Contact Thermography which involves direct contact of phosphor with the work, applied in the form of paint or tape; and Projection Thermography which involves optical projection of thermal radiation from the work onto a screen of phosphor.[1]

The method has been used for a variety of purposes, including nondestructive testing of metal parts, and recent improvements of phosphors and screens and development of phosphor-resin tapes is expected to encourage wider application. The contact technique sometimes does not require very high sensitivity phosphor. With this technique, if the phosphor is coated on the work, the phosphor temperature will correspond closely to that of the part. In this case, some applications require a useful temperature range far above room temperature. Phosphors are available which operate as high as 400°C. The higher temperature phosphors are less sensitive than those designed for use at lower temperatures. We find that four different phosphors are needed to cover the range from below room temperature to about 400°C. The tape contact technique allows more flexibility with respect to temperature, since with parts having nearly plane surfaces on which a moving tape can be used, the temperature of the tape may not reach that of the parts.

With the projection technique, the phosphor screen can always be held in the most favorable temperature range, therefore, the highest sensitivity phosphor is used. But in this case, there is no limit to the object temperature range. Since this type phosphor is quite sensitive to near infrared radiation, sensitivity is not a particular problem with high temperature work. Low temperatures and great distance call for the ultimate in phosphor sensitivity.

In Figure 1, log brightness-temperature curves are shown for four phosphors covering temperatures up to about 400°C. In Figure 2, the data for the near-room temperature phosphor, No. 1807, are shown on expanded temperature scale. The slopes of the curves are measures of the sensitivity, usually expressed in terms of per cent change of brightness per degree Centigrade change of temperature. The family of curves for each phosphor demonstrates the effectiveness of excitation intensity as a control on brightness, sensitivity, and useful temperature range. Thus, a given phosphor can have high sensitivity and still be useful over a relatively wide temperature range. The practical upper limit of temperature at which a phosphor can be used will be determined in a given situation by the amount of ultraviolet radiation that can be applied and by the lowest useful brightness. But the higher sensitivity phosphors are capable of showing good contrast patterns over a wide range of conditions. On the arbitrary scale of ultraviolet irradiation indicated in

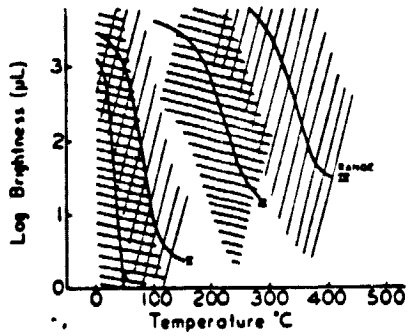

Figure 1—Log brightness-temperature data for four thermographic phosphors.
Range I: ZnCdS:Ag:Ni,
U. S. Radium Corporation No. 1807.
Range II: ZnCdS:Ag:Ni,
U. S. Radium Corporation No. 3215.
Range III: ZnS:Cu:Ni,
U. S. Radium Corporation No. 2090.
Range IV: ZnS:Cu,
U. S. Radium Corporation No. 3003.
Solid curves correspond to one unit of ultraviolet irradiation (see text). Upper edges of shaded areas correspond to 10 units, lower edges to 0.1 unit.

the figures, one unit corresponds to one 100-watt flood-type mercury arc lamp plus U. V. filter at a distance of 53 inches or to two 15-watt fluorescent blacklite lamps (purple glass bulbs) at a distance of 30 inches. A brief discussion of thermographic phosphor properties in terms of theory is given in the Appendix.

In specific situations, the thermographic phosphor method offers certain advantages over other methods. Surface oxidation of metal parts is not a problem. Control of performance through regulation of intensity of excitation allows a degree of flexibility which is important. In testing of bonding of laminates or of thin sheets to substructures, there is no

Reprinted from the May-June, 1961 issue of Nondestructive Testing

limit to the thinness of sheets which can be tested. Since heat flow is involved, the method tests the actual efficiency of bonding rather than just presence or absence of bonding material. The method is adaptable to production line testing, using photocell sensing with feed-back controls if needed. An interesting possibility, for example, is testing lap welding of cable sheathing. Of course, the method is ideally suited to testing of cooling rates. In relation to most widely used methods, the thermographic phosphor method employs simple, inexpensive equipment. Comparing the projection technique to some other imaging methods, it is clean and fast.

On the negative side, in applications involving visual observation, subdued ambient light is indicated. In work with parts of irregular shape, control of heat flow may sometimes be a problem although this may in some cases be handled by preheating or by heating with infrared radiation through the phosphor layer. Lateral flow of heat imposes limitations on depth at which discontinuities can be observed. This varies with heat conductivity of the part and with size of the defect but may generally be expected to be less than 50 mils for metal. With the paint coating technique, if the situation requires the utmost in contrast sensitivity, the coating thickness should be uniform since a nonuniform phosphor layer may yield brightness differences not related to temperature differences. This is not a problem with tape but, with tape, it is important to provide good uniform contact with the surface.

Equipment and Materials

Equipment required will vary greatly with type of test. Qualitative visual observation with the contact technique requires only a phosphor sheet or coating, one or more ultraviolet lamps arranged to provide reasonably uniform irradiation, and means for providing heat flow through or from the part. Phosphor-resin sheets have been developed and can be made to suit varied requirements. The four phosphors of Figure 1 are available, but the higher temperature ones are not expected to be used in ordinary tape due to temperature limitation (about 140°C) of thermoplastic resins. Lacquer and thinner for use in making paint for spray or brush application are available. The resin is chosen for good working properties and relative freedom from fluorescence. Ventilation should be provided to remove solvent vapors. A slurry with two parts by weight phosphor and one part lacquer thinned to working consistency with thinner is suggested. For qualitative work in situations where high contrast and definition are not needed, brush application may be acceptable. Otherwise the spray method is preferred. A DeVilbis type T.G.A., series 501 spray gun is satisfactory for general purpose work. Frequent agitation to insure suspension of phosphor is indicated. A silica binder such as Ludox (DuPont) is suitable for use with the higher temperature phosphors. Optimum coat thickness may vary with the situation. It must be thick enough to provide acceptable light output and uniformity but too great thickness leads to loss of definition; 2 to 5 mils is thought to be the proper range.

Wherever space limitations do not prevent their use, fluorescent blacklite bulbs provide a good uniform ultraviolet source. Mercury arc floodlights or spotlights with near ultraviolet filters are also useful.

For stationary work, electric strip or rod heaters and infrared lamps or glass panels are useful heat sources.

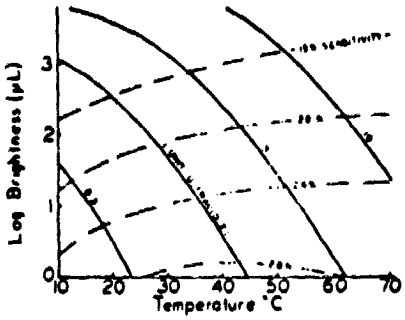

Figure 2—Log brightness-temperature data for Range 1 thermographic phosphor, No. 1807. Dashed curves show sensitivity (per cent brightness change per degree Centigrade change of temperature) against brightness and temperature.

For continuous production line flow, the heat uniformity requirements are less severe. It is sometimes advantageous to play a stream of air on the phosphor surface thereby reducing lateral flow of heat. This tends to increase contrast and makes it possible to hold the pattern for careful study or photography.

At present, no commercial projection equipment is available. However, phosphor screens on cardboard or glass support are available. Equipment arrangements are suggested in U. S. Patent 2,642,538 and royalty-free licensing is available.

An Application Example

The photograph of Figure 3 represents application of the contact thermographic technique in testing a section of stainless steel honeycomb. Panels of this kind are used as structural parts on aircraft and it is important to have a quality control test which can detect faulty bonding between sheets and honeycomb substructure.

The panel was spray-coated with a layer of Range 1 phosphor (see Fig. 2) about 4 mils thick. Heat from a U-shaped electric rod unit was passed into the back side of the panel at a rate of about 0.5 watts/in.^{2} The phosphor was excited by two 15-watt blacklite fluorescent lamps oriented parallel to the two panel edges at an angle of 45 degrees and distance of 16 in. Room air was played on the phosphor surface at a rate of about 1 CFM/in.^{2} With this arrangement, the brightness contrast pattern pattern was steady over a period of many minutes.

The higher temperature dark areas are areas where heat flows in at a rate relatively high compared with the rate at which it escapes. This corresponds to areas where there is good metallic contact between sheet and honeycomb. In a perfect panel, these areas should form an unbroken pattern but in this case, some breaks are observed. We find similar results with phosphor layers applied in the form of pressure sensitive tape or decal sheets. The large-area shadows are thought to be due to

an overall unevenness in thickness of solder.

In addition to the available controls related to phosphor performance, pattern contrast is influenced so by rate of heat flow. Thus, thin weaks may be obscured by choosing very high contrast conditions. Also, is possible to run a gamut of nditions and arrive at an estimate of relative magnitudes of different ws. Intermediate contrast conditions were chosen for the photograph of Figure 3.

ariations of Method

Whenever it is desirable to photograph the contact pattern, this may be done by use of a K-2 filter to clude reflected ultraviolet and blue ght. The film may be of interest as a permanent record but it also rovides a good technique for quan-tative work, especially in cases where it is desirable to plot isoterms. The film may be calibrated y photographing the phosphor-coated surface of a simple calibrating device the temperature of which an be varied in measured steps. It is, of course, necessary to coat this device with the same phosphor at ne same thickness as that used for ne work, to expose it to the same intensity ultraviolet, and to develop ne film under the same conditions. or routine quantitative work, the procedure can be considerably simplified by using the above calibrating evice to calibrate a fluorescent step wedge which is then used for the outine exposures.

Photocell sensing is not as convenient for isotherm mapping as the photographic method, but it serves or quantitative work in cases where only spot areas are of interest or for continuous recording.

pecial Applications

Thermographic phosphors are being used to study air flow patterns ver surfaces. A technique for doing his has been described.[2] A somewhat similar technique has been used to id in design of air jets for cooling.[3]

Thermographic phosphor screens have been used in experimental ultrasonography.[4]

The contact method has been found

Figure 3—Brightness contrast pattern shown by a layer of Range I, No. 1807, thermographic phosphor on a section of steel honeycomb panel as heat is passed through the panel.

useful in testing uniformity of distribution of electrically conductive coatings. When current is passed through the coating, variations in thickness give rise to variations in resistance and hence to variations in temperature. This method is being used also for testing insulation in refrigerator walls.

APPENDIX

Thermographic Phosphor Theory

Solid state theory provides a useful, although not complete, picture of the mechanisms involved in thermographic phosphors. According to the energy band picture, in an ideal crystal there are no allowed electron energy levels between the top of the valence band and the bottom of the conduction band. In preparation of phosphors, the lattice is distorted by addition of foreign atoms or by heat treatment and this introduces new levels just above the valence band (activator levels) and usually also some new levels nearer the conduction band (trapping levels). Excitation by ultraviolet radiation, etc. raises electrons from the activator ground level or the valence band to the conduction band. If the electron returns directly to the ground state, radiation (fluorescence) is emitted. If, instead, it is captured in a trapping state, it may either be lifted again to the conduction band by thermal energy or in some cases, it may find its way back to the ground state by a nonradiative path. This nonradiative return can be pictured in terms of a series of short jumps between trapping states or in terms of the whole-crystal energy picture in which the configurational coordinate curves of the excited and ground states approach one another closely, allowing the transition to occur. The energy is thus dissipated in the form of infrared radiation or thermal vibration. The ratio of radiative to nonradiative returns may be decreased either by increase of temperature of the crystal or by irradiation with infrared. This may be due to one or both of two effects: 1. Thermal vibration or infrared radiation may raise electrons from the valence band to the activator level thus making this level unavailable for receiving excited electrons; 2. Thermal vibration may encourage nonradiative returns by allowing close approach of the configurational coordinate curves.

These are a few of the features of phosphor theory which apply particularly to phosphors having bimolecular phosphorescence decay, such as the sulfides which are adaptable to design of good thermographic phosphors. By using as base material a combination of cadmium and zinc sulfide rather than zinc sulfide alone, the forbidden energy region is narrowed and this favors nonradiative returns. By using silver activator rather than copper, the activator level is nearer the valence band and this favors nonradiative returns because electrons are more easily raised from the valence band to the activator level by thermal energy. By adding a "killer" such as nickel, nonradiative returns are fa-

vored because new relatively deep trap levels are added, etc. Thus, zinc cadmium sulfide activated by silver and "poisoned" by nickel is found to be the most sensitive material for the near-room temperature range. The relative rate constants of the radiative, trap-emptying, and other mechanisms are such that the useful temperature range for a given phosphor can be increased by increasing the intensity of excitation. But there is, of course, a practical limit and for the most sensitive near-room temperature type, this limit is around 90°C. In order to extend the useful temperature range, some of the design parameters must be varied; e.g., cadmium content, nickel content, or kind of activator.

REFERENCES

(1) The Observation of Temperature Distributions and of Thermal Radiation by Means of Non-linear Phosphors, F. Urbach, N. R. Nail, and D. Pearlman, J. Opt. Soc. Am., Vol. 39, No. 12, pp. 1011-1019 (1949). Thermography, F. Urbach, The Photographic Journal, Vol. 90B, pp. 109-114 (1950). Measurement of Temperature Distribution on the Surface of Solid Bodies, F. Urbach, U. S. Patent 2,551,650, May 8, 1951. Thermal Radiography Using Phosphors, F. Urbach, U. S. Patent 2,642,538, June 16, 1953.

(2) A Temperature-Sensitive Phosphor Used to Measure Surface Temperatures in Aerodynamics, Lee C. Bradley, Review of Scientific Instruments, Vol. 24, No. 3, pp. 219-220 (1953).

(3) Temperature-Sensitive Phosphors for the Evaluation of Air Jets Designed to Cool Motion Picture Film, F. J. Kolb and F. Urbach, Soc. of Motion Picture and Television Engineers, Vol. 62, No. 5, pp. 364-376 (1954).

(4) New Methods of Ultrasonoscopy and Ultrasonography, Paul J. Ernst and Charles W. Hoffman, J. Acoustical Soc. Am., Vol. 24, No. 2, pp. 207-211 (1952).

data sheet 40.40

thermographic phosphors and contact thermography

This bulletin is concerned with use of certain special phosphors for detection or measurement of variation of temperature over surface areas. These special phosphors are inorganic crystalline materials which emit light under excitation by ultraviolet radiation and exhibit marked change of brightness with change of temperature. The method originated with Dr. Franz Urbach and his associates at Eastman Kodak Research Laboratories. They developed phosphors with good sensitivity. They also developed and patented basic methods of application. More recently, U. S. Radium Corp. has developed phosphors of still higher sensitivity and studied specific application problems. We are in position now to supply the phosphors in quantity and to offer suggestions relative to their use.

A layer of thermographic phosphor applied to a surface forms an effective thermometer extended in two dimensions. This is being used to study surface phenomena such as air flow patterns and variable electrical conductivity of thin surface layers. By causing heat to flow through the body of an object, discontinuities in the body may be revealed through temperature differences at the surface. In fact, this provides a non-destructive testing technique which is useful in some cases where the x-ray method fails. Since heat flow is involved, lateral flow of heat tends to reduce surface temperature differentials. Therefore, best results are shown where the discontinuity is near the surface or is relatively large: For example, it is particularly effective in showing flaws in bonding of laminates or bonding of sheets to substructures and is now in regular use for such purposes. A demonstration of this type of application is shown in Fig. 1.

In the photograph of Fig. 1, the object under study is a brass ring—stainless steel sheet brazed assembly. The brass ring is 3/8" thick, 3" diameter with a series of equally spaced ¼" holes and a groove about ⅛" deep concentric with the large center hole. The 0.015" thick steel sheet is cut away to show the structure of the brass ring. The steel is covered with a 0.005" layer of Radelin* No. 1807 thermographic phosphor with Radelin* thermographic binder, applied by spray. The phosphor is excited by a set of two 15 watt blacklite fluorescent lamps at a distance of 12 inches. The surface is heated by radiation from two 600 watt hot plates, in which the coils are totally enclosed to avoid visible radiation, placed at a distance of 7 inches. Areas of the steel plate which make good contact with the brass appear as bright areas because heat generated at those surface areas flows freely into the brass so that the temperature remains relatively low. In addition to the dark areas corresponding to the circular groove and holes, a dark radial line is observed. This represents a shallow groove cut in the brass ring surface simulating a flaw in the brazing.

The best conditions for controlling heat flow will vary with the physical situation. In some cases it may be best to flow heat into the body from the reverse side. Also, it is sometimes advantageous to "freeze" the temperature pattern by playing a stream of air on the phosphor surface.

Ideally, both infrared and ultraviolet radiation should be uniform over the surface area under observation. Also, there should not be excessive visible radiation from either source. In fact, in situations where heat is supplied from the phosphor side, it is advisable to avoid short wavelength infrared because this directly reduces phosphor

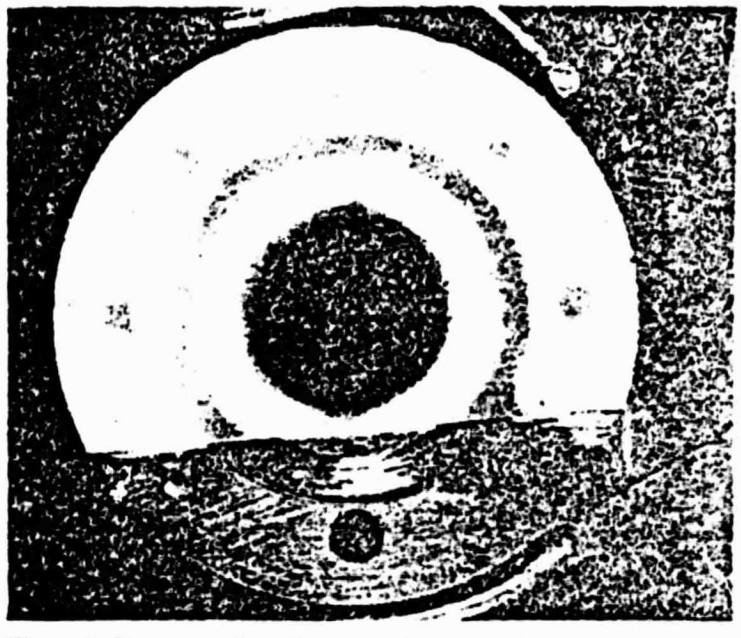

Figure 1. Demonstration of contact thermography indicating discontinuities in bonding of stainless steel sheet to brass.

brightness and has the effect of reducing contrast. Strip heaters or hot plates operated at intermediate temperatures serve the purpose. Wherever space limitations do not prevent their use, fluorescent blacklite bulbs provide a good ultraviolet source. Mercury arc floodlights or spotlights with near ultraviolet filters are also useful (See appendix for partial list of suppliers of ultraviolet lamps).

*Trademark

Phosphor Properties

Phosphors in general exhibit variation of efficiency with change of temperature but many of the more efficient ones show relatively little variation in the near-room temperature range. Therefore, phosphors useful for thermography must be specially designed to show large change of brightness with small change of temperature. Sensitivity is expressed in terms of percent change of brightness per degree Centigrade change of temperature.

Preliminary work in the field indicates that for the near-room temperature range, zinc cadmium sulfide with silver activator and a trace of nickel as "poison" is most useful. This type phosphor is best excited by near ultraviolet radiation and emits broad band radiation with dominant wavelength in the yellow. United States Radium's standard near-room temperature type thermographic material, Radelin *phosphor No. 1807, is a fine crystalline material with average particle size below ten microns. Performance of this phosphor can best be discussed by reference to Fig. 2.

The solid curves of Fig. 2 show the effect of temperature on brightness at four levels of ultraviolet excitation. On this arbitrary scale of ultraviolet irradiation, one unit corresponds to one 100-watt flood-type mercury arc lamp, plus U.V. filter, at a distance of 53 inches or to two 15-watt fluorescent blacklite lamps (purple glass bulbs) at a distance of 30 inches. The slopes of these curves at the various points represent sensitivity of the phosphor at corresponding temperature and brightness. The dashed curves are iso-sensitivity curves drawn in each case through points on the solid curves where the slope is the same. This shows that in the intermediate range of brightness and over the range of temperature from room temperature to above 80° C., sensitivity holds nearly constant at a given brightness level. Also, it is observed that a given brightness level may be held over this range of temperature by adjusting the level of ultraviolet excitation. And at a given temperature both brightness and sensitivity are functions of level of excitation. Therefore, the phosphor is capable of showing good contrast patterns over a wide range of conditions. The practical upper limit of temperature at which this phosphor can be used will be determined in a given situation by the amount of ultraviolet radiation that can be applied and by the lowest useful brightness.

For higher temperature applications, phosphors of different design must be used. While it is expected that most applications will require the near-room temperature type, we are prepared to supply phosphors for use at higher temperatures. Performance data on these phosphors will be available at a later date.

Phosphor Coating

The phosphor should be applied uniformly by spray, brush, screen or settling. The binder must be such that it shows a minimum of fluorescence since such fluorescence would tend to reduce contrast of the temperature pattern developed by the phosphor. At temperatures much above 100° C., thermal stability of the usual resin binders becomes a problem. In this range, either silicate or silica binder such as Ludox* (Du Pont) or one of the newer high temperature thermosetting resin binders may be used. But it is expected that most applications will involve the range below 100° C. and United States Radium has developed a lacquer for this range which is suitable for brush or spray application and is prepared to supply it and thinner for use with it. We suggest a slurry with two parts by weight phosphor and one part lacquer thinned to working consistency with the thinner. These materials, in common with all such materials, should be handled under ventilated conditions away from sparks, flame, or excessive heat. Thinner can be used to remove the phosphor coating. We invite consultation relative to any special binder problems.

For qualitative work in situations where high contrast and definition are not needed, brush application may be acceptable. Otherwise the spray method is preferred. Optimum coat thickness will vary with the situation. It must be thick enough to provide good light output and acceptable uniformity. On the other hand, too great thickness leads to loss of definition. We find a thickness of 0.005" to be the right order of magnitude. A DeVibilis type T.G.A., series 501 spray gun is satisfactory for general purpose work. Frequent agitation to insure suspension of phosphor is indicated.

Special Techniques

Although most industrial testing may require only qualitative visual observation of the brightness pattern, there may be situations where it is desirable to photograph the pattern. This may be done simply by use of a K-2 filter to exclude reflected ultraviolet and blue light. The film may be of interest as a permanent record but it also provides a good technique for quantitative work, especially in cases where it is desirable to plot isotherms. The film may be calibrated by photographing the phosphor-coated surface of a simple calibrating device the temperature of which can be varied in measured steps. It is, of course, necessary to coat this device with the same phosphor at the

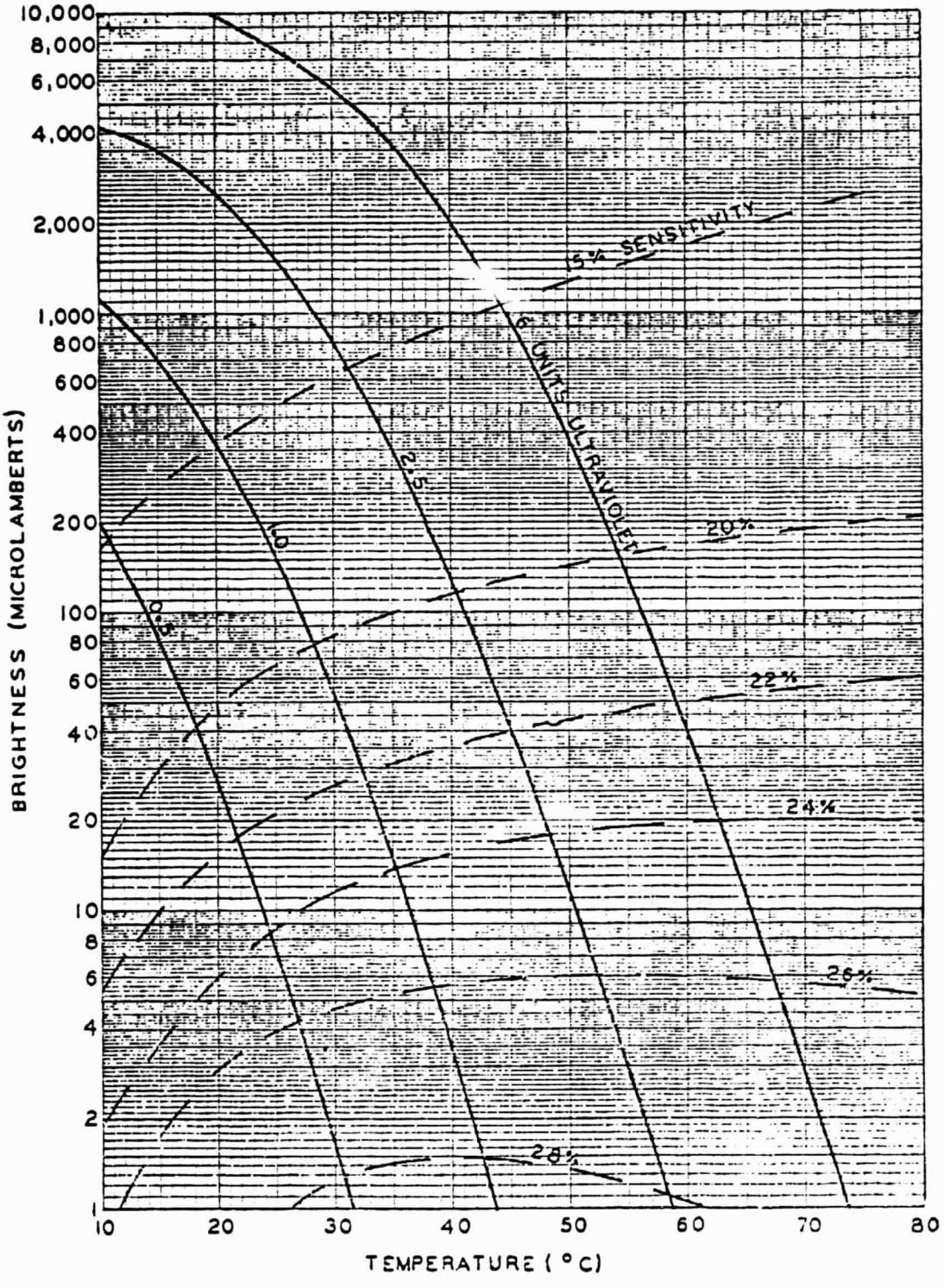

Figure 2. Performance of Radelin thermographic phosphor No. 1807. Solid curves show brightness against temperature at four levels of ultraviolet excitation. Dashed curves show sensitivity (per cent brightness change per degree Centigrade change of temperature) against brightness and temperature.

same thickness as that used for the work to expose it to the same intensity ultraviolet, and to develop the film under the same conditions. For routine quantitative work, the procedure can be considerably simplified by using the above calibrating device to calibrate a fluorescent step wedge which is then used for the routine exposures.

Photocell sensing is obviously not as convenient for isotherm mapping as the photographic method, but it serves for quantitative work in cases where only spot areas are of interest. Also, the photocell method is ideal for assembly line sensing and can be set up to actuate devices for marking locations of flaws or performing other operations on the work.

The preceding discussion applies only to methods involving application of the phosphor directly to the object, i.e., contact thermography. Since thermographic phosphor responds to infrared radiation, a screen of the phosphor can be used to detect distant sources of heat radiation and by optically projecting an image of the source on the screen, the temperature pattern of the source can be seen and photographed (projection thermography). This method allows study of objects at very high temperatures. This bulletin deals primarily with contact thermography but it should be mentioned that United States Radium is also prepared to supply thermographic screens as well as phosphor, lacquer, and thinner.

Appendix

A Partial List of Suppliers of Black Lights

* Black Light Eastern Corporation
33-00 Northern Boulevard
Long Island City 1, N. Y.

* Burton Manufacturing Company
2520 Colorado Boulevard
Santa Monica, Calif.

* Century Lighting, Inc.
521 W. 43rd Street
New York 36, N. Y.

\ Charlotte Chemical Laboratories
Charlotte 1, N. C.

* George W. Gates & Co., Inc.
Franklin Square
Long Island, N. Y.

* Hanovia Chemical & Manufacturing Co.
100 Chestnut Street
Newark 5, New Jersey

* Herbach & Rademan, Inc.
1204 Arch Street
Philadelphia 7, Pa.

\ Lawter Chemicals, Inc.
3550 Toughy Avenue
Chicago 45, Illinois

\ Luminous Resins Inc.
166 W. Washington Street
Chicago 2, Illinois

* Magnaflux Corporation
5900 Northwest Highway
Chicago 31, Illinois

\ * Norco Manufacturing Company
392 Bleecker Street
New York 14, New York

\ * Research Specialties Company
2005 Hopkins Street
Berkley 7, Calif.

\ * Shannon Luminous Materials Co.
7354 Santa Monica Blvd.
Hollywood 46, Calif.

\ * Strobilite Company
75 West 45th Street
New York 36, N. Y.

\ Vietze Luminescent Company
Baldwin, Long Island, N. Y.

\ Western Fluorescent Lighting, Inc.
3224 W. Roosevelt Road
Chicago 24, Illinois

\ Indicates suppliers of fluorescent type
* Indicates suppliers of mercury arc type

Printed in U. S. A.

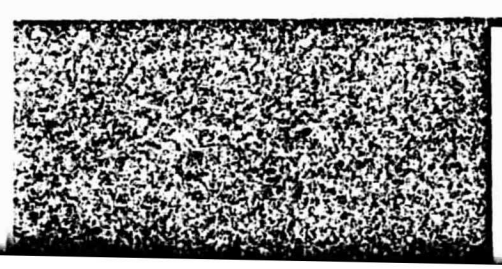

UNITED STATES RADIUM CORPORATION
Morristown, N.J.

RADIUM